

https://dspace.org/

Hybrid lipopolysaccharide-based nanosystem for the delivery of anti-tuberculosis therapeutics

Sumaila, Mumuni

2021

https://hdl.handle.net/10539/32545

Downloaded from a DSpace repository. https://dspace.org/

HYBRID LIPOPOLYSACCHARIDE-BASED NANOSYSTEM FOR THE DELIVERY OF ANTI-TUBERCULOSIS THERAPEUTICS

Mumuni Sumaila



A dissertation submitted to the Faculty of Health Sciences, University of the Witwatersrand, in fulfilment of the requirements for the degree of Master of Pharmacy

Supervisor:

Professor Viness Pillay

Department of Pharmacy and Pharmacology, Faculty of Health Sciences, University of the Witwatersrand, Johannesburg, South Africa

Co-Supervisors:

Professor Yahya E. Choonara

Associate Professor Pradeep Kumar

Department of Pharmacy and Pharmacology, Faculty of Health Sciences, University of the Witwatersrand, Johannesburg, South Africa

Johannesburg, 2021

DECLARATION

I, Mumuni Sumaila, declare that this dissertation is my own work. It has been submitted for the degree of Master of Science in Pharmacy in the Faculty of Health Sciences at the University of the Witwatersrand, Johannesburg, South Africa. It has not been submitted before for any degree or examination at this or any other University.



This …2nd.. day of ……February…….. 2021

RESEARCH OUTPUTS

Research Publication

Sumaila, M. *et al.* (2019) 'Lipopolysaccharide Polyelectrolyte Complex for Oral Delivery of an Anti-tubercular Drug', AAPS PharmSciTech, 20(3), pp. 107. doi: 10.1208/s12249-019-1310-6.

Conference Proceedings

Poster Presentations

Mumuni Sumaila, Viness Pillay, Yahya E. Choonara, Lisa C. du Toit, Pradeep Kumar and PP Kondiah. Synthesis and Characterization of Lipopolysaccharide Nanoparticles for Dual Delivery of Rifampicin and Isoniazid. Poster presented at the School of Therapeutic Sciences Biennial Research day, 10 September 2019, University of the Witwatersrand, Johannesburg, South Africa. (Abstract in Appendix B).

ABSTRACT

Tuberculosis (TB) is reported as one of the leading causes of morbidity and mortality globally, accounting for about 10 million new cases and 1.5 million deaths annually with the poorest and socially excluded groups bearing the largest burden of the disease. The conventional treatment approach for susceptible cases involves a daily oral dose of four first-line drugs, such as rifampicin, isoniazid, pyrazinamide and ethambutol (RIPE), which are scheduled into an initial intensive phase of two months with RIPE regimen and a continuous phase of four months with rifampicin/isoniazid regimen. Currently, the treatment of tuberculosis still remains a global challenge due to inconsistent drug bioavailability, dose-related side effects, systemic drug toxicity and poor patient compliance, which could be attributed to poor delivery of conventional anti-TB therapeutics. Therefore, the issue of drug resistance, non-targeted delivery, sub-optimal dosage at disease sites and side effects on healthy cells have rendered conventional treatment approach inefficient and ineffective in combating the disease even after combination chemotherapy. This research aimed to address the shortfalls associated with oral delivery of anti-TB therapeutics by employing nanotechnological approach to design a novel nano-enabled surface-functionalized drug delivery system (DDS) that will specifically target the infection site of *Mycobacterium tuberculosis* (Mtb) following oral administration. Alveolar macrophages, the reservoir for Mtb, displays special surface receptors, such as mannosyl, galactosyl, and lectin, which can be explored in the design of a smart and intelligent nanodelivery system to improve the preferential accumulation of anti-TB drugs within the alveolar macrophages, thereby reducing systemic side-effects and enhancing therapeutic activity. Based on this concept, we have designed, optimized and characterized a smart ligand-functionalized nano-construct – referred to herein as a 'mannosylated hybrid lipopolysaccharide-based (MHLP) nanosystem' – with encapsulated rifampicin and isoniazid for targeted and controlled delivery to Mtb infection site following oral administration.

The physicochemical parameters that characterized the design of a smart nano-construct in TB therapeutics including satisfactory size, shape and surface properties, good gastrointestinal permeability, cellular uptake and internalization by RAW 264.7 macrophages, as well as low cellular toxicity to healthy cells informed the fabrication of the MHLP nanosystem. In this study, an optimized CT-SL nano-conjugate was developed and surface-functionalized with mannose as targeting moiety. Fourier Transform Infrared (FTIR) spectroscopy, Differential Scanning Calorimetry (DSC), Thermogravimetric analysis (TGA) and Phenol-Sulphuric acid assay confirmed the successful grafting and functionalization of the nano-conjugates while Dynamic Light Scattering (DLS) analyses confirmed the synthesis of MHLP nanoparticles with an average size less than 300 nm and surface charge of +20 to +30 mV. Scanning Electron Microscopy (SEM) results confirmed the morphology of the MHLP nanosystem to be spherical with uneven surfaces and a spongy appearance due to the attachments of the functionalized moiety. Optical scattering analysis confirmed the stability profile of the nanosystem in suspension while the *in vitro* dissolution study showed a sustained release of rifampicin and isoniazid at the simulated physiological pH, indicating a positive influence of lipopolysaccharide architecture on drug release kinetics. Additionally, *ex vivo* permeability studies demonstrated a 2-fold increase in gastrointestinal rifampicin permeability within 8-hour study period in comparison with the free drug solution. Interestingly, MHLP nanoparticle uptake and intracellular drug accumulation studies showed an enhanced rifampicin/isoniazid delivery to RAW 264.7 macrophages when compared with the unmodified nanosystem and the free drug solution. Cytotoxicity assay demonstrated a good biocompatibility with greater than 80% cell viability achieved at nanoparticle concentrations 120 µg/mL during 24-hour treatment time.

Overall, detailed *in vitro* and *ex vivo* experimental results validated the fabricated MHLP nanoparticulate systems as efficient cargo system for rifampicin and isoniazid delivery to alveolar macrophages for enhanced anti-TB therapeutics. While rifampicin and isoniazid were selected as the model drugs in this study due to their established anti-mycobacterial activities and limitations, the novel MHLP nanosystem can also be employed to incorporate other anti-TB chemotherapeutics for enhanced on-site delivery of the bioactives.

RESEARCH AWARDS AND RECOGNITIONS

1. University of the Witwatersrand CTG Postgraduate Grant, 2018.
2. National Research Foundation (NRF) Innovation Master's Scholarship 2019. Award Reference: SFH180525334818.

ACKNOWLEDGEMENTS

At the completion of this work I am eternally humbled and deeply grateful to the countless individuals for their generosity of spirit in guiding and assisting me through this most rewarding and challenging task. Without each of you this journey would have held much less value, educational and life lessons.

Of greatest importance, I lay my gratitude at the feet of the Almighty God, constant and everlasting companion of my heart, for bringing me to and through this invaluable experience from which I have gained unquantifiable rewards and lessons.

My sincere and profound gratitude goes to my supervisor, Professor Viness Pillay. His mentorship, supervision, relentless guidance, supports and attention to detail contributes immensely to the successful completion of this study. I am most grateful for giving me the platform to explore my undying quest for excellence which WADDP represents. To my co-supervisor - Professor Yahya E Choonara; I say thank you for your constructive and meticulous advice, research planning and editing of research outputs during the course of this study. A hearty thanks to my co-supervisor - Professor Pradeep Kumar. Your immense contributions to the successful completion of this study are greatly appreciated from conceptualisation to design, and from analyses to editing of research reports. You have provided a window into a world that encourages us to think out of the box and feel comfortable (even inspired) in the realm of outrageous ideas, uncertain outcomes and fearless exploration of the unknown that may indeed bring forth a concept that will change the world someday. Thank you for pushing the boundaries, testing me, frustrating me and teaching me. It was all worthwhile!

Special thanks to the National Research Foundation and the University of the Witwatersrand for the bursary and research grant given to me during the period of this study. Your generosity and support did ease the financial burden that goes with this study.

My heartfelt appreciation to Professor Winnie Nhlengethwa and Dr Bongani Sibandze for your kind assistance and inspirational contribution towards completing this research work.

To my ever-loving wife, Patience Oiza Sumaila: I am at a loss for words to adequately express my gratitude for your unwavering support, help and encouragement. Thank you for making my work a priority and going far beyond every expectation to make life smooth and easy for me. Thank you for having faith in me when mine was dwindling, wiping the many tears, indulging my crazy antics and always reminding me of the wonder that lay ahead. You are a symbol of all that is good, and you truly inspire me to do and be better. To my adorable daughter - Jassiel

and loving son – Jesh, I say thank you for believing in your daddy in the pursuit of academic excellence.

To the friends that have become family, Onyinye, Alex, Hillary, Yasar and Samson: Each one of you has provided something unique that has helped, inspired and motivated me. Thank you for the coffee/lunch/shopping expeditions that were a welcomed distraction, the hours of laughter and conversation on and off campus and for always having an encouraging word when things just weren't working. Thank you for the willingness to help with my work and provide guidance or share the lessons learned through each of your own research. Most of all thank you for all the things that only amazing friends can provide!

A special thank you to Dr Philemon Ubanako and Dr Poornima Ramburrun for always being there to lend a helping hand during my cell work. Thank you for the constant encouragement, support and insight into the 'bigger picture'. Your kindness and generosity have made a huge contribution to this experience.

To my friends and colleagues at WADDP: Funi, Kate, Pakama, Gillian, Sarah, Dalton, Femi, Jonathan, Lara, Zakkiyya and all other postgraduate students, I extend my gratitude for the assistance each of you have provided during my research and for being a part of my journey.

A heartfelt thank you to Professor Pierre P. Kondiah and Dr Thashree Marimuthu for your unselfish nature and the many hours you have spent assisting, guiding and encouraging me.

This list is by no means complete. There have been countless acts of kindness and amazing people that have assisted me on this journey. I would like to express my gratitude to everyone that I may have mistakenly omitted.

DEDICATION

With gratitude to God, this research work is whole-heartedly dedicated to my mother: Mrs Aminetu Sumaila, who crafted in me the quest for and pursuit of academic excellence.

TABLE OF CONTENTS

DECLARATION i
RESEARCH OUTPUTS ii
ABSTRACT iii
RESEARCH AWARDS AND RECOGNITIONS iv
ACKNOWLEDGEMENTS v
DEDICATION vii
TABLE OF CONTENTS viii
LIST OF FIGURES xvii
LIST OF TABLES xxi
LIST OF EQUATIONS xxii
LIST OF ABBREVIATIONS xxiii

CHAPTER 1

INTRODUCTION

1.1. Tuberculosis: Causative organism and pathology ……..1

1.2. Background of the study 2

1.3. Rationale for this study..... 5

1.4. Aim and objectives..... 6

1.5. Novelty of this study..... 7

1.6. Overview of the dissertation 7

1.7. Conclusion..... 9

1.8. References..... 9

CHAPTER 2

LIPOPOLYSACCHARIDE NANOTECHNOLOGICAL STRATEGIES FOR EFFICIENT ORAL DRUG DELIVERY

2.1. Introduction 12
2.2. Molecular transport mechanisms across the gastrointestinal tract 14
2.2.1. Paracellular transport 14
2.2.2. Transcellular transport 15
2.2.3. Carrier-mediated transport 15
2.2.4. Receptor-mediated transport 16
2.3. Barriers associated with oral drug delivery 16
2.3.1. Physiological barriers 17
2.3.2. Biochemical barrier 18
2.3.3. Physicochemical barrier 19
2.4. Rationale for the use of polymer-lipid hybrid nanosystems 20
2.5. Nanotechnological approaches of lipopolysaccharide in oral drug delivery 21
2.5.1. Polysaccharide-associated lipid nanoparticles 22
2.5.2. Modified chitosan-associated lipid nanoparticles 23
2.5.2.1. Quaternized Chitosan Derivatives 24
2.5.2.1.1. TMC – associated lipid nanosystem 24
2.5.2.1.2. CMC-associated lipid nanosystem 25
2.5.2.1.3. HACC-associated lipid nanosystem 26
2.5.3. Layer by layer polysaccharide-associated lipid nanoparticles 28
2.6. Conclusion 32
2.7. References 32

CHAPTER 3

DESIGN OF LIPOPOLYSACCHARIDE POLYELECTROLYTE COMPLEX FOR ORAL DELIVERY OF AN ANTI-TUBERCULAR DRUG

3.1. Introduction 45
3.2. Materials and methods 47
3.2.1. Materials 47
3.2.2. Preparation of rifampicin-loaded SL-CT lipopolysaccharide particulates 48
3.2.2.1. Preparation of loose nanoparticle powders 48
3.2.2.2. Preparation of PEC particulate tablets 49
3.2.2.3. Evaluation of particle size distribution, zeta potential and conductivity 49
3.2.2.4. Determination of RFP-loading capacity and encapsulation efficiency in response to changes in SL concentration 49
3.2.2.5. Determination of molecular vibrational transitions and analysis of PEC formation 50
3.2.2.6. Analysis of the thermodynamic properties of the synthesized lipopolysaccharide PEC and RFP-loaded PEC particulates 50
3.2.2.7. X-ray powder diffraction (XRPD) analysis 50
3.2.2.8. Evaluation of rheological properties of the synthesized lipopolysaccharide complex and RFP-loaded PEC particulates 51
3.2.2.9. Textural profiling of RFP-loaded lipopolysaccharide complex nanoparticle tableted formulations 51
3.2.2.10. Optical characterization and stability of the lipopolysaccharide PEC particulates in suspension 51
3.2.2.11. In vitro drug release of lipopolysaccharide PEC particulates and kinetic modelling of release data 52
3.2.2.12. Analysis of the hydrodynamic and swelling characteristics of the RFP-loaded lipopolysaccharide PEC tableted PEC particulates 52
3.2.2.13. *Ex vivo* Permeability of RFP from the Lipopolysaccharide PEC Particulates across Porcine Intestinal Tissue 53
3.3. Results and Discussion 54
3.3.1. Evaluation of particle size and zeta potential 54

3.3.2. Determination of RFP loading capacity and encapsulation efficiency in response to changes in SL concentrations 54
3.3.3. Determination of mucoadhesive properties in response to SL:CT and RFP variations 55
3.3.4. Analysis of molecular vibrational transitions indicating PEC formation 57
3.3.5. Analysis of thermal stability and degradation induced by SL-CT-RFP polyelectrolyte complexation 58
3.3.6. X-Ray Powder Diffraction (XRPD) analysis 59
3.3.7. Evaluation of rheological properties of the synthesized lipopolysaccharide complex and RFP-loaded PEC particulates 61
3.3.8. Textural transitions in response to variations in SL in the RFP-loaded lipopolysaccharide PEC nanoparticulate tablets 61
3.3.9. Optical characterization and stability of the lipopolysaccharide PEC particulates in aqueous suspension 63
3.3.10. Evaluation and mathematical modelling of RFP release from the lipopolysaccharide PEC particulates 65
3.3.11. Evaluation of hydration dynamics controlling swelling and erosion behaviors of the RFP-loaded lipopolysaccharide PEC nanoparticulate tablets 68
3.3.12. Ex vivo Evaluation of RFP Permeation Across Porcine Intestinal Tissue from the Lipopolysaccharide PEC Particulates 70
3.4. Conclusion 72
3.5. References 73

CHAPTER 4

DESIGN OF MANNOSE-FUNCTIONALIZED HYBRID LIPOPOLYSACCHARIDE NANOPARTICLES FOR MACROPHAGE-TARGETED DELIVERY OF RIFAMPICIN AND ISONIAZID

4.1. Introduction 79
4.2. Materials and Methods 80
4.2.1. Materials 80
4.2.2. Methods 81
4.2.2.1. Preparation of the Lipopolysaccharide Formulations 81
4.2.2.1.1. Preparation of Hybrid Chitosan-Lecithin RFP-ISN-loaded (CT-SL-RFP-ISN) Nanoparticles 81
4.2.2.1.2. Preparation of mannosylated Nanoparticles 81
4.2.2.2. Characterization of the Lipopolysaccharide Formulations 82
4.2.2.2.1. Evaluation of Particle Size, polydispersity index, Zeta Potential, Conductivity, and Structural Morphology 82
4.2.2.2.2. Quantification of mannose linkage on the surface of functionalized lipopolysaccharide nanoparticles 83
4.2.2.2.3. Determination of RFP-ISN-Loading Capacity and Encapsulation Efficiency of the Nanoparticles 83
4.2.2.2.4. Analysis of molecular vibrational transitions using Fourier Transform Infrared (FTIR) Spectroscopy 84
4.2.2.2.5. Analysis of the Thermodynamic Properties of the Synthesized Nanoparticles 84
4.2.2.2.6. Stability profiling and optical characterization of Mn-CT-SL-RFP-ISN and CT-SL-RFP-ISN nanoparticles in suspension 84
4.2.2.2.7. *In vitro* evaluation of RFP and ISN release from the Mn-CT-SL-RFP-ISN and CT-SL-RFP-ISN nanoparticles 85
4.2.2.3. Cellular studies 85
4.2.2.3.1. Culturing and expansion of the macrophage RAW 264.7 cell line 85
4.2.2.3.2. Determination of cell density and viability 86
4.2.2.3.3. In vitro cytotoxicity assay of the formulated nanoparticles 86
4.2.2.3.4. Evaluation of nanoparticle internalization and drug accumulation in cultured macrophage RAW 264.7 cells 87
4.3. Results and Discussion 88

4.3.1. Nanoparticle synthesis and evaluation of particle size, surface charge, morphology, drug association efficiency and degree of mannose-functionalization 88
4.3.2. Evaluation of molecular vibrational transitions induced by RFP-ISN incorporation and Schiff's base formation. 93
4.3.3. Analysis of thermodynamic behaviour of the synthesized nanoparticles and the effect of mannosylation on nanoparticle thermal stability 96
4.3.4. Evaluating the stability and optical characterization of Mn-CT-SL-RFP-ISN and CT-SL-RFP-ISN nanoparticles in suspension 97
4.3.5. In vitro release of RFP and ISN from CT-SL-RFP-ISN and Mn-CT-SL-RFP-ISN nanoformulations 100
4.3.6. Assessment of the cytotoxicity effect of the formulated nanoparticles 101
4.3.7. Assessing the influence of CT-SL-RFP-ISN surface functionalization on nanoparticle uptake via fluorescence microscopy and drug accumulation study in cultured macrophage RAW 264.7 cells 103
4.4. Conclusion 107
4.5. References 108

CHAPTER 5

CONCLUSIONS, LIMITATIONS AND FUTURE RECOMMENDATIONS

5.1. Conclusions 127

5.2. Limitations of the research 129

5.3. Future recommendations 129

APPENDICES

APPENDIX A.....132
APPENDIX B.....133
APPENDIX C 134
APPENDIX D 135

LIST OF FIGURES

Figure 1.1. Schematic showing the synthetic mechanism involved in the fabrication of hybrid CT-SL RFP-ISN-loaded nanoparticles. The solvent injection technique encourages polyelectrolyte complexation between CT and SL, which drives the formation of the hybrid lipopolysaccharide nanostructure. RFP: rifampicin. ISN: isoniazid. 6

Figure 2.1. Schematic summary (not to scale) of several possible transport mechanisms across the gastrointestinal mucosa barrier; paracellular route provides a channel where the drug passively diffuses between cells at the intercellular tight junctions, transcellular route allows drugs to permeate the cell passively by partitioning to cell membranes at both apical and basolateral sides, receptor-mediated and carrier-mediated transport routes, an energy-dependent active transport where the drug is vectorized via receptor-drug and carrier-drug interaction, respectively. Figure adapted from (Mohammadzadeh and Javadzadeh, 2018). 14

Figure 2.2. Reaction scheme of N-trimethyl chitosan (TMC). 25

Figure 2.3. The chemical structures of chitosan and the various derivatives of carboxymethyl chitosan (CMC). 26

Figure 2.4. Reaction scheme illustrating the synthesis of N-(2-hydroxy)-propyl-3-trimethylammonium chitosan chloride (HACC) in the presence of epoxypropyl trimethyl ammonium chloride (EPOTAC)……27

Figure 2.5. Schematic representation of the transport mechanisms of HACC-modified bioactive-loaded SLN across GI epithelial cells; permeation mechanism is largely related to caveolae-mediated endocytosis, M cell phagocytosis, and reversible tight junction opening. Reprinted with permission from (Shi *et al.*, 2016). Copyright (2016) American Chemical Society……28

Figure 3.1. Schematic representation of the synthesis of lipopolysaccharide-based PEC particulates via the solvent injection technique. 49

Figure 3.2. Representation of %MBE of RFP-loaded and RFP-free nanoparticle formulations in response to SL: CT and RFP variations. All values represented as mean ± SD (n=3). 57

Figure 3.3. FTIR spectra of a) SL-CT-RFP, b) SL-CT, c) RFP, d) CT and e) SL. 58

Figure 3.4. DSC thermograms of a) SL-CT-RFP 3:1, b) SL-CT-RFP 1:1, c) SL-CT 3:1, d) SL-CT 1:1, e) CT, f) SL and g) RFP 59

Figure 3.5. X-ray Powder Diffraction (XPRD) spectra of CT, SL, RFP, the SL-CT complex and the SL-CT-RFP PEC particulates. 61

Figure 3.6. Kinetic gelation plots of a) SL-CT 1:1 and SL-CT 3:1, and b) SL-CT-RFP 1:1 and SL-CT-RFP 3:1 presenting the shear storage modulus (G') (Pa) observed over a 5-hour timeframe at 37^0C..... 63

Figure 3.7. Representation of the destabilization kinetics of a) SL-CT 1:1, b) SL-CT 3:1, c) SL-CT-RFP 1:1 and d) SL-CT-RFP 3:1 suspension, indicating ΔBS and T measured at 25 ± 0.5 ^{0}C for 5-minutes duration. 65

Figure 3.8. *In vitro* release profile of RFP from various indicated formulations at 37 ^{0}C and pH 6.8 (n=3, mean ± SD). 68

Figure 3.9. MRI acquisition illustrating the progression of fluid ingress and hydration of nanoparticulate tablets formulated from a) SL-CT-RFP 1:1 and b) SL-CT-RFP 3:1 (formation of a distinct swelling zone encircled in red) over a time-period of 16 hours. 69

Figure 3.10. Images representing the instant hydration and swelling behaviours of (a) SL-CT-RFP 3:1 and (b) SL-CT-RFP 1:1 nanoparticle tablet after 5 minutes contact with PBS solution (pH6.8). 70

Figure 3.11.Cumulative RFP permeation across pig intestinal tissue from SL-CT-RFP 1:1, SL-CT-RFP 3:1 and Free RFP formulations (37°C). 71

Figure 4.1: Reaction scheme for the mannosylation of CT-SL RFP-ISN-loaded nanoparticles. A = Acetate buffer at pH 4.0, B = Constant stirring for 48 hours, CT-SL-RFP-ISN = unmannosylated Rifampicin/Isoniazid-loaded nanoparticle, Mn-CT-SL-RFP-ISN = mannosylated Rifampicin/Isoniazid-loaded nanoparticle. Mannose isomerizes, in the presence of acetate buffer at pH 4.0, formed an open ring molecule, which then interacted with the positively charged suface of the CT-SL-RFP-ISN nanoparticles to produce the mannose-functionalized nanostructure, Mn-CT-SL-RFP-ISN. 82

Figure 4.2. Graphical illustration of the Size distribution by intensity of CT-SL-RFP-ISN (A) and Mn-CT-SL-RFP-ISN (C) Nanoparticles, using Dynamic Light Scattering, and their Apparent zeta potentials (B and D, respectively). The nanoparticles expressed a positive surface charge, which prevents flocculation/coalescence of the nanoparticles in suspension, and this may contribute to their stability. In both formulations n=3 and SD < 0.3……..…90

Figure 4.3. Gold sputtered scanning electron micrographs of (A) CT-SL-RFP-ISN (scale bar: 70μm; magnification: 1580x) and (B) Mn-CT-SL-RFP-ISN (scale bar: 20μm;

magnification: 4550x) nanoparticles. Particles in both formulations exhibited spherical shape morphology with uneven surfaces. 91

Figure 4.4. Digital images of drug-loaded mannosylated CT-SL nanoformulation (Mn-CT-SL-RFP-ISN). (A) Synthesized Mn-CT-SL-RFP-ISN nanoparticle suspension, (B) Sedimented Mn-CT-SL-RFP-ISN nanoparticles post-centrifugation, (C) Lyophilized Mn-CT-SL-RFP-ISN nanoparticles with a soft spongy appearance……..92

Figure 4.5. Illustration of the degree of mannose functionalization (expressed in µg/mg of nanoparticle) versus stirring time in hour. Experimental data showed an optimal surface sugar coverage of nanoparticles achieved within 48 hours mannose-CT-SL reaction time. Further increase in stirring time produced no significant increase in surface sugar density. (n = 3, bars represent mean ± SD). 93

Figure 4.6. FTIR spectra of pure drugs, pristine polymers, mannosylated and unmannosylated nanoparticles showing the various molecular compositions and transitions upon polymer hybridization, drug incorporation and mannose-functionalization. (A) Mn, CT, SL, ISN, and RFP; (B) Mn-CT-SL-RFP-ISN, CT-SL-RFP-ISN, Mn-CT-SL, and CT-SL. CT-SL = unmannosylated chitosan-lecithin nanoparticles; CT-SL-RFP-ISN = unmannosylated rifampicin-isoniazid-loaded chitosan-lecithin nanoparticles; Mn-CT-SL = mannosylated chitosan-lecithin nanoparticles; Mn-CT-SL-RFP-ISN = mannosylated rifampicin-isoniazid-loaded chitosan-lecithin nanoparticles; CT = Chitosan; SL = L-α-Lecithin soybean; RFP = rifampicin; ISN = isoniazid. 95

Figure 4.7. Illustrating the side-by-side comparison of the vibrational peaks of mannosylated and unmannosylated nanoparticles in order to delineate the molecular transitions of the nanosystems upon RFP-ISN incorporation. (A) CT-SL-RFP-ISN and CT-SL; (B) Mn-CT-SL-RFP-ISN and Mn-CT-SL. CT-SL = unmannosylated chitosan-lecithin nanoparticles; CT-SL-RFP-ISN = unmannosylated rifampicin-isoniazid-loaded chitosan-lecithin nanoparticles; Mn-CT-SL = mannosylated chitosan-lecithin nanoparticles; Mn-CT-SL-RFP-ISN = mannosylated rifampicin-isoniazid-loaded chitosan-lecithin nanoparticles……..96

Figure 4.8. Percentage weight versus temperature thermograms depicting the transitions in thermal degradation properties of (A) CT, SL, CT-SL and CT-SL-RFP-ISN, and (B) CT-SL, Mn-CT-SL, CT-SL-RFP-ISN, and Mn-CT-SL-RFP-ISN. 98

Figure 4.9. Delta transmission (top) and delta backscattering (bottom) for CT-SL-RFP-ISN nanoformulation (A) and Mn-CT-SL-RFP-ISN nanoformulation (B) measured at 25°C for 60-minutes duration. BS = Backscattering. 99

Figure 4.10. In vitro RFP and ISN release profile from CT-SL-RFP-ISN (A) and Mn-CT-SL-RFP-ISN (B) nanoparticles in pH 4.8, 6.8 and 7.4, and at 37°C (n = 3, mean ± SD). 101

Figure 4.11. Effect of RFP-ISN-loaded nanoformulations, corresponding placebos and Free RFP+ISN solution on the viability of murine macrophage RAW 264.7 cells assessed by MTT after 24-hour period. The positive control group consisted of cells without any treatment and the negative control group consisted of cells treated with 4% DMSO. RFP+ISN was a physical mixture of RFP and ISN in equivalent concentrations as contained in the nanoformulations. (n = 3, mean ± SD)……..….102

Figure 4.12. Fluorescent images illustrating the cellular uptake and internalization of FITC-labelled lipopolysaccharide nanoparticles in macrophage RAW 264.7 cells after 24-hour treatment period; (A) the fluorescence image of FITC-labelled Mn-CT-SL (green). (B) the fluorescence image of FITC-labelled CT-SL (green). (C & D) the fluorescence field of RAW 264.7 cells stained with CellTracker Deep Red dye. (E) the superimposed image of (A) and (C). (F) overlaid image of (B) and (D). (E) showed a higher density of Mn-CT-SL-FITC green fluorescence overlaid on RAW 264.7 red fluorescence indicating a greater degree of intracellular nanoparticle trafficking in comparison with CT-SL-FITC nanoparticle (overlaid red fluorescence in F). Scale bar: 20μm; magnification: 40x……..…105

Figure 4.13. In vitro uptake characteristics of lipopolysaccharide nanoformulations by cultured RAW 264.7 cells incubated at 37 ^{0}C over a 24-hour period. (A) represent the percentage extracellular versus intracellular concentration of RFP, and (B) indicate the percentage extracellular versus intracellular concentration of ISN. (n = 3, bars represent mean ± SD). 106

LIST OF TABLES

Table 1.1. Standard treatment regimen for new and previously treated TB for adult and children greater than 8 years (TB-Guidelines, 2017). 3

Table 2.1. Illustration of various lipopolysaccharide approaches successfully designed to improve oral drug delivery. 30

Table 3.1. Particle size, zeta potential, conductivity and PdI of RFP-loaded and RFP-free nanoparticle formulations. 54

Table 3.2. Encapsulation efficiency (%EE) and Loading capacity (%LC) of RFP-loaded and RFP-free nanoparticle formulations. 55

Table 3.3. %MBE comparison of RFP-loaded and RFP-free nanoparticle formulations as a function of time. 56

Table 3.4. Profiling the Hardness, Compressibility and Fracture energy of SL-CT-RFP 1:1 and SL-CT-RFP 3:1 as a function of the SL:CT ratio 63

Table 3.5. Mathematical modeling for RFP release kinetics. 68

Table 3.6. Cumulative amount of RFP permeated (M), Flux Value (J), and permeability (P) of RFP from SL-CT-RFP 1:1, SLCTLWCT-RFP 3:1, and free RFP formulations after 8-h exposure time. 72

Table 4.1. Physicochemical characteristics of the synthesized nanoparticles, indicating the various average hydrodynamic diameters, zeta potentials, conductivities and polydispersity indexes. 89

Table 4.2. Percentage Encapsulation Efficiency and Loading Capacity of RFP-ISN-loaded nanoformulations and corresponding placebos. 93

LIST OF EQUATIONS

EQUATION 3.1 ……....49
EQUATION 3.2 ……..49
EQUATION 3.3 ……..50
EQUATION 3.4 ……..52
EQUATION 3.5 ……..52
EQUATION 3.6 ……..52
EQUATION 3.7 ……..52
EQUATION 3.8 ……...52
EQUATION 3.9 ……...53
EQUATION 3.10 ……53
EQUATION 3.11 ……53
EQUATION 4.1 ……83
EQUATION 4.2 ……83
EQUATION 4.3 ……....86
EQUATION 4.4 ……..86
EQUATION 4.5 ……...86

LIST OF ABBREVIATIONS

ABCB1	ATP-binding cassette, subfamily B member 1
AM	Alveolar Macrophage
ASP	Aspirin
ATDs	Antitubercular drugs
ATP	Adenosine triphosphate
AUC	Area under plasma drug concentration-time curve
BBB	Blood-brain barrier
BS	Backscatter
BSC	Biopharmaceutical system of classification
CMC	Carboxymethyl chitosan
CMC-C-SLN	CMC coated curcumin-loaded solid lipid nanoparticles
CT	Chitosan
CT-SL	Hybrid chitosan soybean lecithin
CT-SL-RFP-ISN	Rifampicin-isoniazid-loaded chitosan soybean lecithin
DDS	Drug delivery system
DDW	Double deionized water
DLS	Dynamic light scattering
MEM	Dulbecco's Modified Eagle's medium
DMSO	Dimethyl sulfoxide
DPPC	1,2-dipalmitoyl-sn-glycero-3-phosphocholine
DSC	Differential Scanning Calorimeter
DT	Decomposition temperature
DTX	Docetaxel
EDTA	Ethylenediaminetetraacetic acid
EE	Encapsulation efficiency
POTAC	Epoxypropyl trimethyl ammonium chloride
ETOH	Ethanol
FA	Ferulic acid
FAE	Follicle-associated epithelium
FBS	Fetal bovine serum
FDA	Food and Drug Administration
FTIR	Fourier Transform Infrared
GI	Gastrointestinal
GMO	Glyceryl monooleate

HACC	Hydroxypropyl trimethyl ammonium chloride chitosan
HACC-g-DTX-SLN	HACC-grafted docetaxel-loaded solid lipid nanoparticles
HIV	Human immunodeficiency virus
ISN	Isoniazid
LBL	Layer by Layer
LBL-HA-CT-g-SLN	Layer by Layer hyaluronic acid-chitosan-coated solid lipid nanoparticle
LBN	Lipid-based nanosystem
LC	Loading capacity
LP	Lipopolysaccharide
CT	Low molecular weight chitosan
MBE	mucin-binding efficiency
MDR-TB	Multidrug resistant tuberculosis
MHLP	mannose-functionalized hybrid lipopolysaccharide-based
Mn-CT-SL	Mannosylated hybrid chitosan soybean lecithin
Mn-CT-SL-RFP-ISN	Mannosylated rifampicin-isoniazid-loaded hybrid chitosan soybean lecithin
MRI	Magnetic Resonance Imaging
MTT	3-(4,5-dimethylthiazol-2-yl)-2,5-diphenyltetrazolium bromide
MWCO	Molecular weight cut-off
NDSs	Nanodelivery systems
NPs	Nanoparticles
PBS	Phosphate buffered saline
PC	Phosphatidylcholine
PdI	Polydispersity index
PEC	Polyelectrolyte complex
P-gp	P-glycoprotein
PLN	Polysaccharide-associated lipid nanoparticles
PTX	Paclitaxel
RFP	Rifampicin
RFP+ISN	Physical mixture of rifampicin and isoniazid solution
RI	Rifampicin, Isoniazid
RIPE	Rifampicin, Isoniazid, Pyrazinamide, Ethambutol
SEM	Scanning Electron Microscopy
SGF	Simulated gastric fluid
SIF	Simulated intestinal fluid
SL	L-α-lecithin Soybean
SLN	Solid lipid nanoparticle

SPC	Soybean phosphatidylcholine
TB	Tuberculosis
TGA	Thermogravimetric analysis
TMC	Trimethyl chitosan
TMDSC	Temperature Modulated Differential Scanning Calorimeter
WHO	World Health organisation
XDR-TB	Extensively drug resistant tuberculosis
XRPD	X-ray powder diffraction
ZP	Zeta potential

CHAPTER 1
INTRODUCTION

1.1. Tuberculosis: Causative organism and pathology

Tuberculosis (TB) is an infectious disease caused by the mycobacterium species in the *Mycobacterium tuberculosis* (Mtb) complex. Whilst Mtb is identified as the causative organism for the majority of cases, other species have been implicated as well, including *Mycobacterium bovis, Mycobacterium microti, Mycobacterium africanum, and Mycobacterium canettii* (Nachiappan *et al.*, 2017). Airborne Mtb are spread by droplets (1–5 μm in diameter) which are usually expelled into the air when a person with active TB coughs, speaks, sings, or sneezes (Nachiappan *et al.*, 2017). It is worthy to note that not all persons exposed to Mtb get infected. The chances of getting infected depends on several factors such as virulent nature of the tuberculosis source, the environment and exposure period, and the strength of the immune system (Nachiappan *et al.*, 2017). Following inhalation of the airborne droplets, the Mtb is deposited in the terminal airspaces of the lungs, where it infects the alveolar macrophages. In ~5% of infected individuals, the immune response is not strong enough to adequately eliminate the initial infection, hence, the disease progresses to active TB within the first one to two years (Leung, 1999). This is known as primary TB. Also, there are other group of individuals (~5%) in which their immune system is strong enough to control the initial infection, however, some viable Mtb remain dormant and reactivate at a later time (Leung, 1999). These kind of cases are referred to as post-primary or reactivation tuberculosis. Majority of Mtb infected individuals (~90%) present as asymptomatic, harbouring the infection at subclinical level, which is referred to as latent tuberculosis infection. These individual are the major reservoir of Mtb, but they are not contagious. In this case, the activities of the host immune system suppress the mycobacteria and prevent it from multiplication and spread (Nachiappan *et al.*, 2017) . The nature of immune response to Mtb infection has become an important determinant of the clinical presentations of TB, especially in immunocompromised patients.

The pathological manifestation of Mtb impacts the normal physiological performance of the lungs in regards to respiration. The lung is the most commonly affected organ in TB infection, with about 79% - 87% lung involvement in an individuals with active cases (Farer, Lowell and Meador, 1979; Lyon and Rossman, 2017). While the main pulmonary focus is generally sub-pleural, the disease could spread into the pleural space resulting to the development of a tuberculous pleurisy with effusion. This usually leads to the classic but nonspecific symptoms of pleurisy. Local spread to the hilar lymph nodes and other areas of the body has also been

reported, with the later giving rise to extra-pulmonary foci which are responsible for the major clinical manifestations of TB. These spreads can be seen on radiographic images as enlarged lymph nodes or calcification of both the lymph nodes and the parenchymal lesion typically referred to as the classic Ghon's complex. Pulmonary involvement in immunocompetent individual is estimated to be comparable to that of immunocompromised individual, e.g. in cases of human immunodeficiency virus (HIV) coinfection (Lyon and Rossman, 2017). However, immunocompromised individuals are prone to more extra-pulmonary disease (Shafer and Edlin, 1996). Typically, the host response to Mtb infection is characterized as granulomatous inflammation, in which the cells of the mononuclear phagocyte system and the chiefly activated macrophages and their cellular derivatives aggregate in a compact collection of cells (Adams, 1976; Warren, 1982; Williams and Williams, 1983). The immune response is meant to eliminate the invaded pathogen, Mtb. However, there is a rising evidence that suggests that Mtb concurrently adapts to the changing microenvironment of the host immune system (Basaraba and Hunter, 2017). This adaptation gives rise to a non-replicating, drug-tolerant bacilli, which persistently manipulate the host's immunity with the development of a progressive pulmonary/ extra-pulmonary inflammation, as well as multiple organ failure, leading to death (Basaraba and Hunter, 2017). In addition, the granulomas can cause the development of abnormal cell death (necrosis) in the centre of tubercles, appearing to the bare eyes as a soft, white, cheese-like mass called caseous necrosis (Grosset, 2003). It has been suggested that the tissue damage associated with mycobacterial adaptation is a result of a progressive responses to accumulated mycobacterial antigens, suggesting that disease progression may not exclusively depends on bacterial numbers even in the late stages of disease (Basaraba and Hunter, 2017). Hence, the understanding that Mtb can produce disease without necessarily increasing bacterial load could be a major advancement in anti-TB therapeutics and disease managing strategies.

1.2. Background of the study

TB has been a major public health challenge despite all efforts made to improve its treatment and management. It has been reported to cause a high death rate, particularly in immunocompromised systems like in HIV-infected patients (Costa *et al.*, 2016). TB disease has widely spread throughout Africa, Asia and South America, presenting enormous stress on public health with significant economic impact. However, its presence in Europe and North America is minimal (WHO, 2018). The causative organism, *Mycobacterium tuberculosis* (Mtb), is a small rod-shaped bacillus affecting majorly the lungs (pulmonary TB), but other parts of the body can also be affected (extrapulmonary TB) (Rappuoli and Aderem, 2011; Sia and Wieland, 2011). Adequate mycobacterial clearance from an infected human requires early initiation of efficient anti-TB agent. The conventional anti-TB regimen involves the use of

rifampicin, isoniazid, pyrazinamide and ethambutol (RIPE) (Costa *et al.*, 2016). In South Africa, the standard treatment regimen for a new and previously treated TB for adults and children greater than 8 years includes an intensive phase and a continuation phase. The intensive phase runs for a period of two months, while the continuation phase runs for four months. During this period, patients take a combination therapy at a varying dose based on their body weights as illustrated in table 1 below (TB-Guidelines, 2017).

Table 1.1. Standard treatment regimen for new and previously treated TB for adult and children greater than 8 years (TB-Guidelines, 2017).

Body weight before treatment	**Intensive Phase (Daily dose for two months)**	**Continuation Phase (Daily dose for four months)**	
	RIPE (150/75/400/275) per tablet	RI (150/75) per tablet	RI (300/150) per tablet
30-37 kg	2 Tablets	2 Tablets	-
38-54 kg	3 Tablets	3 Tablets	-
55-70 kg	4 Tablets	-	2 Tablets
>70 kg	5 Tablets	-	2 Tablets

However, the need for a long treatment schedules (about 6 months) usually comes with serious adverse effects, leading to poor adherence to therapy. In addition, the pill burden further discourages the patient from complying with treatment (Pinheiro and Reis, 2011). This obviously contributes to the emergence of multidrug resistant strains and treatment's inefficacy (Vieira *et al.*, 2018). The rise in the incidence of resistance to drug therapy is an issue of public health concern, as it causes a relapse and disease propagation. Multidrug resistant TB (MDR-TB) and extensively drug resistant TB (XDR-TB) necessitate the use of second-line anti-tubercular drugs (ATDs), which are hard to purchase and are much more toxic and costly than the first-line ATDs (du Toit *et al.*, 2006). Consequently, effective delivery technologies are required in order to remedy these therapeutic drawbacks. Improving drug delivery strategies for the existing drugs may be useful in reducing the length of TB chemotherapy, avoiding resistance and improving patient compliance to treatment (Vieira *et al.*, 2018).

Whilst the development of new ATDs is a reasonable advancement in the fight against TB, improving the efficacy of existing drugs can be seen as a faster approach. In this regard, the need to improve the therapeutic index of existing ATDs, majorly by encapsulating them into

nanodelivery systems (NDSs), should be well thought out (Pradhan, 2011). This basically aims at increasing the amount of drugs that reach the infected sites and minimizing toxic effects (Pradhan, 2011). The exceptional physicochemical properties of these delivery systems, such as small and suitable size, controlled release ability, excellent surface area to mass ratio and high reactivity with structure, have given a lead in optimizing anti-TB therapeutics. The usefulness of these properties is very important, as it eliminates the need for frequent drug administration, provide doses reduction, help the patient to adequately comply to therapy and by extension improves therapeutic outcome (Mustafa *et al.*, 2015). An anti-TB dosage form that can be orally administered once weekly would be ideal for patient compliance (Flynn, 1982). In addition, the advantage of escaping the degradation and absorption problem encountered with conventional oral formulation is maintained (Mohammed *et al.*, 2017).

Most importantly in anti-TB therapeutics is alveolar macrophage (AM) targeting, as these cells represent the key reservoir for Mtb. The discovery of surface receptors like mannosyl, lectin, and galactosyl on the surface of macrophage cells has revolutionized anti-TB therapeutics, where nanostructures carrying anti-TB drugs can be functionalized with specific ligands to target these receptors, thus enhancing particulate internalization (Kaur *et al.*, 2008; Saraogi et al., 2011). The macrophage cells can recognize and phagocytize particulate carriers with the help of these surface receptors and consequently enhancing the intracellular drug delivery and therapeutic efficacy. Several studies have surface functionalized nanoparticles (NPs) with mannose aimed at targeting the AMs. Nimje and co-workers, 2009 coated solid lipid NPs bearing Rifabutin with mannose (Nimje *et al.*, 2009), Kumar and co-workers, 2006 mannosylated 5G EDA–PPI dendrimers to deliver rifampicin (Kumar *et al.*, 2006), Saraogi and co-workers, 2010 mannosylated gelatin NPs bearing isoniazid (Saraogi *et al.*, 2011) and Jain and co-workers, 2008 fabricated similar system to deliver Didanosine for anti-HIV therapeutics (Jain *et al.*, 2008).

This study investigated a mannose-functionalized Lipopolysaccharide (LPPS) nanosystem as an excellent strategy for simultaneous oral delivery of rifampicin (RFP) and isoniazid (ISN). The nano-architect combines the advantages of biodegradable polysaccharide (for example structure integrity and physical stability) and biodegradable lipid (such as high drug loading capacity and sustained release ability). In addition, they offer the advantages of higher degree of biocompatibility, versatility, safety and efficacy (Patidar *et al.*, 2010). The choice of oral route stems from the ease of drug administration and higher compliance tendency usually associated with oral drug delivery. Moreover, this route of drug administration is widely accepted, and it requires neither specialized training nor administration device.

1.3. Rationale for this study

There are several questions arising from the clinical management of TB. Victims of this deadly and 'hard to eradicate' bacteria (Mtb) suffer severely because of the problem of ineffective chemotherapy available to them (Sosnik *et al.,* 2010; Matthys *et al.*, 2009). The current TB therapeutics is challenged with the problem of drug degradation before reaching the target site, low drug concentrations at the infection site, primary drug resistance or the poor cell drug penetration (Cardona *et al*., 2006). The long (about 6-9 months) and compulsory treatment schedule of ATDs usually gives rise to serious toxic effects (especially the second-lines ATDs), and it predisposes to poor patient compliance (Pinheiro and Reis, 2011) . This is one of the reasons why there is a wide spread of resistant strains of Mtb. Furthermore, there are several factors, such as low drug solubility, premature degradation before reaching the target sites, intestinal malabsorption, and drug-drug interaction, which predispose current TB drugs to poor bioavailability (Sosnik *et al.,* 2010). Hence, current medicine fails to effectively focus the treatments and instead overflows the entire body with poisonous chemicals and consequently toxic results (Pradhan, 2011). These challenges necessitate appropriate actions to develop a delivery system that could optimize anti-TB therapeutics.

Considering the therapeutic viewpoint, existing anti-TB chemotherapeutic agents have demonstrated acceptable anti-mycobacterial activity against various susceptible strains of Mtb. However, non-targeted delivery and the associated toxicity alongside poor oral bioavailability contributed to failure in the fight against TB. The design of a delivery system with the capacity to shield the encapsulated drug(s) from gastrointestinal degradation, deliver the payload to a target cell and minimise systemic toxicity could significantly improve the clinical outcome of TB management. Active targeting of AMs (reservoir for Mtb) presents several-folds of advantages. Targeting the AMs could increase the intracellular deposition of ATDs at infection site by favourably altering biodistribution of the drug after oral administration, while minimizing toxicity to healthy tissue. Hence, the anti-mycobacterial efficacy could significantly improve whilst the unwanted side effects associated with conventional therapy substantially reduce. Furthermore, this strategy may help lessen the challenges of drug-drug interactions in cases of concurrent treatment of co-morbidities due to site-specific drug delivery.

The rising cost of conventional anti-TB drugs, particularly the second line regimen, and the increasing incidence of TB in some countries undoubtedly impact on the healthcare system, which is unaffordable for developing countries. Improved drug efficacy will significantly decrease the amount of anti-TB drug needed to eradicate Mtb, hence permitting a reduction in cost. Additionally, an effective targeted carrier system designed to deliver the payload in a

sustained release kinetics allow for reduction in dose frequency and duration of therapy, which will minimize pill burden and improve patient compliance.

Thus, the current study designed, optimized and characterized a mannosylated hybrid lipopolysaccharide based (MHLP) nanosystem capable of encapsulating, targeting and controlling the simultaneous release of rifampicin (RFP) and isoniazid (ISN). Figure 1.1 depicted the synthetic mechanism encompassing the nanoformulation, which incorporated low molecular weight Chitosan (CT) and Soybean Lecithin (SL) into the lipopolysaccharide backbone.

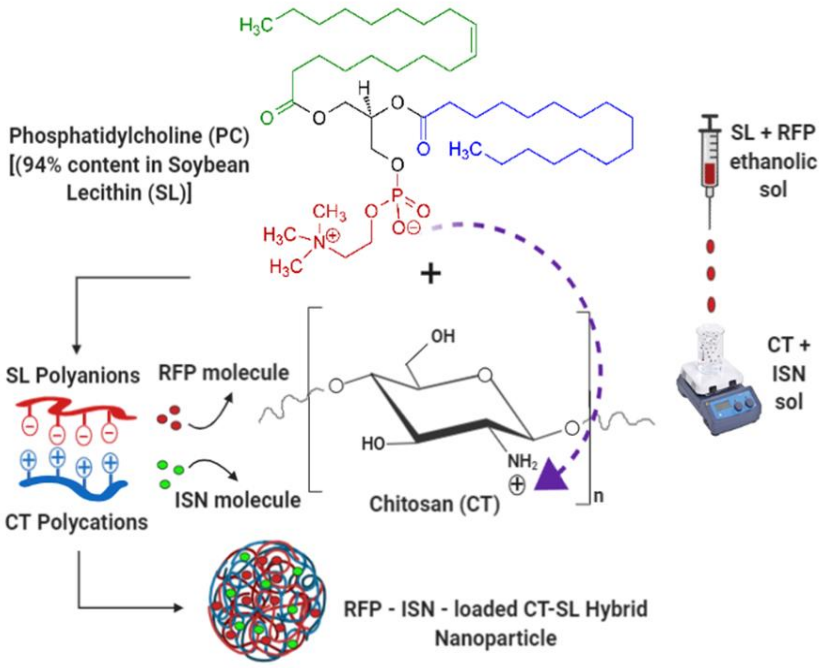


Figure 1.1. Schematic showing the synthetic mechanism involved in the fabrication of hybrid CT-SL RFP-ISN-loaded nanoparticles. The solvent injection technique encourages polyelectrolyte complexation between CT and SL, which drives the formation of the hybrid lipopolysaccharide nanostructure. RFP: rifampicin. ISN: isoniazid.

1.4. Aim and objectives

To overcome the challenges associated with conventional anti-TB therapeutics, this work aims to fabricate a surface functionalized hybrid lipopolysaccharide based NDSs, having application as a controlled release and site-specific delivery system with the goal of improving the therapeutic efficacy of the bioactive. To achieve this design strategy, the following objectives were identified:

a) To synthesize a hybrid lipopolysaccharide (CT-SL) nanoparticles with polyelectrolyte complex architect for improved structural integrity and drug-loading efficiency.
b) To prepare hybrid CT-SL RFP-ISN-loaded nanoparticles for enhanced drug delivery.
c) To conjugate CT-SL RFP-ISN-loaded nanoparticles with mannose to facilitate active targeting.
d) To determine the degree of functionalization of the mannosylated CT-SL NPs.
e) To analyze the chemical and functional transformations of CT, SL, RFP-ISN-free mannosylated CT-SL hybrid and RFP-ISN-loaded mannosylated CT-SL hybrid.
f) To describe the physicochemical and morphological characteristics, such as, particle size, zeta potential, structural morphology, thermal transition, drug loading capacity, polydispersity index, thermal decomposition, encapsulation efficiency and elastic properties of the NPs.
g) To investigate the release of RFP-ISN from the NDSs.
h) To determine the biocompatibility as well as cellular uptake of RFP-ISN-loaded mannosylated CT-SL NPs using RAW 264.7 macrophages.

1.5. Novelty of this study

The two strategies underlisted presented the novelty of this project.

1. The design and characterization of CT-SL nano-constructs with a polyelectrolyte complex structure for the oral delivery of anti-TB therapeutics.
2. The synthesis of a mannose-functionalized CT-SL nanosystem encapsulated with RFP and ISN for smart targeting of the alveolar macrophages, the reservoir for Mtb.

1.6. Overview of the dissertation

The dissertation is sectioned into interwoven chapters that offers a logical and holistic understanding of the design strategies, as well as the characterization technique applied in the formulation of lipopolysaccharide-based nanosystem for anti-TB therapeutics.

Chapter 1 of this dissertation presented a concise introduction into tuberculosis as an infectious disease outlining the global burden and standard treatment guidelines of the disease, with particular focus on Africa as one of the highly affected continents in the world. Furthermore, this chapter highlighted the study rationale by detailing the numerous drawbacks associated with the current conventional anti-TB therapeutics. In addition, the chapter provided a detailed description of the proposed lipopolysaccharide nano-enabled drug delivery system that can potentially be used to overcome the alarming therapeutic challenges of TB treatment. A schematic illustration of the synthetic mechanism employed in the nanoformulation was also provided to better demonstrate the reaction mechanism associated

with the nanosystem fabrication. The novelty of this study as well as the aims and objectives were presented herein.

Chapter 2 discussed the transport mechanisms driving the movement of molecules across the gastrointestinal tract and also the various barriers, such as physiological, biochemical and physicochemical barricades, associated with oral delivery of molecule or bioactives. More also, it provided an insight into the unique properties of lipopolysaccharide NDSs that could enable the system to bypass the harsh gastrointestinal environment during oral administration. This chapter further reviewed numerous current lipopolysaccharide nanotechnological strategies reported to show significant efficacy in the oral delivery of several bioactive towards various disease management.

Chapter 3 delineated the stepwise approach adopted in the nanofabrication of RFP-loaded CT-SL nanoparticles investigating the polyelectrolyte complex (PEC) structure inherent in the nanostructure and its impact on the delivery of RFP. It further explored the influence of CT-SL ratio on the physicochemical properties as well as the drug-loading and entrapment efficiency of various nanoformulations. In addition, the various conventional techniques employed to validate the successful complexation of the polycation (from CT) and polyanion (from SL) were also presented herein. Finally, the mucoadhesive properties, in vitro drug release profile, and gastrointestinal permeability of the nanoformulations were described giving more insight into the optimal formulation parameters with respect to the desired measured responses.

Chapter 4 highlighted the influence of surface-functionalization, via mannosylation, of the synthesized CT-SL nanoparticles on cellular uptake and intracellular drug accumulation. Nanoparticle internalization and intracellular RFP-ISN concentration assays were undertaken quantitatively and qualitatively to validate the efficacy of the synthesized nanosystem as regards targeted delivery of the experimental drugs. This chapter revealed that RAW 264.7 macrophage cells are better targeted by mannose-functionalized nanoparticles when compared with unmannosylated and the free drug solution counterpart. The accumulation of intracellular RFP and ISN was higher in the mannose-functionalized experimental formulation in comparison with the unmannosylated and the free drug solution. Ex vivo cytocompatibility study revealed a ‘cyto-friendly’ nanosystem demonstrating acceptable safety profile ideal for NDSs.

Chapter 5 presented the summary of the overall findings from this research work and appropriate recommendations as regards further exploration into the utilization of the lipopolysaccharide-based nanosystem in anti-TB therapeutics.

1.7. Conclusion

The management of TB has become a nightmare to clinicians due to several drawbacks associated with anti-TB therapeutics, such as poor oral bioavailability, dose-associated side effects, toxicity and the issue of patient compliance. Anti-TB drugs are themselves very active as regards anti-mycobacterial action, however, the clinical benefit of these chemotherapeutic agents is hindered due to poor drug delivery to the diseased site. As a result, these chemicals are taken at high doses to achieve therapeutic plasma concentration, thus flooding the system with toxic chemicals. Nanotechnological approach has proven to be a better alternative drug delivery strategy to remedy the challenges of anti-TB therapeutics. The design of a smart and intelligent mannose-functionalized lipopolysaccharide nanosystem that can enable direct and specific targeting of the alveolar macrophages, where Mtb reside, to deliver the anti-TB drugs will be a gold standard for enhanced treatment TB.

1.8. References

Adams, D. (1976) 'The Granulomatous Inflamatory Response', American Journal of Pathology, 84(1), pp. 164–192. doi: 10.1007/s12138-004-0006-8.

Basaraba, R. J. and Hunter, R. L. (2017) 'Pathology of Tuberculosis: How the Pathology of Human Tuberculosis Informs and Directs Animal Models', Microbiology Spectrum, 5(3), pp. 1–13. doi: 10.1128/microbiolspec.tbtb2-0029-2016.

Cardona, P. J., *et al.* (2006) 'RUTI: a new chance to shorten the treatment of latent tuberculosis infection', Tuberculosis 86. pp. 273 – 289.

Costa, A. *et al.* (2016) 'The formulation of nanomedicines for treating tuberculosis', Advanced Drug Delivery Reviews. Elsevier B.V., 102, pp. 102–115. doi: 10.1016/j.addr.2016.04.012.

du Toit, L. C., Pillay, V. and Danckwerts, M. P. (2006) 'Tuberculosis chemotherapy: Current drug delivery approaches', Respiratory Research, 7(118), pp. xxxx. doi: 10.1186/1465-9921-7-118.

Farer, L., Lowell, A. and Meador, M. (1979) 'Extrapulmonary tuberculosis in the United States', Am J Epidemiol, 109(2), pp. 205–217. doi: 10.1164/ajrccm/141.2.347.

Flynn, G.L., (1982) 'Considerations in controlled release drug delivery system'. Pharm. Tech., (6), pp. 33-39.

Grosset, J. (2003) 'Mycobacterium tuberculosis in the extracellular compartment: An underestimated adversary', Antimicrobial Agents and Chemotherapy, 47(3), pp. 833–836. doi: 10.1128/AAC.47.3.833-836.2003.

Jain, S. K. et al. (2008) 'Mannosylated gelatin nanoparticles bearing an anti-HIV drug

didanosine for site-specific delivery', Nanomedicine: Nanotechnology, Biology, and Medicine, 4(1), pp. 41–48. doi: 10.1016/j.nano.2007.11.004.

Kaur, A., Jain, S. and Tiwary, A. K. (2008) 'Mannan-coated gelatin nanoparticles for sustained and targeted delivery of didanosine: In vitro and in vivo evaluation', Acta Pharmaceutica, 58(1), pp. 61–74. doi: 10.2478/v10007-007-0045-1.

Kumar, P. V. *et al.* (2006) 'Intracellular macrophage uptake of rifampicin loaded mannosylated dendrimers', Journal of Drug Targeting, 14(8), pp. 546–556. doi: 10.1080/10611860600825159.

Leung, A. N. (1999) 'Pulmonary tuberculosis: The essentials', Radiology, 210(2), pp. 307–322. doi: 10.1148/radiology.210.2.r99ja34307.

Lyon, S. and Rossman, M. (2017) 'Pulmonary Tuberculosis', in Tuberculosis and Nontuberculous Mycobacterial Infections, pp. 285–297. doi: 10.1201/b13511-16.

Matthys, F *et al.* (2009) 'Outcome after chemotherapy with WHO category II regimen in a population with high prevalence of drug resistance tuberculosis', Plus ONE 4 (11), pp. e7954. doi: 10. 1371/journal.pone.0007954

Mohammed, M. A. *et al.* (2017) 'An Overview of Chitosan Nanoparticles and Its Application in Non-Parenteral Drug Delivery', 9(4), pp. 53, doi: 10.3390/pharmaceutics9040053.

Mustafa, S. *et al.* (2015) 'Nanocarrier-based interventions for the management of MDR/XDR-TB', Journal of Drug Targeting, 23(4), pp. 287–304. doi: 10.3109/1061186X.2015.1009076.

Nachiappan, A. C. *et al.* (2017) 'Pulmonary tuberculosis: Role of radiology in diagnosis and management', Radiographics, 37(1), pp. 52–72. doi: 10.1148/rg.2017160032.

Nimje, N. *et al.* (2009) 'Mannosylated nanoparticulate carriers of rifabutin for alveolar targeting.', Journal of drug targeting, 17(10), pp. 777–787. doi: 10.3109/10611860903115308.

Patidar, A. *et al.* (2010) 'A review on novel lipid based nanocarriers', Int. J. Pharm. Pharm Sci. 2 (4), pp. 30–35.

Pinheiro, M. and Reis, S. (2011) 'Liposomes as drug delivery systems for the treatment of TB Review', Jornal of Nanomedicine, 6(8), pp. 1413–1428.

Pradhan, S. (2011) 'Targeting of Nanocarriers for Chemotherapy of Tuberculosis', International Journal of Biomedical and Advance…, 2(2011). Available at: http://ssjournals.com/index.php/ijbar/article/view/78.

Rappuoli, R. and Aderem, A. (2011) 'A 2020 vision for vaccines against HIV, tuberculosis and

malaria', Nature. Nature Publishing Group, 473(7348), pp. 463–469. doi: 10.1038/nature10124.

Saraogi, G. K. *et al.* (2011) 'Mannosylated gelatin nanoparticles bearing isoniazid for effective management of tuberculosis', Journal of Drug Targeting, 19(3), pp. 219–227. doi: 10.3109/1061186X.2010.492522.

Shafer, R. W. and Edlin, B. R. (1996) 'Tuberculosis in patients infected with human immunodeficiency virus: Perspective on the past decade', Clinical Infectious Diseases, 22(4), pp. 683–704. doi: 10.1093/clinids/22.4.683.

Sia, I. G. and Wieland, M. L. (2011) 'Current concepts in the management of tuberculosis', Mayo Clinic Proceedings. Mayo Foundation for Medical Education and Research, 86(4), pp. 348–361. doi: 10.4065/mcp.2010.0820.

Sosnik, A. *et al.* (2010) 'New old challenges in tuberculosis: Potentially effective nanotechnologies in drug delivery ☆', Advanced Drug Delivery Reviews. Elsevier B.V., 62(4–5), pp. 547–559. doi: 10.1016/j.addr.2009.11.023.

South African National TB Guidelines (2017) 'Standard treatment of new and previously treated TB for adults and children > 8 years and > 30 kg'.

Vieira, A. C. C. *et al.* (2018) 'Mannosylated solid lipid nanoparticles for the selective delivery of rifampicin to macrophages', Artificial Cells, Nanomedicine, and Biotechnology. Informa UK Limited, trading as Taylor & Francis Group, 1401, pp. 1–11. doi: 10.1080/21691401.2018.1434186.

Warren, K. S. (1982) 'The Secret of the Immunopathogenesis of Schistosomiasis: IN VIVO Models', Immunological Reviews, 61(1), pp. 189–213. doi: 10.1111/j.1600-065X.1982.tb00377.x.

WHO (2017) 'Global tuberculosis report'. WHO Library Cataloguing-in-Publication data.

WHO (2018) 'Global tuberculosis report'. WHO Library Cataloguing-in-Publication data.

Williams, G. T. and Williams, W. J. (1983) 'Granulomatous inflammation - A review', Journal of Clinical Pathology, 36(7), pp. 723–733. doi: 10.1136/jcp.36.7.723.

CHAPTER 2

LIPOPOLYSACCHARIDE NANOTECHNOLOGICAL STRATEGIES FOR EFFICIENT ORAL DRUG DELIVERY

2.1. Introduction

Delivery of active pharmaceutical ingredients through the oral route is a widely accepted and most preferred because of high patient compliance rate, convenience, cost-effectiveness, ease of formulation and administration. In addition, oral formulations are now designed to facilitate the gradual release of its bioactive over a prolonged duration, thereby permitting spaced dosing while still maintaining optimal therapeutic plasma or target tissue concentration. The gastrointestinal (GI) epithelium of humans interestingly provides a wide absorptive surface braced with finger-like protrusions (villi) that further broaden the total surface area available for absorption (Vertzoni *et al.*, 2019). Greater than seventy percent of all medications are orally administered either as solid drug formulations (that is tablet and capsule) or liquid drug formulations (that is suspensions and solutions) (Reinholz, Landfester and Mailänder, 2018). However, orally given medicines, in comparison with those administered parenterally are not readily available in the plasma to produce their desired therapeutic effects. Usually, they 'journey' via the GI tract, through which they get absorbed before reaching the systemic circulation. Due to this, oral drug delivery predisposes to delayed onset of action in comparison with parenteral delivery, and in a worst case scenario, the bioactive may not even get into the blood (Berardi and Bisharat, 2014). Orally ingested medications encounter several challenges before they could make it down to the systemic circulation. The drug must survive the harsh acidic environment in the stomach after ingestion. In addition, protein drugs must escape the effect of the digestive enzymes such as, proteases, pepsin and cathepsin. Furthermore, a drug that makes it through the stomach into the small intestine is faced with additional enzymatic degradation from the action of sucrases, lactases and maltases that digest oligosaccharides and disaccharides to simple sugars (i.e. glucose, galactose, mannose, and fructose). In addition, lipids and peptides are cleaved by pancreatic lipases and proteolytic enzymes (i.e. chymotrypsin, trypsin, aminopeptidase, dipeptidase and carboxypeptidase). Finally, after successfully overcoming these major obstacles, the drug must be absorbed mainly through the small intestinal enterocyte and overcome the intestinal efflux pump to access the systemic circulation. Currently, several biopharmaceuticals have failed to achieve adequate absorption into the bloodstream, with subsequent poor bioavailability as a result of these and other challenges (Mei *et al.*, 2013; Reinholz, Landfester and Mailänder, 2018).

Efforts to prevent drug degradation and improve the rate of intestinal absorption with the aim of enhancing oral bioavailability of drugs have been steered from formulation science ranging from the enteric coating to the more advanced nano-based formulation (Mei *et al.*, 2013; Mohammadzadeh and Javadzadeh, 2018). The enteric coating is made up of polymeric layer that demonstrates some level of stability at low pH values with consequent shielding of the bioactive from dissolving in the stomach, but then disintegrates at the alkaline pH of the small intestine to release its contents into the intestinal fluid. However, such enteric coating alone still doesn't give expected solution to the challenges of poor bioavailability of oral drug delivery especially as it relates to protein and antibody medicine delivery (Zelikin, Ehrhardt and Healy, 2016; Brown, Whitehead and Mitragotri, 2020). A major promising strategy to counter the obvious obstacles and proffer solution to the drawbacks of oral drug delivery involves the use of nanomedicine (Chen *et al.*, 2015; Press, 2016). Nanomedicine, the medical application of nanotechnology (agent in nanometric scale, less than 1000 nm), may be applied in pharmaceuticals to achieve bioactive protection, sustained drug release, specific targeting, enhanced drug dissolution and absorption, and reduced bioactive cytotoxicity (Hanifi, Fathi and Mir Mohammad Sadeghi, 2010; Mohammadzadeh, 2013; Singh *et al.*, 2017; Sithole *et al.*, 2017; Sumaila *et al.*, 2019).

Lipopolysaccharide (LP)-based nanosystems are nanostructures containing both lipid and polysaccharide components. They combine excellent properties of biodegradable lipids (i.e. high drug-loading and sustain-release capacity) and biodegradable polysaccharides (i.e. structure integrity and physical stability) (Nagpal, Singh and Mishra, 2010; Rawal *et al.*, 2018). Moreover, LP-based nanosystems offer the benefits of enhanced biocompatibility, adaptability, safety and efficacy with comparatively cost-effective naturally derived polymers (Patidar *et al.*, 2010; Salomon, Goycoolea and Moerschbacher, 2017).

In recent times, lipid-based nanosystem (LBN) has gained much attention as an effective oral drug delivery system (Hallan *et al.*, 2016; Al-Remawi *et al.*, 2017; Dora *et al.*, 2017b; Nirbhavane *et al.*, 2017; Singh *et al.*, 2017; Patil and Deshpande, 2018), basically because they have demonstrated a higher level of biocompatibility, safety and versatility (Müller, Radtke and Wissing, 2002; Erdine and De Andrés, 2006). Consequently, about thirty-six different lipid-based drug delivery formulations have been enlisted in the U.S. Food and Drug Administration (FDA) approved register for lipid-based drug delivery systems (Wishart, 2006; Savla *et al.*, 2017). The fact that lipid-based formulations can be adapted in several ways to satisfy varieties of product requirement as regards the administration route, disease state, product cost, stability, and efficacy, has lightened the scientists' job and heightened the desire for more exploration into this line of research. Therefore, lipid-based drug carriers have become very important lately due to their intrinsic capacity to improve the solubility and

bioavailability of poorly water-soluble drugs. In this review, the key challenges precluding the success of oral drug delivery are discussed, and the various LP nanotechnological strategies employed to remedy these drawbacks are also detailed.

2.2. Molecular transport mechanisms across the gastrointestinal tract

The GI tract provides various transportation pathways for the delivery of molecules to the systemic circulation with notable ones being paracellular, transcellular, carrier-mediated, and receptor-mediated (Fig. 2.1). The movement of molecules through these pathways depends on the physicochemical properties of these molecules, such as hydrophobicity, molecular weight, pH, and ionization constants along with biological barriers that hinders the absorption of large molecules like proteins from the GI tract. (Yun, Cho and Park, 2013). Therefore, a thorough understanding of biomolecular materials and the underlying mechanisms behind their transport through the GI tract are significant in fabricating oral drug delivery systems.

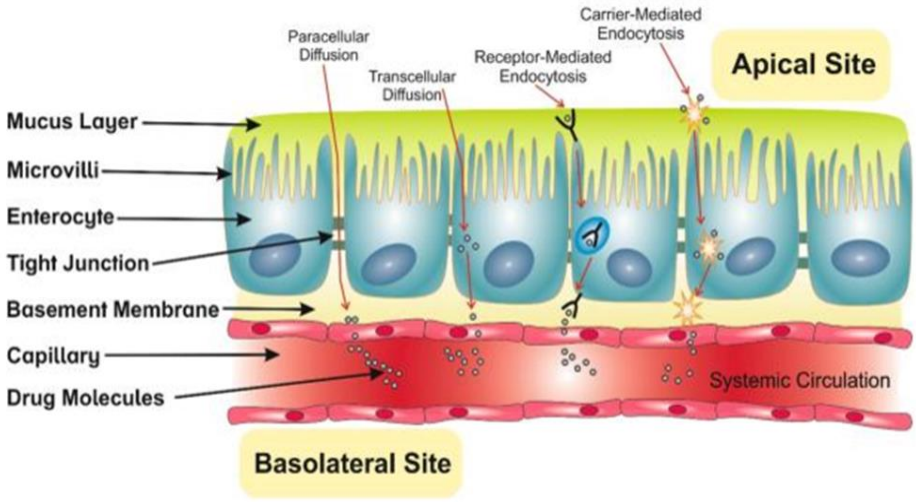


Figure 2.1. Schematic summary (not to scale) of several possible transport mechanisms across the gastrointestinal mucosa barrier; paracellular route provides a channel where the drug passively diffuses between cells at the intercellular tight junctions, transcellular route allows drugs to permeate the cell passively by partitioning to cell membranes at both apical and basolateral sides, receptor-mediated and carrier-mediated transport routes, an energy-dependent active transport where the drug is vectorized via receptor-drug and carrier-drug interaction, respectively. Figure adapted from (Mohammadzadeh and Javadzadeh, 2018).

2.2.1. Paracellular transport

The aqueous extracellular channel that exists between epithelial cells linked together by intercellular junctions is referred to as a *paracellular pathway* (Zheng, Trivedi and Siahaan,

2006; Deli, 2009; Laksitorini *et al.*, 2014). This curvy channel, which is about 80 nm long, runs the entire lateral side of the cells and allows the trafficking of small molecules and ions across the mucosa barrier of the intestine (Adson *et al.*, 1994) . This transport mechanism is passive and involve simple diffusion regulated by the tight junctions. However, these tight junctions create major barricades for the permeation of ions and larger molecules (Madara, 1998). The human intestine has variable average pore sizes created by the epithelial tight junctions and this play a major role as regards selectivity in the type of molecule transported across the epithelial tight junction (Buckley and Turner, 2018). The jejunum, ileum and colon with average paracellular pore sizes of approximately 7–9 Å, 3–4 Å, and 8–9 Å, respectively, suggests that molecules greater than 15 Å (~3.5 kDa) cannot permeable through this route (Tomita *et al.*, 1988; Rubas *et al.*, 1996).

2.2.2. Transcellular transport

Transcellular transport allows molecules transit the GI epithelial cells via a mechanism called transcytosis, a process that involves the cellular uptake of particulate materials. This transport mechanism, initiated by endocytosis at the cell apical membrane, is typically exemplified in glucose movement from the intestinal lumen to the extracellular compartment. Particulate transportation via transcellular route depends on numerous factors: (1) particle physicochemical properties (e.g. size, shape, surface charge, lipophilicity, hydrogen-bonding potential, surface hydrophobicity or ligand) (Kiptoo, Calcagno and Siahaan, 2016); (2) gastrointestinal tract physiology; and (3) the animal model used for uptake study (Burton, Conradi and Hilgers, 1991; Ganesan *et al.*, 2018). Enterocytes and M cells, specialized cells lining the GI tract and dominating the Peyer's patch epithelium, respectively, are primarily involved in particulate transportation. Furthermore, M cells are characterized by a high endocytosis ability and thus represent a potential portal for oral delivery of proteins and peptide drugs. In addition, the high transcytotic capacity of M cells have made them a good target for the transport of nanoparticles (Clark, Hirst and Jepson, 2000). The surface of M cell is adapted to convey antigens from the intestinal cavity to lymphoid tissue, thereby producing a mucosal immune response (Toorisaka *et al.*, 2012). The nanoparticulate uptake and transport efficiency of M cells are significantly greater than that of intestinal cells. However, the absence of a complete glycocalyx structure evident in glycosyl arrangement, together with the sparsely developed apical membrane microvilli encourages the contact and fusion of nanoparticles with cells (Shakweh, Ponchel and Fattal, 2004).

2.2.3. Carrier-mediated transport

Carrier-mediated transport mechanism is an active absorption, energy-dependent, adenosine triphosphate (ATP) process that allows the uptake of specific molecules by carrier proteins. In

this transport mechanism, bioactives are moved across the cell membrane or the whole cell and then deposited into the systemic circulation from the enterocyte's basal surface. The carrier agents identify target molecules via membrane-bound receptors and transport them across the cell membranes into the gastrointestinal epithelium. Transportation of materials in this process is against concentration gradient and usually in trace amounts, as seen in the transcellular movement of some molecules like amino acids, di- and tripeptide, and monosaccharides (Bai and Amidon, 1992; Shah and Shen, 1996).

2.2.4. Receptor-mediated transport

Receptor-mediated transport has long been utilized to improve the oral bioavailability of drugs. These mechanisms offer a pathway for the transfer of bioactive materials into the cell (endocytosis) and across the cell (transcytosis), facilitated by the binding of a ligand to a precise cell surface receptor (Russell-Jones, 1996). Ligand-receptor complexes are internalized into the cell in the vesicular form unlike the carrier-mediated process that depends on energy (ATP or cotransport) to shuttle their substrate across the cell membrane. Collectively, these processes of membrane invagination and subsequent vesicular formation are referred to as 'endocytosis' and include phagocytosis, pinocytosis, receptor-mediated endocytosis (clathrin-mediated), and potocytosis (non-clathrin-mediated) (Swaan, 1998). Drugs or bioactive materials transported to the gastrointestinal tract access the systemic circulation via two distinct absorption pathways: intestinal lymphatics and the portal blood. The amount of administered drug absorbed through these dual pathways is strongly dependent on the physicochemical and metabolic disposition of the drug.

2.3. Barriers associated with oral drug delivery

Orally administered drugs are either intended to exert a local effect in the GI tract or are absorbed into the bloodstream for a systemic effect. A huge surface area for absorption and long resident time, offer better chances for drug absorption, particularly in the small intestine. However, several environmental factors impact drug integrity and absorption along the intestinal segments: (i) length of the segment, (ii) thickness of the mucus layer, (iii) segment pH, (iv) drug resident time, and (v) segmental bacterial diversity and population (Rouge, Buri and Doelker, 1996; Ensign, Cone and Hanes, 2012; Homayun, Lin and Choi, 2019). The biological and physicochemical interactions that exist between oral therapeutic agents and the GI tract physiology regulate the absorption of drugs into the systemic circulation and subsequently determines the bioavailability and therapeutic effect. Thus, developing oral drugs with adequate bioavailability comes with serious challenges broadly classified into physiological, biochemical, and physicochemical barriers. Moreover, large molecule

biopharmaceuticals like proteins, peptides, and oligonucleotides are even more challenging than small molecular drugs (Kiptoo, Calcagno and Siahaan, 2016; Kompella and Lee, 2001).

Several biological hurdles are naturally designed to protect the body and separate every organ system based on their specific functions. The protection could be against invading pathogens such as bacteria, viruses, and toxins. The human skin offers the widest barrier to the human body protecting it from the harmful external environment. On the other hand, the blood–brain barrier (BBB), is a highly specific barrier protecting the brain against undesirable molecular trafficking from the bloodstream to the brain. Likewise, the GI mucosa barrier eliminates harmful germs and toxins from ingested materials and stop them from entering the bloodstream. These are very important natural self-defence body structures; however, it also precludes the delivery of biotherapeutic agents orally or centrally. Hence, sound knowledge of the structural and biological design of the GI mucosa barrier alongside the physicochemical properties of the drug is vital in the design of an oral delivery system with improved drug bioavailability.

2.3.1. Physiological barriers

The GI tract is an extended conduit in which the luminar surface is covered with an aqueous glycoprotein-rich mucus layer secreted by the goblet cells. Orally administered drugs have to infiltrate the mucus layer (thickness, 100 to 150 micrometres) before gaining access into the epithelial cell layer of the GI mucosa barrier (Fricker and Drewe, 1996). The mucus layer precludes particles larger than 600 to 800 Da molecular weights from penetration, and thus acting as a 'biological filter' (Turner, 2009). In addition, a single layer of columnar epithelial cells linked together by tight intercellular junctions underneath the mucus layer further barricade drug molecules from crossing in to the systemic circulation (Kompella and Lee, 2001; Turner, 2009; Laksitorini *et al.*, 2014). Lipophilic drug molecules, seemingly, are more amenable to permeate the intestinal mucosa barrier through the transcellular route due to their cell membrane partitioning ability. However, such molecules must have optimal lipophilicity-solubility balance. On the other hand, hydrophilic drugs cannot partition into the cell membrane but rather they are transported via the aqueous paracellular channel. This is the most likely route for the transport of peptide and protein drugs, but the large size of these molecules precludes their permeation through the tight-junctions inherent in the paracellular route.

Finally, another notable barrier to drug trafficking across intestinal mucosa is the ATP-dependant p-glycoprotein efflux transporter. P-glycoprotein (P-gp), also called ATP-binding cassette, subfamily B member 1 (ABCB1), is an efflux membrane protein that is vastly expressed on the apical surface of the superficial columnar epithelial cells of the intestine. The density of P-gp decreases proximally from the colon to the duodenum with the colon and ileum

expressing a vast amount (Takano, Yumoto and Murakami, 2006). Drug interaction with the efflux transporters often results in poor absorption and low oral bioavailability because the drug is readily expelled back into the intestinal lumen and removed from the body (Sugano *et al.*, 2010). It has been estimated that more than 25 percent of lipophilic drugs are P-gp substrate (Nassar *et al.*, 2009).The efflux pumps remove harmful molecules like toxins from the epithelial cell membrane of the intestinal mucosa (Shepard *et al.*, 2003; V. Varma *et al.*, 2011).

2.3.2. Biochemical barrier

The stomach and intestinal region of the GI tract offer the most active biochemical barricade to the bioavailability of orally administered drugs (Allen and Carroll, 1985; Brown, Whitehead and Mitragotri, 2020). Drug molecules are faced with the first hurdle of having to overcome the unfavourable environment of hydrochloric acid and proteolytic pepsin mixture within the stomach segment. Hydrochloric acid in the stomach makes this region the most acidic environment (pH 1 to 2) in the human body, a condition suitable for pepsin activity. Due to this, pepsin is present at high concentration in the stomach acting as a broad-spectrum endopeptidase with the ability to hydrolyze peptide linkages of aromatic residues such as tyrosine, tryptophan, and phenylalanine (Brown, Whitehead and Mitragotri, 2020). Lipases are also well distributed in the stomach region catalyzing the hydrolysis of fats, oils, and triglycerides. Getting down to the small intestine, ingested drugs are faced with barrier posed by the pancreatic enzymes, chymotrypsin, trypsin, elastase, and carboxypeptidases. These enzymes are capable of degrading 30 to 40 percent of large proteins and small peptides within ten minutes (Fricker and Drewe, 1996). In addition, the small intestinal enterocytes produce numerous carboxypeptidases, aminopeptidases, endopeptidases, and gamma-glutamyl transpeptidases (Whitcomb and Lowe, 2007).

Phase I and II metabolizing enzymes have also been found in the intestine and this could predispose to a premature drug metabolism, particularly for agents designed for systemic action. CYP superfamily are the most notable phase I enzymes exhibiting a minimal concentration of P-450 enzymes in the wall of the intestine. Though the amount of intestinal P-450 enzymes is about twenty times less than that in the liver, the potency is comparable to hepatic P-450 as regards drug metabolizing activity (Agoram, Woltosz and Bolger, 2001; Engman *et al.*, 2001). P-450 enzymatic activity is greatest at the proximal segment of the GI tract, while toward the distal part a decreasing activity is displayed (Agoram, Woltosz and Bolger, 2001). The CYP1, CYP2, and CYP3 subfamilies are associated with the metabolism of xenobiotics, and each of these isoenzymes' subfamilies are substrate specific. CYP1A1, CYP2C, CYP2D6, and CYP3A4 enzymes are located in the small intestine (Doherty and Charman, 2002). CYP3A4 makes up 70-percent of the intestinal CYP enzymes and as such

regarded as the most abundant P-450 enzyme (Benet *et al.*, 1999). There is much structural resemblance between intestinal and liver CYP enzymes; however, they are regulated independently (Doherty and Charman, 2002). Ingested foods have been shown to interact with intestinal CYP enzymes and thus regulate enzymatic activity. some foods are enzyme inducers (e.g. grilled/smoked foods-CYP1A1 enzyme interaction), while others are enzyme inhibitors (e.g. grapefruit- CYP3A enzyme interaction) (Doherty and Charman, 2002). Intestinal phase II enzymes (e.g. glucuronyltransferase, N-acetyltransferase, sulfotransferase, and glutathione-S-transferase) are viewed as metabolizing and conjugating enzymes that demonstrate high activity at the intestinal mucosa barrier (Doherty and Charman, 2002). The activities of all these GI enzymes, alongside intestinal pH gradient, GI motility and varying the gastric emptying rate, strongly impact the pharmacokinetics of orally administered drugs (Brown, Whitehead and Mitragotri, 2020). Therefore, the design of a delivery system with the architectural disposition to bypass these biochemical barriers is important for effective delivery of oral drugs.

2.3.3. Physicochemical barrier

Physicochemical properties such as size, charge, hydrophilicity and hydrogen-bonding potential can impact the partitioning and transportation of drug molecules across cell membranes, particularly biopharmaceuticals (Kiptoo, Calcagno and Siahaan, 2016; Pauletti, Okumu and Borchardt, 1997). Several studies have investigated the relationship between particulate size and membrane permeability applying the Caco-2 cell monolayer model (Liao *et al.*, 2010; de Angelis and Turco, 2011; Sakai-Kato *et al.*, 2014), and supported the fact that drug permeation across the paracellular channel depends on particulate size. The sieving property of the intercellular junction further explains the size-permeability relationship of drug particles crossing the intestinal epithelium. Particulate transport across the already negatively charged paracellular pathway is charge-dependent; however, the exact mechanism is not well known (Kiptoo, Calcagno and Siahaan, 2016). One study reported that a positive surface charge favours particulate uptake and transport across the intestinal epithelium (Du *et al.*, 2018), but another findings suggested that anions confer an increase in particles permeation across the intestinal wall due to their relaxation effect on tight junction (Lamson *et al.*, 2020). Pauletti and co-worker (1997) suggested that the effect of charge on peptide permeation across the cellular membrane is negligible as the molecular size increases (Pauletti, Okumu and Borchardt, 1997). Molecular hydrophobicity can modify the route of peptide permeation. An increase in lipophilicity shifts peptide permeation from paracellular to transcellular route. The ability of drug molecules to form hydrogen bond with water has also been reported to influence drug trafficking across the intestinal barrier; drugs with lesser hydrogen-bonding potential (e.g. two hydrogen bond) to water molecule have greater membrane permeation than

those with greater hydrogen-bonding potential (e.g. eight hydrogen bond) (Kiptoo, Calcagno and Siahaan, 2016).

2.4. Rationale for the use of polymer-lipid hybrid nanosystems

Nanotechnology-based drug delivery systems can be an effective strategy to improve the therapeutic benefits of most bioactives, particularly as it relates to manoeuvring the GI milieu to enhance bioactive absorption. Nanotechnology when applied in the medical context, results in Nanomedicines (agents in nanometric scale, less than 1000 nm), and have been applied in pharmaceuticals to achieve bioactive protection, sustained drug release, specific targeting, enhanced drug dissolution and absorption, and reduced bioactive cytotoxicity (Singh *et al.,* 2017; Sithole *et al.,* 2018; Sumaila *et al.,* 2019). In addition, nanosizing could help to improve drug-membrane interaction, enhance drug permeability as well as bioavailability (Sumaila *et al.,* 2019). In this regards, several polymeric nanocarriers have been designed, which can be sub-divided into i) nanocapsules (one or more drug encapsulated inside polymer shells), ii) nanospheres (polymer matrix system accommodating an even distribution of the one or more bioactive within the matrix), and iii) drug-polymer hybrids (systems that have one or more drug attached to the polymer externally), and others (Ding *et al.,* 2019). Polymeric nanostructure, unlike the lipid system, imparts the benefit of GI tract stability and a better bioactive protection (Viswanathan, Muralidaran and Ragavan, 2017). In addition, polymeric materials are versatile as they can be modified for optimum physico-chemical properties congruent to oral drug delivery, can be fabricated via different methods (e.g. solvent extraction-evaporation, precipitation technique, spray-drying, and others), and polymeric nanodelivery systems could be used as a transporter for a wide variety of bioactives (Plapied *et al.,* 2011).

Moreover, the advancements in polymer chemistry permits excellent control over the nano-architectural design as well as bio-physical properties of the polymeric nanocarrier, facilitating a controlled or triggered drug delivery design (Raemdonck *et al.,* 2014). However, despite these attractive advantages, polymeric nanocarriers are limited by inadequate encapsulation of lipophilic bioactives and issues of burst release (Rao and Prestidge, 2016). Moreover, only a limited number of polymers have gained approval for oral drug delivery application. Thus, the chances of translation into clinical relevance are limited. Similarly, Lipid carriers offer nascent opportunities in oral delivery of challenging therapeutics. Firstly, the existence of diverse lipid-based excipients had given rise to versatile nanoformulation designs viz; solid lipid nanoparticles (SLN), nano-emulsions, nanostructured lipid carrier (NLC), self-emulsifying nanosystems, nanoliposomes, and others. Secondly, in regards to application in the delivery of poorly water-soluble drugs, lipidic nanocarriers could be beneficial in i) improving drug solubility by forming a lipophilic micro-environment; ii) enhancing drug uptake by inhibiting P-glycoprotein (P-gp) efflux and/or preventing pre-systemic drug degradation inside the

enterocyte; and iii) by-passing first pass metabolism by encouraging lymphatic route of drug transport (Singh, Gangadharappa and Mruthunjaya, 2017). Furthermore, lipid-based nanosystems could be applied to shield sensitive bioactives, such as proteins and peptides through encapsulation, from the degradative effect of the gastrointestinal (GI) enzymes (Manosroi and Bauer, 1990). However, lipid nanocarriers when exposed to the harsh acidic/enzymatic environment of the stomach and gastrointestinal (GI) tract (Fricker *et al.,* 2010) are susceptible to lipolysis. This could disrupt the stability of the lipid system and results in undesired burst release of the encapsulated drug(s) and subsequent premature metabolism. In addition, the altered structure and composition of the ruptured lipid nanocarriers could led to a reduction in its solubilization ability. Hence, regardless of the outstanding pre-clinical potential of lipid-based nanosystems, the highlighted drawbacks have limited their extensive clinical relevance.

Recently, a more sophisticated carrier system was proposed, which recognized lipid-polymer hybrid system as a more promising platform for efficient oral drug delivery (Joyce *et al.,* 2020). The introduction of biopolymer hybrids was aimed at combining the much-needed features of lipid-based and polymeric nanosystems in a single carrier. A wide variety of polymeric materials have been incorporated into the hybrid system, ranging from naturally derived (e.g. polysaccharides) to semi-synthetic/synthetic (e.g. Carboxy methyl ethyl cellulose/ poly lactic-co-glycolic acid) biopolymers (Maghrebi, Prestidge and Joyce, 2019). However, given that most synthetic polymer-based nanocarriers are limited by the challenges of safety and biocompatibility, polysaccharides which are naturally derived, have been widely investigated for application in lipopolysaccharide oral drug delivery design. Moreover, the eco-friendly property and the simple fabrication procedure associated with polysaccharides make it a more acceptable excipient for lipid-polymer hybrid system (Sumaila *et al.,* 2019). Lipid-polysaccharide hybrids, herein called lipopolysaccharide hybrid systems, has been widely investigated for biopharmaceutical performance towards oral absorption and bioavailability enhancement of difficult therapeutic agents (Ling et al., 2010; Ramalingam and Ko, 2016; Liu *et al.,* 2018; Mohammadzadeh and Javadzadeh, 2018). The lipopolysaccharide composition as well as the fabrication method typically played a role in the physicochemical properties and the performance of the nanosystem in oral drug delivery. Thus, a good knowledge of the structure-bioactivity relationships associated with lipopolysaccharide nanocarriers in regard to GI transport is vital when designing an effective lipopolysaccharide system.

2.5. Nanotechnological approaches of lipopolysaccharide in oral drug delivery

Nano-formulation technology is exploring the benefit of combining both polysaccharides and phospholipids in the design of drug delivery system (DDS) as shown in table 2.1. Due to their biocompatibility, biodegradability, nontoxicity, and versatility, the most commonly used

members of naturally derived polysaccharide in this hybrid system include chitosan, alginate, pectin, and dextran (Seyednejad *et al.*, 2011; Mandal *et al.*, 2013). Some designs have utilized chemically modified polysaccharide in order to improve the physical and chemical properties of the polymer while retaining their unique properties. Typical examples include N-trimethyl chitosan (TMC), Carboxymethyl chitosan (CMC), and Hydroxypropyl trimethyl ammonium chloride chitosan (HACC), which are used for their improved water solubility (Wang *et al.*, 2020). Lipids used are often phospholipids, which may be anionic, cationic or neutral for example, lecithin, compritol 888, Stearic acid, Soybean phosphatidylcholine (SPC), Lipoid S75, glyceryl monooleate (GMO), 1,2-dipalmitoyl-sn-glycero-3-phosphocholine (DPPC), cetyl palmitate and others (Luo *et al.*, 2015; Shi *et al.*, 2016, 2017; Thakkar *et al.*, 2016; Vieira *et al.*, 2018; Liang *et al.*, 2018; Senna *et al.*, 2018; Basha *et al.*, 2020).These naturally derived polymers have been designed into nanoparticles or nanoliposomes with both polymeric components complementing each other to improve desirable properties. For instance, the polysaccharide component impact GI stability (Luo *et al.*, 2015) and mucoadhesiveness (Vieira *et al.*, 2018) to the architecture while the phospholipid component influence extended bioactive release and high loading capacity (Harde, Das and Jain, 2011). LP-based architecture can positively influence the GI absorption of drugs via various mechanisms such as; drug release modification, lymphatic uptake motivation, drug-induced side effect reduction, bioavailability enhancement among others. This section will focus on solid lipid nanoparticles and liposomal formulations enhanced with polysaccharide backbone to improve oral drug delivery.

2.5.1. Polysaccharide-associated lipid nanoparticles

Polysaccharide-associated lipid nanoparticles (PLN) are nanosized particles comprising of polysaccharide-phospholipid core-shell or hybridized architecture, which integrate complementary characteristics of both polysaccharide nanoparticles and liposomes. This integrated nanostructure can mitigate the drawbacks associated with liposomal and polymeric nanosystems in the delivery of bioactives perorally (Mandal *et al.*, 2013).

Thakkar and co-workers (2015), explored the application of this novel architect in cancer therapeutics. They investigated the potential application of chitosan-coated solid lipid nanosystem (SLN) in the oral delivery of combined ferulic acid (FA) and aspirin (ASP) for pancreatic cancer chemoprevention. In their study, the human pancreatic cancer cells MIA PaCa-2 and Panc-1 models were used to investigate cell viability. They reported that combined FA + ASP loaded chitosan-coated SLN significantly reduced the dose of FA and ASP required for effective tumour suppression by 5- and 40- fold, respectively. Moreover, in comparison to the free FA + ASP, an increased apoptosis of 35 and 31 percent were observed in MIA PaCa-2 and Panc-1 cells, respectively (Thakkar *et al.*, 2015). Their findings were

supported by an *in vivo* study done in the same lab using the MIA PaCa-2 pancreatic tumour xenograft mice model (Thakkar *et al.*, 2015). They reported a 45 percent increase in tumour growth suppression after peroral doses of combined 75mg/kg and 25mg/kg of FA+ ASP loaded chitosan-coated SLN when compared to the vehicle control group (Thakkar *et al.*, 2015). Most recently, Azandaryani and colleagues (2019) also demonstrated the efficiency of chitosan-lipid nanocomplex in the oral delivery of letrozole, a non-steroidal aromatase inhibitor known for its hydrophobicity and low oral bioavailability (Azandaryani *et al.*, 2019). In their study, they reported that letrozole loaded hybrid chitosan-stearic acid nanocomplex, designed using modified ionic crosslinking technique, yielded a 7- to 10-fold GI permeability in comparison to the free drug (Azandaryani *et al.*, 2019). Furthermore, they reported a substantial cytotoxicity (IC_{50} of 67.85 ± 0.55 nM) against breast cancer cell line, MCF-7 (Azandaryani *et al.*, 2019).

In a another study, Dong and associates (Dong *et al.*, 2018) designed a hybrid chitosan-solid lipid nanoparticles (NPs) to improve the GI absorption of enoxaparin, a hydrophilic macromolecule clinically used for its anticoagulant activity. This LP-based system, fabricated from the hybridization of chitosan and glyceryl monooleate, produced a 4.5-fold increase in the area under the plasma drug concentration-time curve (AUC) as compared to plain enoxaparin solution (Dong *et al.*, 2018). The enhanced oral bioavailability of the drug may be attributed to the high mucoadhesivity and improved GI epithelial cell permeation impacted by the chitosan-solid lipid nanostructure. There are other numerous studies (Vieira *et al.*, 2018; Liang *et al.*, 2018; Senna *et al.*, 2018; Khan *et al.*, 2019), which have demonstrated the efficacy of this novel PLN architect in the delivery of bioactive molecules for treatment of various diseases.

2.5.2. Modified chitosan-associated lipid nanoparticles

Chitosan, a deacetylated product of chitin, has been widely investigated for nanotechnological application due to their biological activities and outstanding properties such as; biocompatibility, biodegradability, bioactivity, and non-toxicity (Brasselet *et al.*, 2019). However, the use of this natural polysaccharide in various fields is limited by its low solubility in water and most organic solvents. This drawback can be remedied through chemical modification of chitosan, and at the same time improving on the previously mentioned outstanding properties (Wang *et al.*, 2020). The presence of reactive functional groups, -OH and $-NH_2$, allow for chemical modification of chitosan via N-acylation, N-alkylation, C-6 oxidation, and quaternization reactions to improve the biotechnological application. Chitosan derivatives have been utilized in the design of LP-based nanosystem for application as a drug carrier system (Chen *et al.*, 2016; Shi *et al.*, 2016; Tian *et al.*, 2018). This section will focus on chitosan quaternization as applicable to LP nanostructure in oral drug delivery.

2.5.2.1. Quaternized Chitosan Derivatives

Quaternization is a reaction process that improves the water solubility of chitosan. This reaction involves ionic interaction between alkyl iodide and chitosan under basic condition. Several studies have revealed the possibility to modify the cation (NH_3^+) of chitosan to enhance its solubility in a wide pH range, as well as in neutral or slightly alkaline medium (Ortona *et al.*, 2008; Mohamed *et al.*, 2013; Luan *et al.*, 2018). Quaternized chitosan remain positively charged at pH ≥ 6.5, whereas unmodified chitosan loses its cations as the medium become more acidic. This change in chemical behaviour impacts the use of chitosan in oral drug delivery design.

Quaternized chitosan derivatives associated with lipid nanostructure, administered orally, can improve the plasma concentration and tissue distribution of encapsulated bioactive. This could be possible based on the following factors; (i) high affinity of cationic quaternized chitosan towards the anionic surface of cell membranes, (ii) improved drug transport through the paracellular pathways by the opening of the tight junction between epithelial cells, and (iii) the lipophilicity of quaternized chitosan-associated lipid architecture that allows permeation across cellular membranes.

2.5.2.1.1. TMC – associated lipid nanosystem

N-trimethyl chitosan (TMC) is a partially quaternized chitosan derivative that can be obtain from reductive methylation of chitosan using methyl iodide in the presence of a strong base such as sodium hydroxide (figure 2.2) (Bose and Wong, 2018). The unique properties of this water-soluble chitosan derivative such as; mucoadhesiveness and absorption-enhancing capability, have aroused the interest of many research scientists (Thanou *et al.*, 2001; Hamman, Stander and Kotzé, 2002). TMC has the ability to open epithelial tight junctions through ionic interactions between the positively charged amino groups (NH_3^+) on the carbon-2 position and the negatively charged sites on the cell membrane and/or in the tight junctions (Hamman, Schultz and Kotzé, 2003). Due to the membrane-permeating and tight junction-opening properties, TMC has been applied in numerous nanotechnological designs, particularly in combination with phospholipids (Brasselet *et al.*, 2019). Ramalingam and co-worker (2015, 2016), in separate studies, investigated the efficiency of TMC-grafted palmitic acid nanoparticles in oral delivery of curcumin and resveratrol (Ramalingam and Ko, 2015, 2016). In both studies, they reported that this nanostructure prevented burst release of the bioactives in simulated gastric fluid (SGF, pH 1.2), indicating that the nano- architect is stable in acidic medium. However, the nanosystem encouraged a sustained release of the drugs in simulated intestinal fluid (SIF, 7.4) (Ramalingam and Ko, 2015, 2016). This information detailed the ability of TMC-grafted lipid nanosystem to protect the bioactives against acidic degradation, and consequently improve oral bioavailability of the drug. Furthermore, this group

evaluated the oral bioavailability and brain distribution of curcumin from the novel nanostructure in mice. They show that TMC-associated lipid nanostructure increases the relative oral bioavailability of curcumin and resveratrol 23-folds (Ramalingam and Ko, 2015) and 3.8-folds (Ramalingam and Ko, 2016), respectively, when compared to corresponding curcumin and resveratrol solutions. A significant increase in mice brain distribution of curcumin, impacted by the TMC-grafted lipid structure, was also reported (Ramalingam and Ko, 2015). In a related study, Chen and colleagues (2016) also investigate the performance of this novel TMC-associated lipid structure in oral delivery of harmine, a β-carboline compound with antitumor activity (Chen *et al.*, 2016). They observed an oral delivery efficacy of the fabricated TMC-coated liposome similar to that described by Ramalingam and co-worker (Ramalingam and Ko, 2015, 2016; Chen *et al.*, 2016).

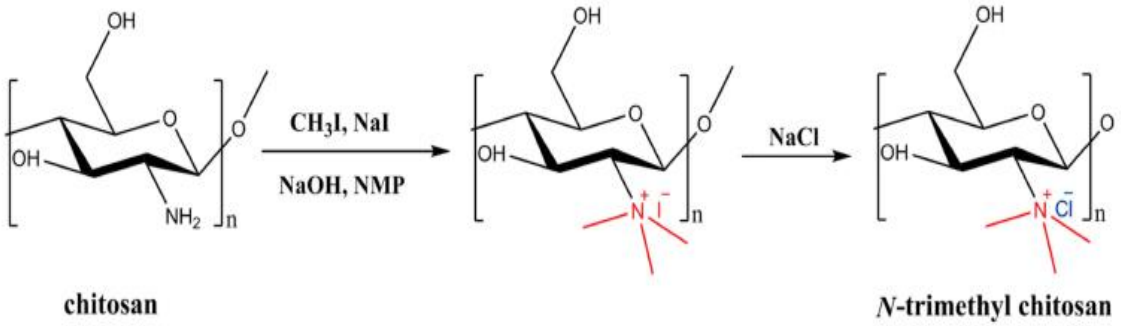


Figure 2.2. Reaction scheme of N-trimethyl chitosan (TMC).

2.5.2.1.2. CMC-associated lipid nanosystem

Carboxymethyl chitosan (CMC) is famous for its excellent water-solubility, ampholytic property, ease of synthesis, and a wide range of applications (Aizat and Aziz, 2018). CMC is derived from the carboxymethylation of chitosan, in which some of the – NH_2 and primary -OH sites of the glucosamine units of chitosan are substituted by carboxyl group (- COOH). This reaction, based on the position of substitution, can yield O-carboxymethyl chitosan (O-CMC), N, N-carboxymethyl chitosan (N, N-CMC), and N, O-carboxymethyl chitosan (N, O-CMC) (figure 2.3). Like the TMC-grafted lipid nanostructure, CMC has been intercalated with liposome/ SLN to impact desirable properties such as GI stability and ease of transport across the mucosa barrier (Baek and Cho, 2017; Tian *et al.*, 2018). Baek and colleague (2017) designed a CMC coated curcumin-loaded SLN (CMC-C-SLN) to demonstrate the bioavailability-enhancing capacity of the modified chitosan-associated SLN (Baek and Cho, 2017). They reported a 6.3- and 9.5-fold increase in lymphatic uptake and oral bioavailability of CMC-C-SLN, respectively, compared to curcumin solution (Baek and Cho, 2017). Their work showed that the improvement in bioavailability with a corresponding increase in

cytotoxicity of CMC-C-SLN may be due to the enhanced cellular and lymphatic uptake impacted by CMC-associated lipid system.

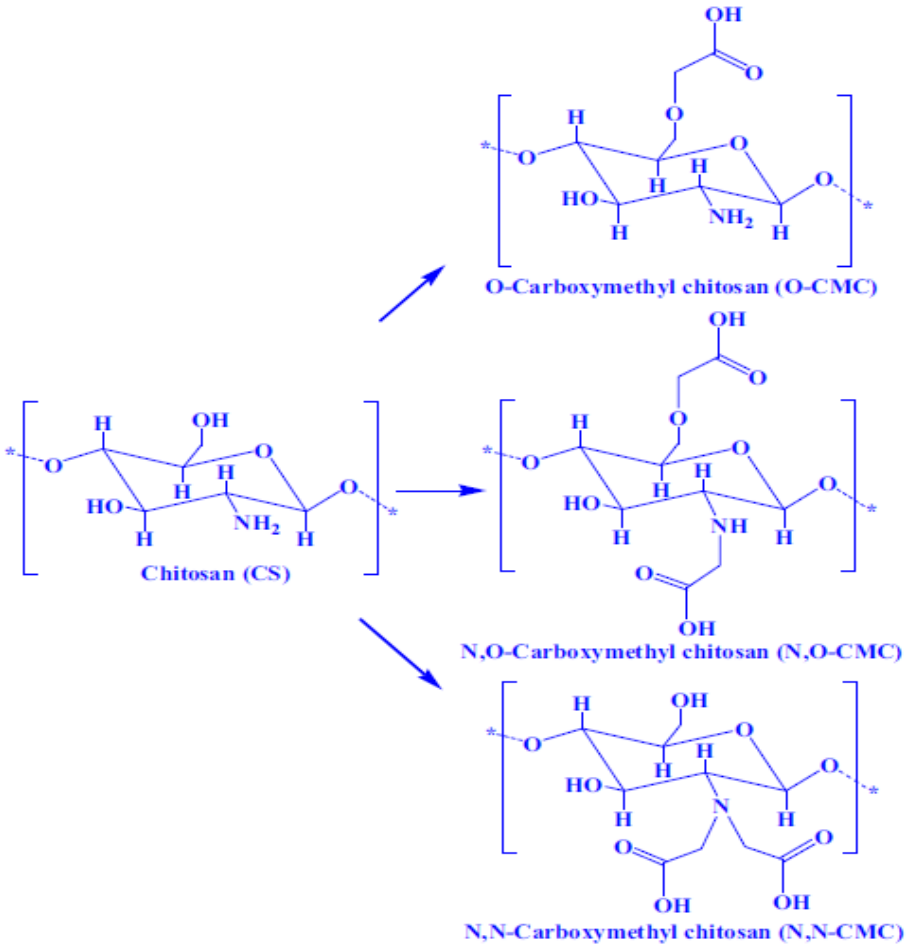


Figure 2.3. The chemical structures of chitosan and the various derivatives of carboxymethyl chitosan (CMC).

2.5.2.1.3. HACC-associated lipid nanosystem

N-(2-hydroxy)-propyl-3-trimethylammonium chitosan chloride (HACC) is a modified chitosan, which is synthesized by the reaction of chitosan with epoxypropyl trimethyl ammonium chloride as shown in (Figure 2.4) (Li *et al.*, 2016; Yang *et al.*, 2019). Like other quaternized chitosan with good solubility profile and GI permeation properties, HACC has been applied in various nanoformulations to improve the oral delivery of poorly water-soluble drugs, particularly in association with phospholipid (Choi *et al.*, 2016; Shi *et al.*, 2016, 2017). Using Caco-2 and follicle-associated epithelium (FAE) cell models, Shi and co-workers (2016) extensively investigated the GI permeation mechanisms of HACC-associated solid lipid nanosystem (Shi *et al.*, 2016). Their work showed that HACC-grafted docetaxel-loaded SLN (HACC-g-DTX-

SLN) demonstrated the highest cellular uptake in Caco-2 cell monolayer when compared to unmodified SLN and DTX solution. Furthermore, they reported that HACC-g-DTX-SLN displayed a higher transport efficacy in follicle-associated epithelium cell monolayer in comparison to that in Caco-2 cell monolayer (Shi *et al.*, 2016). Their findings posit that HACC-modified SLN could reversibly regulate the trans-epithelial electrical resistance and the expressions of tight junction-associated proteins, like occludin, claudin-1, and zonula occludens-1, to favour the vectorization capacity of the nanosystem (Shi *et al.*, 2016). This shows that the mechanism of enhanced absorption impacted by HACC-modified SLN is largely related to caveolae-mediated endocytosis, M cell phagocytosis, and reversible tight junction opening (Figure 2.5) (Shi *et al.*, 2016).

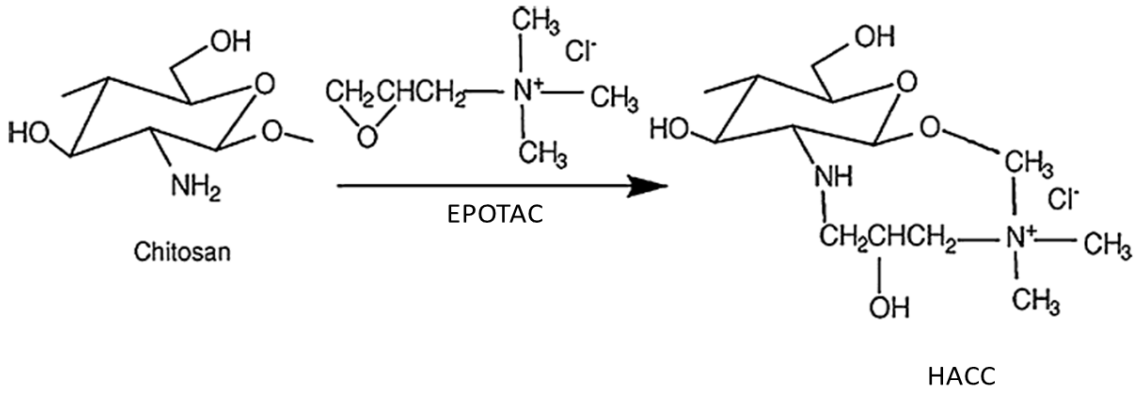


Figure 2.4. Reaction scheme illustrating the synthesis of N-(2-hydroxy)-propyl-3-trimethylammonium chitosan chloride (HACC) in the presence of epoxypropyl trimethyl ammonium chloride (EPOTAC).

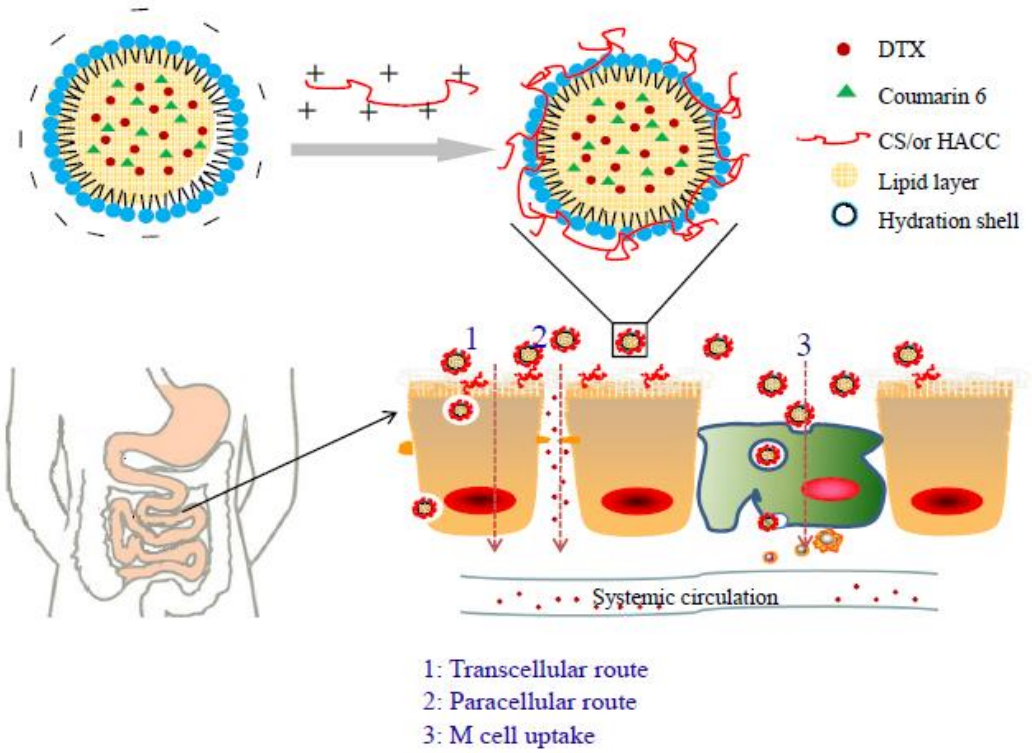


Figure 2.5. Schematic representation of the transport mechanisms of HACC-modified bioactive-loaded SLN across GI epithelial cells; permeation mechanism is largely related to caveolae-mediated endocytosis, M cell phagocytosis, and reversible tight junction opening. Reprinted with permission from (Shi *et al.*, 2016). Copyright (2016) American Chemical Society.

2.5.3. Layer by layer polysaccharide-associated lipid nanoparticles

Layer by layer (LBL) assembly, first introduced by Decher and Hong (Decher and Hong, 1991; G, 1997), has become an effective technique of polymeric coating on two-dimensional and three-dimensional systems, like liposomes, for the delivery of bioactives. The design of this assembly involves alternating depositions of cationic and anionic polyelectrolytes to create a multilayer coating, which is supported primarily, but not entirely, by electrostatic interactions, hydrogen bonds and bio-specific interactions (Lvov Y Ichinose I, Kunitake T, 1995; Cheung, Stockton and Rubner, 1997; Wang *et al.*, 1997). LBL strategy is well acceptable because of the numerous benefits it offers; it allows non-covalent incorporation of many therapeutic agents and biomacromolecules into the LBL structure without compromising their biological properties (Poon *et al.*, 2011). Moreover, since the strategy allows the integration of multiple components, several factors such as the surface chemistry, choice of bioactive moieties to use, and dimensions of the thin films, can be manipulated to produce a sophisticated nanosized drug delivery system with a tailored drug

release kinetics (Poon *et al.*, 2011). Furthermore, LBL nanoparticles can be employed to deliver multiple therapeutic substances with the capacity to control the release of each entrapped substance (Poon *et al.*, 2011). The hybridization of LBL polysaccharide assembly with liposomes which is applicable in the design of high-quality oral delivery system has been well recognized.

Paclitaxel (PTX), a poorly water-soluble chemotherapeutic agent known for its anti-tumour activity was encapsulated in LBL assembled polysaccharide coated SLN to improve its anti-angiogenic effect (Campos, Varas-Godoy and Haidar, 2017). Campos and co-workers (2014), in their work, fabricated a novel shell–core LBL hyaluronan–chitosan coated SLN (LBL–HA–CT–g-SLN) to demonstrate the efficacy of the nanostructure in the delivery of the encapsulated PTX. The design, with hyaluronan (HA) forming the outermost layer of the shell, offers selective targeting of CD44 receptors (HA receptors) in MCF-7 breast cancer cells (Song *et al.*, 2014). They reported that LBL–HA–CT–g–SLN enhanced the intrinsic chemotherapeutic activities of PTX by facilitating the targeting, cellular uptake and time-/dose-controlled delivery and release of PTX (Campos, Varas-Godoy and Haidar, 2017). In a related publication, Tian and colleague (2018) designed a lecithin-based liposome coated with the quaternized chitosan, CMCS and TMC, in an LBL format through electrostatic adsorption, to demonstrate the sustained release and improve oral bioavailability impacted by the LBL-coated nano-assembly (Tian *et al.*, 2018). They reported a 6-fold and 3-fold increase in oral absolute bioavailability of curcumin from the LBL-CMCS-TMC coated liposomes when compared to uncoated liposomes and TMC-coated liposomes, respectively (Tian *et al.*, 2018). Furthermore, they discovered from *in vivo* studies that the LBL assembly could extend the retention time of curcumin in systemic circulation and generate high level of the drug in the liver, spleen and lung (Tian *et al.*, 2018). The ease of LBL-CMCS-TMC coated liposomes to permeate the GI mucosa barrier and then cellular uptake by phagocytes from the reticuloendothelial system could explain the higher blood level of curcumin with a corresponding increase in biodistribution.

Table 2.1. Illustration of various lipopolysaccharide approaches successfully designed to improve oral drug delivery.

Formulation approach	Phospholipid	Polysaccharide	Bioactive	Remarks	References
Chitosan-coated SLN	Stearic acid, lecithin	chitosan	ferulic acid, aspirin	Increased apoptosis in MIA PaCa-2 and Panc-1 cells, and tumour growth suppression in animal model.	(Thakkar *et al.*, 2015)
Chitosan-lipid nanocomplex	Stearic acid, Tripalmitin glyceride	Chitosan	Letrozole	Increased tissue permeability and cytotoxicity against MCF-7	(Azandaryani et al., 2019)
Chitosan-lipid hybrid	Glyceryl monooleate	chitosan	enoxaparin	Produced a 4.5-fold increase in AUC when compared to plain enoxaparin solution.	(Dong *et al.*, 2018)
TMC-grafted SLN	Palmitic acid	TMC	Curcumin, resveratrol	Protected bioactives against acidic degradation, encouraged sustained release in simulated intestinal fluid, and improved oral bioavailability of the drugs. The nanostructure also improved permeation across blood-brain barrier.	(Ramalingam and Ko, 2015, 2016)

TMC-associated lipid structure	Palmitic acid	TMC	Harmine	Possessed stability in gastric acid medium, sustained release capacity, and oral bioavailability enhancing capacity.	(Chen *et al.*, 2016)
CMC- coated SLN	Glyceryl monooleate, soya lecithin	CMC	Curcumin	Increased lymphatic uptake and oral bioavailability of drug by 6.3-fold and 9.5-fold, respectively, compared to curcumin solution.	(Baek and Cho, 2017)
HACC-grafted SLN	Glyceryl monooleate, soya lecithin	HACC	Docetaxel	Enhanced GI permeation and oral bioavailability	(Shi *et al.*, 2016)
Shell–core layer by layer hyaluronan–chitosan coated SLN	Soy-lecithin	Hyaluronan, chitosan	Paclitaxel	Enhanced intrinsic chemotherapeutic activities of paclitaxel via specific tumour targeting, cellular uptake and time-/dose-controlled delivery and release of bioactive.	(Campos, Varas-Godoy and Haidar, 2017)
Layer by layer CMCS-TMC coated liposomes	L-α-Phosphatidylcholine	CMCS, TMC	Curcumin	Increased oral absolute bioavailability by 6-fold and 3-fold in comparison to uncoated liposomes and	(Tian *et al.*, 2018)

	TMC-coated liposomes, respectively. Generated increase biodistribution of drug in tissues.

2.6. Conclusion

Oral route of drug delivery is a generally acceptable form of drug administration due to several benefits that come with it, such as safety, ease of ingestion, pain evasion, patient compliance, among others. However, the harsh environment of the GI tract could degrade pharmacologically active agents and renders them useless. In addition, the P-gp efflux transporters, associated with GI epithelial cell membrane, eliminate ingested drugs from cells, and this consequently reduce *in vivo* drug efficacy. This makes oral drug delivery very challenging and has become the focus in formulation science. In this review, we have reported the various molecular transport mechanisms across the GI tract and presented the barriers that could preclude effective oral delivery of bioactives. Furthermore, we highlighted the influence of lipopolysaccharide nanotechnological architect on vectorization of bioactive through the harsh GI environment and across the GI mucosa barrier. We recognised that lipopolysaccharide nanostructures could increase plasma drug concentration and improve tissue drug distribution for orally administered medications.

2.7. References

Adson, A. *et al.* (1994) 'Quantitative approaches to delineate paracellular diffusion in cultured epithelial cell monolayers', Journal of Pharmaceutical Sciences, 83(11), pp. 1529–1536. doi: 10.1002/jps.2600831103.

Agoram, B., Woltosz, W. S. and Bolger, M. B. (2001) 'Predicting the impact of physiological and biochemical processes on oral drug bioavailability', Advanced Drug Delivery Reviews, 50 (2001), pp. S41 –S67. doi: 10.1016/S0169-409X(01)00179-X.

Aizat, M. A. and Aziz, F. (2018) 'Chitosan Nanocomposite Application in Wastewater Treatments', Nanotechnology in Water and Wastewater Treatment, pp. 243-265. Elsevier Inc. doi: 10.1016/B978-0-12-813902-8.00012-5.

Al-Remawi, M. *et al.* (2017) ‘Chitosan/lecithin liposomal nanovesicles as an oral insulin delivery system’, Pharmaceutical Development and Technology, 22(3), pp. 390–398. doi: 10.1080/10837450.2016.1213745.

Allen, A. and Carroll, N. J. H. (1985) ‘Adherent and soluble mucus in the stomach and duodenum’, Digestive Diseases and Sciences, 30(11), pp. 55S-62S. doi: 10.1007/BF01309386.

de Angelis, I. and Turco, L. (2011) ‘Caco-2 cells as a model for intestinal absorption’, Current Protocols in Toxicology, (SUPPL.47), pp. 1–15. doi: 10.1002/0471140856.tx2006s47.

Azandaryani, A. H. *et al.* (2019) ‘A Comprehensive Physicochemical, In Vitro and Molecular Characterization of Letrozole Incorporated Chitosan-Lipid Nanocomplex’, Pharmaceutical Research. Pharmaceutical Research, 36(4), pp. 1–11. doi: 10.1007/s11095-019-2597-4.

Baek, J. S. and Cho, C. W. (2017) ‘Surface modification of solid lipid nanoparticles for oral delivery of curcumin: Improvement of bioavailability through enhanced cellular uptake, and lymphatic uptake’, European Journal of Pharmaceutics and Biopharmaceutics. Elsevier B.V., 117, pp. 132–140. doi: 10.1016/j.ejpb.2017.04.013.

Bai, J. P. F. and Amidon, G. L. (1992) ‘Structural Specificity of Mucosal-Cell Transport and Metabolism of Peptide Drugs: Implication for Oral Peptide Drug Delivery’, Pharmaceutical Research: An Official Journal of the American Association of Pharmaceutical Scientists, pp. 969–978. doi: 10.1023/A:1015885823793.

Basha, S. K. *et al.* (2020) ‘Materials Today: Proceedings Solid lipid nanoparticles for oral drug delivery’, Materials Today: Proceedings. Elsevier Ltd, (xxxx). doi: 10.1016/j.matpr.2020.04.109.

Benet, L. Z. et al. (1999) ‘Intestinal MDR transport proteins and P-450 enzymes as barriers to oral drug delivery’, Journal of Controlled Release, 62(1–2), pp. 25–31. doi: 10.1016/S0168-

3659(99)00034-6.

Berardi, A. and Bisharat, L. (2014) ‘Nanotechnology systems for oral drug delivery: challenges and opportunities’, in Massadeh, S. (ed.) Nanotechnology in Drug Delivery. UK: One Central Press, pp. 52–84.

Bose, A. and Wong, T. W. (2018) ‘Oral colon cancer targeting by chitosan nanocomposites’ in Inamuddin, Abdullah M. Asiri, Ali Mohammad (eds.) Applications of Nanocomposite Materials in Drug Delivery. Cambridge: Elsevier Inc., pp. 409-429. doi: 10.1016/B978-0-12-813741-3.00018-2.

Brasselet, C. et al. (2019) ‘Modification of chitosan for the generation of functional derivatives’, Applied Sciences, 9(7), pp. 1321. doi: 10.3390/app9071321.

Brown, T. D., Whitehead, K. A. and Mitragotri, S. (2020) ‘Materials for oral delivery of proteins and peptides’, Nature Reviews Materials. Springer US, 5(2), pp. 127–148. doi: 10.1038/s41578-019-0156-6.

Buckley, A. and Turner, J. R. (2018) ‘Cell Biology of Tight Junction Barrier Regulation and Mucosal Disease’ in Niessen, CM. and Yap, AS. (eds.) Cold Spring Harb Perspect Biol. USA: Cold Spring Harbor Laboratory Press, pp. 1–16.

Burton, P. S., Conradi, R. A. and Hilgers, A. R. (1991) ‘(B) Mechanisms of peptide and protein absorption. (2) Transcellular mechanism of peptide and protein absorption: passive aspects’, Advanced Drug Delivery Reviews, 7(3), pp. 365–385. doi: 10.1016/0169-409X(91)90014-4.

Campos, J., Varas-Godoy, M. and Haidar, Z. S. (2017) ‘Physicochemical characterization of chitosan-hyaluronan-coated solid lipid nanoparticles for the targeted delivery of paclitaxel: A proof-of-concept study in breast cancer cells’, Nanomedicine, 12(5), pp. 473–490. doi: 10.2217/nnm-2016-0371.

Chen, W. L. *et al.* (2016) ‘Liposomes coated with N-trimethyl chitosan to improve the absorption of harmine in vivo and in vitro’, International Journal of Nanomedicine, 11, pp. 325–336. doi: 10.2147/IJN.S95540.

Chen, Y. D. et al. (2015) ‘Development of oral dispersible tablets containing prednisolone nanoparticles for the management of pediatric asthma’, Drug Design, Development and Therapy, 9, pp. 5815–5825. doi: 10.2147/DDDT.S86075.

Cheung, J. H., Stockton, W. B. and Rubner, M. F. (1997) ‘Molecular-level processing of conjugated polymers. 3. Layer-by-layer manipulation of polyaniline via electrostatic interactions’, Macromolecules, 30(9), pp. 2712–2716. doi: 10.1021/ma970047d.

Choi, K. O. *et al.* (2016) ‘Positively charged nanostructured lipid carriers and their effect on the dissolution of poorly soluble drugs’, Molecules, 21(5), pp. 672. doi: 10.3390/molecules21050672.

Clark, M. A., Hirst, B. H. and Jepson, M. A. (2000) ‘Lectin-mediated mucosal delivery of drugs and microparticles’, Advanced Drug Delivery Reviews, 43(2–3), pp. 207–223. doi: 10.1016/S0169-409X(00)00070-3.

Decher, G. and Hong, J. D. (1991) ‘Buildup of Ultrathin Multilayer Films by a Self-Assembly Process: II. Consecutive Adsorption of Anionic and Cationic Bipolar Amphiphiles and

Polyelectrolytes on Charged Surfaces', Berichte der Bunsengesellschaft für physikalische Chemie, 95(11), pp. 1430–1434. doi: 10.1002/bbpc.19910951122.

Decher, G. (1997) 'Fuzzy Nanoassemblies: Toward Layered Polymeric Multicomposites', Science, 277(5330), pp. 1232–1237.

Deli, M. A. (2009) 'Potential use of tight junction modulators to reversibly open membranous barriers and improve drug delivery', Biochimica et Biophysica Acta - Biomembranes. Elsevier B.V., 1788(4), pp. 892–910. doi: 10.1016/j.bbamem.2008.09.016.

Ding, X. *et al.* (2019) 'Biodegradable Antibacterial Polymeric Nanosystems: A New Hope to Cope with Multidrug-Resistant Bacteria', Small, 15(20), pp. 1–29. doi: 10.1002/smll.201900999.

Dong, W. *et al.* (2018) 'Chitosan based polymer-lipid hybrid nanoparticles for oral delivery of enoxaparin', International Journal of Pharmaceutics, 547(1–2), pp. 499–505. doi: 10.1016/j.ijpharm.2018.05.076.

Dora, C. P. *et al.* (2017) 'Improved oral bioavailability and therapeutic efficacy of erlotinib through molecular complexation with phospholipid', International Journal of Pharmaceutics. Elsevier B.V., 534(1–2), pp. 1–13. doi: 10.1016/j.ijpharm.2017.09.071.

Du, X. J. *et al.* (2018) 'The effect of surface charge on oral absorption of polymeric nanoparticles', Biomaterials Science, 6(3), pp. 642–650. doi: 10.1039/c7bm01096f.

Engman, H. A. *et al.* (2001) 'CYP3A4, CYP3A5, and MDR1 in human small and large intestinal cell lines suitable for drug transport studies', Journal of Pharmaceutical Sciences, 90(11), pp. 1736–1751. doi: 10.1002/jps.1123.

Ensign, L. M., Cone, R. and Hanes, J. (2012) 'Oral drug delivery with polymeric nanoparticles: The gastrointestinal mucus barriers', Advanced Drug Delivery Reviews. Elsevier B.V., 64(6), pp. 557–570. doi: 10.1016/j.addr.2011.12.009.

Erdine, S. and De Andrés, J. (2006) 'Drug delivery systems', Pain Practice, 6(1), pp. 51–57. doi: 10.1111/j.1533-2500.2006.00059.x.

Fricker, G. and Drewe, J. (1996) 'Current concepts in intestinal peptide absorption.', Journal of peptide science : an official publication of the European Peptide Society, 2(4), pp. 195–211. doi: 10.1002/psc.66.

Fricker, G. *et al.* (2010) 'Phospholipids and lipid-based formulations in oral drug delivery', Pharmaceutical Research, 27(8), pp. 1469–1486. doi: 10.1007/s11095-010-0130-x.

Ganesan, P. *et al.* (2018) 'Recent developments in solid lipid nanoparticle and surface-modified solid lipid nanoparticle delivery systems for oral delivery of phyto-bioactive compounds in various chronic diseases', International Journal of Nanomedicine, 13, pp. 1569–1583. doi: 10.2147/IJN.S155593.

Hallan, S. S. *et al.* (2016) 'Lipid polymer hybrid as emerging tool in nanocarriers for oral drug delivery', Artificial Cells, Nanomedicine and Biotechnology, 44(1), pp. 334–349. doi: 10.3109/21691401.2014.951721.

Hamman, J. H., Schultz, C. M. and Kotzé, A. F. (2003) 'N-trimethyl chitosan chloride: Optimum degree of quaternization for drug absorption enhancement across epithelial cells', Drug Development and Industrial Pharmacy, 29(2), pp. 161–172. doi: 10.1081/DDC-120016724.

Hamman, J. H., Stander, M. and Kotzé, A. F. (2002) 'Effect of the degree of quaternisation of N-trimethyl chitosan chloride on absorption enhancement: In vivo evaluation in rat nasal epithelia', International Journal of Pharmaceutics, 232(1–2), pp. 235–242. doi: 10.1016/S0378-5173(01)00914-0.

Hanifi, A., Fathi, M. H. and Mir Mohammad Sadeghi, H. (2010) 'Effect of strontium ions substitution on gene delivery related properties of calcium phosphate nanoparticles', Journal of Materials Science: Materials in Medicine, 21(9), pp. 2601–2609. doi: 10.1007/s10856-010-4123-4.

Harde, H., Das, M. and Jain, S. (2011) 'Solid lipid nanoparticles: An oral bioavailability enhancer vehicle', Expert Opinion on Drug Delivery, 8(11), pp. 1407–1424. doi: 10.1517/17425247.2011.604311.

Holmes, R., Hourihane, D. O. B. and Booth, C. C. (1961) 'The mucosa of the small intestine', Postgraduate Medical Journal, 37(434), pp. 717–724. doi: 10.1136/pgmj.37.434.717.

Homayun, B., Lin, X. and Choi, H. J. (2019) 'Challenges and recent progress in oral drug delivery systems for biopharmaceuticals', Pharmaceutics, 11(3). doi: 10.3390/pharmaceutics11030129.

Joyce, P. *et al.* (2020) 'Polymer lipid hybrid (PLH) formulations: A synergistic approach to oral delivery of challenging therapeutics', Delivery of Drugs: Volume 2: Expectations and Realities of Multifunctional Drug Delivery Systems. Elsevier Inc. pp. 1-27. doi: 10.1016/B978-0-12-817776-1.00001-8.

Khan, M. M. *et al.* (2019) 'Lipid-chitosan hybrid nanoparticles for controlled delivery of cisplatin', Drug Delivery. Taylor & Francis, 26(1), pp. 765–772. doi: 10.1080/10717544.2019.1642420.

Kiptoo, P., Calcagno, A. M. and Siahaan, T. J. (2016) 'Physiological, Biochemical, and Chemical Barriers to Oral Dru g Delivery' in Wabg, B, Longqin Hu, and Siahaan, TJ. (eds.) Drug Delivery: Principles and Applications. USA: John Wiley & Sons, Inc, pp. 20-33.

Kompella, U. B. and Lee, V. H. L. (2001) 'Delivery systems for penetration enhancement of peptide and protein drugs: Design considerations', Advanced Drug Delivery Reviews, 46(1–3), pp. 211–245. doi: 10.1016/S0169-409X(00)00137-X.

Lamson, N. G. *et al.* (2020) 'Anionic nanoparticles enable the oral delivery of proteins by enhancing intestinal permeability', Nature Biomedical Engineering. Springer US, 4(1), pp. 84–96. doi: 10.1038/s41551-019-0465-5.

Li, W. *et al.* (2016) 'Synthesis, antioxidant and cathepsin D inhibition activity of quaternary ammonium chitosan derivatives', Carbohydrate Polymers. Elsevier Ltd., 136, pp. 884–891. doi: 10.1016/j.carbpol.2015.09.111.

Liang, J. *et al.* (2018) 'Chitosan-functionalized lipid-polymer hybrid nanoparticles for oral delivery of silymarin and enhanced lipid-lowering effect in NAFLD', Journal of Nanobiotechnology. BioMed Central, 16(1), pp. 1–12. doi: 10.1186/s12951-018-0391-9.

Liao, C. D. *et al.* (2010) 'Nano/sub-microsized lignan glycosides from sesame meal exhibit higher transport and absorption efficiency in Caco-2 cell monolayer', Food Chemistry. Elsevier Ltd, 119(3), pp. 896–902. doi: 10.1016/j.foodchem.2009.07.056.

Ling, G. *et al.* (2010) 'Development of novel self-assembled DS-PLGA hybrid nanoparticles for improving oral bioavailability of vincristine sulfate by P-gp inhibition', Journal of Controlled Release, 148(2), pp. 241–248. doi: 10.1016/j.jconrel.2010.08.010.

Liu, W. *et al.* (2018) 'Encapsulation of β-carotene-loaded oil droplets in caseinate/alginate microparticles: Enhancement of carotenoid stability and bioaccessibility', Journal of Functional Foods, 40, pp. 527–535. doi: 10.1016/j.jff.2017.11.046.

Luan, F. *et al.* (2018) 'Preparation and characterization of quaternized chitosan derivatives and assessment of their antioxidant activity', Molecules, 23(3). doi: 10.3390/molecules23030516.

Luo, Y. *et al.* (2015) 'Solid lipid nanoparticles for oral drug delivery: Chitosan coating improves stability, controlled delivery, mucoadhesion and cellular uptake', Carbohydrate Polymers. Elsevier Ltd., 122, pp. 221–229. doi: 10.1016/j.carbpol.2014.12.084.

Lvov Y Ichinose I, Kunitake T, A. K. (1995) 'Layer-by-layer Architectures of Concanavalin', J. Chem. Soc., Chem. Commun., pp. 2313–2314.

Madara, J. L. (1998) ‘Regulation of the Movement of Solutes Across Tight Junctions’, Annual Review of Physiology, 60(1), pp. 143–159. doi: 10.1146/annurev.physiol.60.1.143.

Maghrebi, S., Prestidge, C. A. and Joyce, P. (2019) ‘An update on polymer-lipid hybrid systems for improving oral drug delivery’, Expert Opinion on Drug Delivery, 16(5), pp. 507–524. doi: 10.1080/17425247.2019.1605353.

Mandal, B. *et al.* (2013) ‘Core-shell-type lipid-polymer hybrid nanoparticles as a drug delivery platform’, Nanomedicine: Nanotechnology, Biology, and Medicine. Elsevier Inc., 9(4), pp. 474–491. doi: 10.1016/j.nano.2012.11.010.

Manosroi, A. and Bauer, K. H. (1990) ‘Effects of gastrointestinal administration of human insulin and a human insulin-deae-dextran complex entrapped in different compound liposomes on blood glucose in rats’, Drug Development and Industrial Pharmacy, 16(9), pp. 1521–1538. doi: 10.3109/03639049009074381.

Mei, L. *et al.* (2013) ‘Pharmaceutical nanotechnology for oral delivery of anticancer drugs’, Advanced Drug Delivery Reviews. Elsevier B.V., 65(6), pp. 880–890. doi: 10.1016/j.addr.2012.11.005.

Mohammadzadeh, R. and Javadzadeh, Y. (2018) ‘An overview on oral drug delivery via nano-based formulations’, Pharmaceutical and Biomedical Research, 4(1), pp. 1–7. doi: 10.18502/pbr.v4i1.139.

Mohamed, N. A. *et al.* (2013) ‘Quaternized N-substituted carboxymethyl chitosan derivatives as antimicrobial agents’, International Journal of Biological Macromolecules. Elsevier B.V., 60, pp. 156–164. doi: 10.1016/j.ijbiomac.2013.05.022.

Mohammadzadeh, R. (2013) ‘Nanosilver as a novel agent in keloid therapy’, Journal of the European Academy of Dermatology and Venereology, 27(2), pp. 1–2. doi: 10.1111/j.1468-3083.2012.04594.x.

Mohammadzadeh, R. and Javadzadeh, Y. (2018) ‘An overview on oral drug delivery via nano-based formulations’, Pharmaceutical and Biomedical Research, 4(1), pp. 1–7. doi: 10.18502/pbr.v4i1.139.

Müller, R. H., Radtke, M. and Wissing, S. A. (2002) ‘Solid lipid nanoparticles (SLN) and nanostructured lipid carriers (NLC) in cosmetic and dermatological preparations’, Advanced Drug Delivery Reviews, 54(SUPPL.), pp. 131–155. doi: 10.1016/S0169-409X(02)00118-7.

Nagpal, K., Singh, S. K. and Mishra, D. N. (2010) 'Chitosan Nanoparticles: A Promising System in Novel Drug Delivery', Chemical & Pharmaceutical Bulletin, 58(11), pp. 1423–1430. doi: 10.1248/cpb.58.1423.

Nassar, T. *et al.* (2009) 'Novel double coated nanocapsules for intestinal delivery and enhanced oral bioavailability of tacrolimus, a P-gp substrate drug', Journal of Controlled Release. Elsevier B.V., 133(1), pp. 77–84. doi: 10.1016/j.jconrel.2008.08.021.

Nirbhavane, P. *et al.* (2017) 'Lipid Nanocarrier-Mediated Drug Delivery System to Enhance the Oral Bioavailability of Rifabutin'. AAPS PharmSciTech, 18(3), pp. 0–8. doi: 10.1208/s12249-016-0559-2.

Ortona, O. *et al.* (2008) 'The aggregative behavior of hydrophobically modified chitosans with high substitution degree in aqueous solution', Carbohydrate Polymers, 74(1), pp. 16–22. doi: 10.1016/j.carbpol.2008.01.009.

Patidar, A. *et al.* (2010) 'A review on novel lipid based nanocarriers', International Journal of Pharmacy and Pharmaceutical Sciences, 2(4), pp. 30–35.

Patil, T. S. and Deshpande, A. S. (2018) 'Nanostructured lipid carriers-based drug delivery for treating various lung diseases: A State - of - the - Art Review', International Journal of Pharmaceutics. Elsevier, 547(1–2), pp. 209–225. doi: 10.1016/j.ijpharm.2018.05.070.

Pauletti, G. M., Okumu, F. W. and Borchardt, R. T. (1997) 'Effect of size and charge on the, passive diffusion of peptides across caco-2 cell monolayers via the paracellular pathway', Pharmaceutical Research, 14(2), pp. 164–168. doi: 10.1023/A:1012040425146.

Plapied, L. *et al.* (2011) 'Fate of polymeric nanocarriers for oral drug delivery', Current Opinion in Colloid and Interface Science, 16(3), pp. 228–237. doi: 10.1016/j.cocis.2010.12.005.

Poon, Z. *et al.* (2011) 'Controlling in vivo stability and biodistribution in electrostatically assembled nanoparticles for systemic delivery', Nano Letters, 11(5), pp. 2096–2103. doi: 10.1021/nl200636r.

Raemdonck, K. *et al.* (2014) 'Merging the best of both worlds: Hybrid lipid-enveloped matrix nanocomposites in drug delivery', Chemical Society Reviews, 43(1), pp. 444–472. doi: 10.1039/c3cs60299k.

Ramalingam, P. and Ko, Y. T. (2015) 'Enhanced oral delivery of curcumin from N-trimethyl chitosan surface-modified solid lipid nanoparticles: Pharmacokinetic and brain distribution

evaluations', Pharmaceutical Research, 32(2), pp. 389–402. doi: 10.1007/s11095-014-1469-1.

Ramalingam, P. and Ko, Y. T. (2016) 'Improved oral delivery of resveratrol from N-trimethyl chitosan-g-palmitic acid surface-modified solid lipid nanoparticles', Colloids and Surfaces B: Biointerfaces. Elsevier B.V., 139, pp. 52–61. doi: 10.1016/j.colsurfb.2015.11.050.

Rao, S. and Prestidge, C. A. (2016) 'Polymer-lipid hybrid systems: Merging the benefits of polymeric and lipid-based nanocarriers to improve oral drug delivery', Expert Opinion on Drug Delivery, 13(5), pp. 691–707. doi: 10.1517/17425247.2016.1151872.

Rawal, T. *et al.* (2018) 'Chitosan Nanoparticles of Gamma-Oryzanol: Formulation, Optimization, and *In vivo* Evaluation of Anti-hyperlipidemic Activity', AAPS PharmSciTech. AAPS PharmSciTech, 19(4), pp. 1894–1907. doi: 10.1208/s12249-018-1001-8.

Reinholz, J., Landfester, K. and Mailänder, V. (2018) 'The challenges of oral drug delivery via nanocarriers', Drug Delivery, 25(1), pp. 1694–1705. doi: 10.1080/10717544.2018.1501119.

Rouge, N., Buri, P. and Doelker, E. (1996) 'Drug absorption sites in the gastrointestinal tract and dosage forms for site-specific delivery', International Journal of Pharmaceutics, 136(1–2), pp. 117–139. doi: 10.1016/0378-5173(96)85200-8.

Rubas, W. *et al.* (1996) 'Flux measurements across Caco-2 monolayers may predict transport in human large intestinal tissue', Journal of Pharmaceutical Sciences, 85(2), pp. 165–169. doi: 10.1021/js950267+.

Russell-Jones, G. J. (1996) 'The potential use of receptor-mediated endocytosis for oral drug delivery', Advanced Drug Delivery Reviews, 20(1), pp. 83–97. doi: 10.1016/0169-409X(95)00131-P.

Sakai-Kato, K. *et al.* (2014) 'Physicochemical properties and in vitro intestinal permeability properties and intestinal cell toxicity of silica particles, performed in simulated gastrointestinal fluids', Biochimica et Biophysica Acta - General Subjects. Elsevier B.V., 1840(3), pp. 1171–1180. doi: 10.1016/j.bbagen.2013.12.014.

Salomon, C., Goycoolea, F. M. and Moerschbacher, B. (2017) 'Recent Trends in the Development of Chitosan-Based Drug Delivery Systems', AAPS PharmSciTech. AAPS PharmSciTech, 18(4), pp. 933–935. doi: 10.1208/s12249-017-0764-7.

Savla, R. *et al.* (2017) 'Review and analysis of FDA approved drugs using lipid-based formulations', Drug Development and Industrial Pharmacy, 43(11), pp. 1743–1758. doi: 10.1080/03639045.2017.1342654.

Senna, J. P. *et al.* (2018) 'Dual alginate-lipid nanocarriers as oral delivery systems for amphotericin B', Colloids and Surfaces B: Biointerfaces. Elsevier B.V., 166, pp. 187–194. doi: 10.1016/j.colsurfb.2018.03.015.

Seyednejad, H. *et al.* (2011) 'Functional aliphatic polyesters for biomedical and pharmaceutical applications', Journal of Controlled Release. Elsevier B.V., 152(1), pp. 168–

176. doi: 10.1016/j.jconrel.2010.12.016.

Shah, D. and Shen, W. C. (1996) 'Transcellular delivery of an insulin-transferrin conjugate in enterocyte-like Caco-2 cells', Journal of Pharmaceutical Sciences, 85(12), pp. 1306–1311. doi: 10.1021/js9601400.

Shakweh, M., Ponchel, G. and Fattal, E. (2004) 'Particle uptake by Peyer's patches: A pathway for drug and vaccine delivery', Expert Opinion on Drug Delivery, 1(1), pp. 141–163. doi: 10.1517/17425247.1.1.141.

Shepard, R. L. *et al.* (2003) 'Modulation of P-glycoprotein but not MRP1- or BCRP-mediated drug resistance by LY335979', International Journal of Cancer, 103(1), pp. 121–125. doi: 10.1002/ijc.10792.

Shi, L. L. *et al.* (2016) 'Positively Charged Surface-Modified Solid Lipid Nanoparticles Promote the Intestinal Transport of Docetaxel through Multifunctional Mechanisms in Rats', Molecular Pharmaceutics, 13(8), pp. 2667–2676. doi: 10.1021/acs.molpharmaceut.6b00226.

Shi, L. L. *et al.* (2017) 'Gastrointestinal stability, physicochemical characterization and oral bioavailability of chitosan or its derivative-modified solid lipid nanoparticles loading docetaxel', Drug Development and Industrial Pharmacy, 43(5), pp. 839–846. doi: 10.1080/03639045.2016.1220571.

Singh, C. *et al.* (2017) 'In Vitro-In Vivo Evaluation of Novel Co-spray Dried Rifampicin Phospholipid Lipospheres for Oral Delivery', AAPS PharmSciTech, 18(1), pp. 138–146. doi: 10.1208/s12249-016-0491-5.

Singh, R. P., Gangadharappa, H. V. and Mruthunjaya, K. (2017) 'Phospholipids: Unique carriers for drug delivery systems', Journal of Drug Delivery Science and Technology, 39, pp. 166–179. doi: 10.1016/j.jddst.2017.03.027.

Sithole, M. N. *et al.* (2018) 'A 3D bioprinted in situ conjugated-co-fabricated scaffold for potential bone tissue engineering applications', Journal of Biomedical Materials Research - Part A, 106(5), pp. 1311–1321. doi: 10.1002/jbm.a.36333.

Sithole, M. N. *et al.* (2017) 'Development of a Novel Polymeric Nanocomposite Complex for Drugs with Low Bioavailability', AAPS PharmSciTech. AAPS PharmSciTech, (6). doi: 10.1208/s12249-017-0796-z.

Song, S. *et al.* (2014) 'Hyaluronan-based nanocarriers with CD44-overexpressed cancer cell targeting', Pharmaceutical Research, 31(11), pp. 2988–3005. doi: 10.1007/s11095-014-1393-4.

Sugano, K. *et al.* (2010) 'Coexistence of passive and carrier-mediated processes in drug transport', Nature Reviews Drug Discovery, 9(8), pp. 597–614. doi: 10.1038/nrd3187.

Sumaila, M. *et al.* (2019) 'Lipopolysaccharide Polyelectrolyte Complex for Oral Delivery of an Anti-tubercular Drug', AAPS PharmSciTech, 20(3), pp. 107. doi: 10.1208/s12249-019-1310-6.

Swaan (1998) 'Recent Advances in Intestinal Macromolecular Drug Delivery via Receptor-Mediated Transport Pathways', Pharm Res., 15(6). doi:10.1023/a:1011908128045.

Takano, M., Yumoto, R. and Murakami, T. (2006) 'Expression and function of efflux drug transporters in the intestine', Pharmacology and Therapeutics, 109(1–2), pp. 137–161. doi:

10.1016/j.pharmthera.2005.06.005.

Thakkar, A. *et al.* (2015) 'Ferulic acid combined with aspirin demonstrates chemopreventive potential towards pancreatic cancer when delivered using chitosan-coated solid-lipid nanoparticles', Cell and Bioscience. BioMed Central, 5(1), pp. 1–14. doi: 10.1186/s13578-015-0041-y.

Thakkar, A. *et al.* (2016) 'Preclinical systemic toxicity evaluation of chitosan-solid lipid nanoparticle-encapsulated aspirin and curcumin in combination with free sulforaphane in BALalB/c mice', International Journal of Nanomedicine, 11, pp. 3265–3276. doi: 10.2147/IJN.S106736.

Thanou, M. *et al.* (2001) 'Intestinal absorption of octreotide using trimethyl chitosan chloride: Studies in pigs', Pharmaceutical Research, 18(6), pp. 823–828. doi: 10.1023/A:1011092613951.

Tian, M. P. *et al.* (2018) 'Inducing sustained release and improving oral bioavailability of curcumin via chitosan derivatives-coated liposomes', International Journal of Biological Macromolecules. Elsevier B.V., 120, pp. 702–710. doi: 10.1016/j.ijbiomac.2018.08.146.

Tomita, M. *et al.* (1988) 'Enhancement of Colonic Drug Absorption by the Paracellular Permeation Route', Pharmaceutical Research: An Official Journal of the American Association of Pharmaceutical Scientists, pp. 341–346. doi: 10.1023/A:1015999309353.

Toorisaka, E. *et al.* (2012) 'Intestinal patches with an immobilized solid-in-oil formulation for oral protein delivery', Acta Biomaterialia. Acta Materialia Inc., 8(2), pp. 653–658. doi: 10.1016/j.actbio.2011.09.023.

Turner, J. R. (2009) 'Intestinal mucosal barrier function in health and disease', Nature Reviews Immunology. Nature Publishing Group, 9(11), pp. 799–809. doi: 10.1038/nri2653.

V. Varma, M. *et al.* (2011) 'Targeting Intestinal Transporters for Optimizing Oral Drug Absorption', Current Drug Metabolism, 11(9), pp. 730–742. doi: 10.2174/138920010794328850.

Vertzoni, M. *et al.* (2019) 'Impact of regional differences along the gastrointestinal tract of healthy adults on oral drug absorption: An UNGAP review', European Journal of Pharmaceutical Sciences, 134(April), pp. 153–175. doi: 10.1016/j.ejps.2019.04.013.

Vieira, A. C. C. *et al.* (2018) 'Mucoadhesive chitosan-coated solid lipid nanoparticles for better management of tuberculosis', International Journal of Pharmaceutics. Elsevier B.V., 536(1), pp. 478–485. doi: 10.1016/j.ijpharm.2017.11.071.

Viswanathan, P., Muralidaran, Y. and Ragavan, G. (2017) 'Challenges in oral drug delivery: A nano-based strategy to overcome' in Andronescu, E., Grumezescu, AM. (eds.) Nanostructures for Oral Medicine. Elsevier Inc. pp. 173-201. doi: 10.1016/B978-0-323-47720-8.00008-0.

Wang, L. *et al.* (1997) 'A new approach for the fabrication of an alternating multilayer film of poly(4-vinylpyridine) and poly(acrylic acid) based on hydrogen bonding', Macromolecular Rapid Communications, 18(6), pp. 509–514. doi: 10.1002/marc.1997.030180609.

Wang, W. *et al.* (2020) 'Chitosan Derivatives and Their Application in Biomedicine', International Journal of Molecular Sciences, 21(2), p. 487. doi: 10.3390/ijms21020487.

Whitcomb, D. C. and Lowe, M. E. (2007) 'Human pancreatic digestive enzymes.', Digestive diseases and sciences, 52(1), pp. 1–17. doi: 10.1007/s10620-006-9589-z.

Wishart, D. S. (2006) 'DrugBank: a comprehensive resource for in silico drug discovery and exploration', Nucleic Acids Research, 34(90001), pp. D668–D672. doi: 10.1093/nar/gkj067.

Yang, Y. *et al.* (2019) ‘Hydroxypropyltrimethyl ammonium chloride chitosan activates RAW 264.7 macrophages through the MAPK and JAK-STAT signaling pathways’, Carbohydrate Polymers. Elsevier Ltd., 205, pp. 401–409. doi: 10.1016/j.carbpol.2018.10.101.

Yun, Y., Cho, Y. W. and Park, K. (2013) ‘Nanoparticles for oral delivery: Targeted nanoparticles with peptidic ligands for oral protein delivery’, Advanced Drug Delivery Reviews. Elsevier B.V., 65(6), pp. 822–832. doi: 10.1016/j.addr.2012.10.007.

Zelikin, A. N., Ehrhardt, C. and Healy, A. M. (2016) ‘Materials and methods for delivery of biological drugs’, Nature Chemistry. Nature Publishing Group, 8(11), pp. 997–1007. doi: 10.1038/nchem.2629.

Zheng, K., Trivedi, M. and Siahaan, T. (2006) ‘Structure and Function of the Intercellular Junctions: Barrier of Paracellular Drug Delivery’, Current Pharmaceutical Design, 12(22), pp. 2813–2824. doi: 10.2174/138161206777947722.

CHAPTER 3

DESIGN OF LIPOPOLYSACCHARIDE POLYELECTROLYTE COMPLEX FOR ORAL DELIVERY OF AN ANTI-TUBERCULAR DRUG

AAPS PharmSciTech (2019) 20:107
DOI: 10.1208/s12249-019-1310-6



Research Article
Theme: Lipid-Based Drug Delivery Strategies for Oral Drug Delivery
Guest Editor: Sanyog Jain

Lipopolysaccharide Polyelectrolyte Complex for Oral Delivery of an Anti-tubercular Drug

Mumuni Sumaila,[1] Poornima Ramburrun,[1] Pradeep Kumar,[1] Yahya E. Choonara,[1] and Viness Pillay[1,2]

3.1. Introduction

Tuberculosis (TB) has been a major public health challenge, particularly in Africa, Asia and South America, despite all efforts made to improve its treatment and management (WHO, 2017). Moreover, TB has been associated with high mortality rates, in co-morbid Human Immunodeficiency Virus (HIV) incidences (Costa *et al.*, 2016). The causative organism, *Mycobacterium tuberculosis* (Mtb) primarily affects the lungs as pulmonary TB, however, other parts of the body could also be affected resulting in extrapulmonary TB (Rappuoli and Aderem, 2011). The conventional anti-TB regimen involves the oral administration of rifampicin, isoniazid, pyrazinamide or ethambutol in various combinations often dosed multiple times per day (Costa *et al.*, 2016). Patients of this 'hard to eradicate' bacteria (Mtb) suffer severe adverse effects due to major drawbacks associated with the delivery of this chemotherapy regimen (Sosnik *et al.*, 2010). The current TB therapeutic strategy is challenged with problems of low drug solubility, intestinal malabsorption, pre-mature drug degradation, low drug concentrations at the infection site, and poor cell-drug penetration (Sosnik *et al.*, 2010). All these factors impart poor bioavailability of TB medications. Furthermore, the long (6-9 months) and stringent treatment schedule of anti-tubercular drugs (ATDs) and associated side-effect profiles (particularly the second-lines ATDs) contributes to poor patient compliance (Pinheiro and Reis, 2011). These challenges necessitate action to develop an effective delivery system capable of alleviating these concerns. A nanocarrier system capable of releasing bioactives steadily in therapeutically effective quantities could assist in improving drug target-site

bioavailability, cell-drug penetration, intestinal absorption, and protection against pre-mature drug degradation while reducing the dosage frequency of the medication thereby improving patient compliance.

In an attempt to solve the aforementioned challenges, several studies have successfully fabricated nano delivery systems to efficiently deliver ATDs. Some of which include hybridized lipid-polymer systems (Bachhav *et al.*, 2017a; Petkar *et al.*, 2018), liposomal systems (El-ridy *et al.*, 2007; Patil *et al.*, 2015), natural polymeric systems (Devi and Maji, 2009; Singh *et al.*, 2017), synthetic polymeric systems (Esmaeili, Hosseini-nasr and Rad-malekshahi, 2007; Ohashi *et al.*, 2009b) and systems for local lung delivery (Amarnath *et al.*, 2016; Costa, Sarmento and Seabra, 2018a), to name a few. Formulations with synthetic polymers face some drawbacks as regards safety and biocompatibility. Likewise, inhalational and intravenous formulations may be less cost effective and administration could pose a challenge to the patient. Lipopolysaccharide-based polyelectrolyte complex (PEC) particulates would be an excellent drug delivery strategy for the smart delivery of ATDs orally. The composition of such a system as a polymeric complex combines the advantages of a biodegradable polysaccharide (for structural integrity, physical stability and bioactive protection) (Nagpal, Singh and Mishra, 2010; Rawal *et al.*, 2018) and phospholipid (for high drug-loading capacity and sustained release). In addition, lipopolysaccharide-based PEC particulates offer the advantages of improved biocompatibility, versatility, safety and efficacy (Patidar *et al.*, 2010; Salomon, Goycoolea and Moerschbacher, 2017) with relatively cost-effective naturally-derived polymers.

Low molecular weight chitosan (CT) is a deacetylated linear polysaccharide represented by (1–4)-2-amino-2-deoxy-B-D-glucan. This copolymer of glucosamine and N-acetylglucosamine with a positive surface charge (Bhise *et al.*, 2007), contributes to its reactive ability to form PECs with anionic molecules (Bawa *et al.*, 2011). L-α-Lecithin, Soybean (SL) in contrast, a negatively charged polymer with a high complexation affinity for CT, has gained much attention for the synthesis of solid-lipid nanoparticles, micro- and nano-emulsions and liposomes (Patil *et al.*, 2015).

To the best of our knowledge, there have been no reports of a lecithin-chitosan nano delivery system specifically designed for oral delivery of rifampicin. However, several studies have investigated similar systems, with favourable outcomes, in cancer chemotherapy (Barbieri *et al.*, 2013), transdermal melatonin delivery (Pepic, Hafner and Lovric, 2011) and oral insulin delivery (Al-Remawi *et al.*, 2017). Likewise, the formulation in the present study is based on the PEC that occurs between the free anionic phosphate group of the phospholipid (SL) and the free cationic amine group of the polysaccharide (CT). Polyelectrolyte complexation is a self-sustaining reaction which does not require further reaction initiators, catalysts or cross-

linkers. In addition, the popularized use of cost-effective naturally-derived polymeric materials for the synthesis of drug-delivery systems propose reliable safety and non-toxicity as a result of an ecologically-positive tactic and non-complex formulation procedure (Sahoo *et al.*, 2009; Siyawamwaya *et al.*, 2015). Of particular importance to this study, is the notion that varying degrees of Polyelectrolyte complexation enhances drug bioavailability (Heinen *et al.*, 2013), improves drug encapsulation efficiency and influences drug-release kinetics of nanoparticulate formulations (Cheow and Hadinoto, 2012).

The present study aims to fabricate a lipopolysaccharide-based PEC particulate for application as a sustained-release oral delivery system for ATDs with the goal of improving patient compliance and therapeutic efficacy with regards to bioavailability. This study incorporated CT and SL for the polyelectrolyte complex using the solvent injection technique with rifampicin (RFP) as the model drug. The synthesized RFP-loaded PEC particulates were analyzed for molecular and crystallinity transitions to establish polyelectrolyte complexation with subsequent characterization of rheological properties, formulation stability and light scattering behaviour of the nanoparticle suspension, mucoadhesion, thermodynamic and hydrodynamic properties, permeability and drug release studies. To effectively study the drug release profile of the fabricated particulates as a function of the PEC, a 4 × 2 matrix system was implemented: 1) PEC particulates of interest with encapsulated RFP (SL-CT-RFP), 2) *in situ* mixing of RFP with the formulated SL-CT+RFP complex (where RFP is not encapsulated), 3) *in situ* complex of pristine SL+CT+RFP and 4) *in situ* complex of SL-coated RFP and pristine CT (MSL+RFP+CT). Furthermore, mathematical modelling of the drug release kinetics was performed to elucidate insight into the drug release mechanisms acting upon the various formulations.

3.2. Materials and methods

3.2.1. Materials

Low molecular weight chitosan (CT) (75-85% deacetylated), L-α-Lecithin soybean (a concentrate of soybean lecithin with 94% phosphatidylcholine and < 2% triglycerides), Porcine Mucin (PM) (type 2), Rifampicin (RFP) and phosphate-buffered saline (PBS) were purchased from Sigma-Aldrich (St. Louise, MO, USA). Ethanol (ETOH) and glacial acetic acid were procured from Merck (Pty Ltd., South Africa). All chemicals were of analytical reagent grade and used without prior modification. Double deionized water (DDW) was used for all the preparations.

3.2.2. Preparation of rifampicin-loaded SL-CT lipopolysaccharide particulates

3.2.2.1. Preparation of loose nanoparticle powders

Lipopolysaccharide PEC particulates were prepared using an adapted solvent injection technique (as shown in Figure 3.1) from Sonvico and co-workers, 2006 (Sonvico *et al.*, 2006). Briefly, 300 mg of SL was dissolved in 10 mL of ethanol followed by an addition of 150 mg RFP which was thoroughly dissolved to obtain a homogenous SL-RFP solution. CT solution was prepared by dissolving 100 mg polymer in 40 mL of a 1% $^{v}/_{v}$ acetic acid solution and 50mL DDW. The RFP-loaded nanoparticle suspension of a 3:1 SL-CT weight ratio was obtained by injecting 10 mL of SL-RFP ethanol solution (30 mg/mL) into 90 mL of CT solution through a syringe (inner diameter 0.75 mm, flow rate 40 mL/min) with subsequent mechanical stirring. The resulting nanoparticle suspension was centrifuged at 5000 rpm for 30 minutes, the supernatant decanted and sediment lyophilized to obtain a dried nanoparticle powder. The same procedure was followed for the preparation of PEC particulates of a 1:1 SL-CT weight ratio and RFP-free formulation.

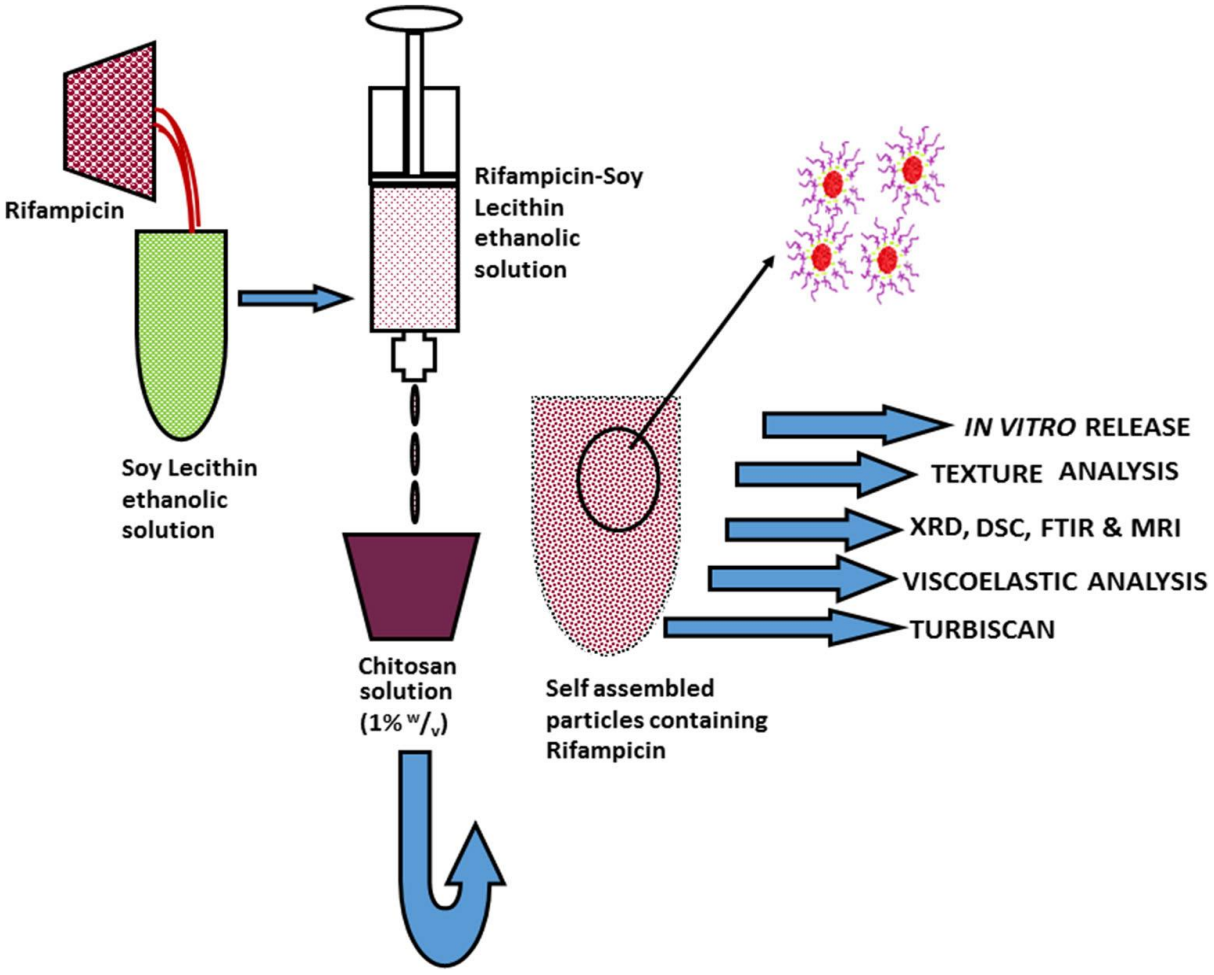


Figure 3.1. Schematic representation of the synthesis of lipopolysaccharide-based PEC particulates via the solvent injection technique.

3.2.2.2. Preparation of PEC particulate tablets

For simplicity of sample preparation for the determination of *in vitro* drug-release profiles, textural profiling and hydration dynamics, the resulting dried nanoparticle powders were compressed into tablets. Batches of nanoparticle powder (SL-CT-RFP 1:1 and 3:1) containing 300 mg RFP was compressed into tablets using a die punch fitted into a hydraulic unit model tablet press machine (Carver, Inc. Wabash, USA) under an applied pressure of 1400 psi. The preparation of SL-CT+RFP tablets involved the mixing of RFP with pre-formulated SL-CT complex. For the preparation of SL+CT+RFP tablets, pristine polymers and RFP (300 mg SL + 300 mg CT +300 mg RFP) were mixed together before punching. The preparation of MSL+RFP+CT tablets required melting of 300 mg SL at 45^0C which was then subsequently used to coat 300 mg RFP. Thereafter, SL-coated RFP was mixed with 300 mg pristine CT and then punched into tablets.

3.2.2.3. Evaluation of particle size distribution, zeta potential and conductivity

Briefly, 100 mg of the synthesized PEC particulates were dispersed in DDW and sonicated for 30 seconds. A 2 mL sample of the nanoparticle suspension was placed in disposable cuvettes and analyzed at 25 ^{0}C for average particle size, polydispersity index (PdI), zeta potential, and conductivity using the Malvern ZetaSizer Nano ZS (Malvern Instruments, Worcestershire, UK).

3.2.2.4. Determination of RFP-loading capacity and encapsulation efficiency in response to changes in SL concentration

Drug-loaded nanoparticle suspensions (2 mL; n=3), were centrifuged at 5000 rpm for one hour. The concentration of RFP in the clear supernatant was analyzed by UV-Vis spectroscopy (Specord40, Analytik Jena, AG, Germany) set at λ_{max} = 475 nm. Triplicate measurements were carried out to determine the %encapsulation efficiency (%EE) and %drug-loading capacity (%LC) of the PEC particulates using Equations (3.1) and (3.2), respectively:

$$\%\ EE = \frac{Total\ amount\ of\ RFP\ loaded\ -\ Amount\ of\ RFP\ in\ the\ supernatant}{Total\ amount\ of\ RIF\ loaded} \times 100 \qquad (3.1)$$

$$\%\ LC = \frac{Amount\ of\ RFP\ in\ PEC\ particulates}{Weight\ of\ PEC\ particulates} \times 100 \qquad (3.2)$$

Determination of mucoadhesive properties in response to SL: CT and RFP variations

In vitro mucoadhesion analysis was performed using PM to determine %mucin-binding efficiency (%MBE) to confirm interactions between the PEC particulates and PM with regards to the effect of RFP-loading on the mucoadhesive property of the PEC particulates (Pawar, Douroumis and Boateng, 2012). Briefly, 2mL samples of nanoparticle suspension (0.5 mg/mL) was mixed with 2 mL of PM (1 mg/mL) solution prepared in phosphate buffered saline (PBS) (pH 6.8). This colloidal mixture was incubated at 37^0C for 2 hours in an incubation chamber with a rotation of 20-25 rpm. Thereafter, the sample was centrifuged at 5000 rpm for 30 min and the absorbance of the supernatant measured at λ_{max} = 250 nm by UV-Vis spectroscopy. Triplicate measurements were performed and %MBE of the various nanoparticle formulations calculated using Equation (3.3):

$$\%MBE = \frac{C_i - C_p}{C_i} \times 100 \qquad (3.3)$$

Where C_i is the original PM concentration used for incubation and C_p is the concentration of free PM in the supernatant.

3.2.2.5. Determination of molecular vibrational transitions and analysis of PEC formation

Powdered samples of RFP-loaded and RFP-free SL-CT PEC particulates and the native polymers were analyzed for interactions resultant of PEC formation. Samples were analyzed at a resolution of 4 cm^{-1} over a wavelength range of 4000 cm^{-1} to 650 cm^{-1} using the PerkinElmer Spectrum 2000 ATR-FTIR (PerkinElmer 100, Llantrisant,Wales, UK).

3.2.2.6. Analysis of the thermodynamic properties of the synthesized lipopolysaccharide PEC and RFP-loaded PEC particulates

The thermodynamic properties of the SL-CT PEC, SL-CT-RFP PEC particulates and the pristine constituent polymers and drug were evaluated using a Temperature Modulated Differential Scanning Calorimeter (TMDSC) (Mettler Toledo, DSC, STAReSystem, Swchwerzenback, ZH, Switzerland). Samples of 5-10 mg were sealed in aluminium crucibles and heated over a 10-325°C temperature range at a heating rate of 5°C/min under continuous flow of nitrogen gas at 200 mL/min. The DSC thermograms were obtained as plots of heat flow against sample temperature.

3.2.2.7. X-ray powder diffraction (XRPD) analysis

The crystallinity transitions of the RFP-loaded PEC particulates, RFP-free SL-CT complex and native polymers were analyzed using XRPD (Rigaku MiniFlex 600, Tokyo, Japan) sourced with nickel-filtered CuKα radiation (at a voltage of 40 kV and a current of 15 mA).

Diffractograms were obtained using a 2θ scan range over 3-80° at a scanning rate of 5° per minute.

3.2.2.8. Evaluation of rheological properties of the synthesized lipopolysaccharide complex and RFP-loaded PEC particulates

The kinetic gelation properties of the PEC formulations were analyzed using the ElastoSens™ Bio^2 (Rheolution Instruments, Canada) which employed a non-destructive acoustic vibration and laser measurement of rheological responses without sample contact (Ceccaldi *et al.*, 2017). Samples were studied by mixing appropriate volumes of 0.1%$^w/_v$ SL and 0.1%$^w/_v$ CT solutions (in SL-CT ratios of 1:1 and 3:1) in the sample holder where Polyelectrotyte complexation reactions were allowed to occur at 37ºC over a 5-hour duration. The experimental procedure was repeated for the incorporation of RFP into the reaction system (polymer complex:RFP ratio of 5:1). The same solvents, as mentioned earlier, were used for preparation of the polymer solutions. The shear storage modulus G' (Pa) was obtained as a function of time (seconds).

3.2.2.9. Textural profiling of RFP-loaded lipopolysaccharide complex nanoparticle tableted formulations

Textural profiling, in terms of matrix breakpoint (N) and fracture energy (N.mm), of the SL-CT-RFP 1:1 and 3:1 tablets was performed using a texture analyzer (TA.*XTplus*, Stable Microsystems, Surrey, UK) fitted with a flat-tipped stainless steel probe of 2mm in diameter. The test parameters consisted of a pre-test and test speed of 2mm/s, post-test speed of 10mm/s and an Auto-type trigger force of 0.05N with a 5 kg load-cell. The maximum peak point and area under the curve of the Force-Distance textural profile allowed the determination of the force at matrix breakpoint and corresponding fracture energy.

3.2.2.10. Optical characterization and stability of the lipopolysaccharide PEC particulates in suspension

Optical interactions and formulation stability of the formulated nanoparticle suspensions were investigated utilizing the Turbiscan™ LAB (Formulaction, L'Union, France). A 20 mL aliquot of RFP-loaded and RFP-free nanoparticle suspensions were introduced into specialized sample holders and analyzed at pre-determined intervals over a 5-minute duration at 25 (± 0.5)^{0}C. The instrument was fixed with a pulsed near infra-red light source moving vertically along the sample collecting data at 40µm-intervals. A 180° positioned transmission detector detected transmitted light whereas a backscattering detector, positioned at 45°, detected rebounded light in response to the light-scattering effect by the suspended PEC particulates. The changes in backscatter (∆BS) measurements were used to assess formulation stability.

3.2.2.11. In vitro drug release of lipopolysaccharide PEC particulates and kinetic modelling of release data

RFP-loaded nanoparticle tablets (SL-CT ratios of 1:1 and 3:1) containing 300 mg RFP were placed into vessels containing 900 mL of PBS pH 6.8 at 37^0C in a dissolution tester (ERWEKA, USP Apparatus II, DT 126, UK) operated at a paddle revolution of 50 rpm over a 24-hour period. Samples of 5mL of dissolution medium were withdrawn at predetermined time intervals and replaced with equal amounts of fresh PBS (pH 6.8) to maintain sink conditions. The RFP content in each sample was quantified using UV-Vis spectroscopy set at λ_{max} = 475 nm. The comparator formulations studied include 1) *in situ* mixing of RFP with the formulated SL-CT complex (SL-CT+RFP), 2) *in situ* complex of pristine SL+CT+RFP, 3) *in situ* complex of SL-coated RFP and pristine CT (MSL+RFP+CT) and 4) Free RFP. Experimental data were obtained in triplicate and all values are representative of mean ± SD (n=3). The release kinetics of RFP from the formulated nanoparticle-based tablets and comparator formulations were fitted into the Zero-order (Equation 3.4), First-order (Equation 3.5), Higuchi (Equation 3.6), Korsmeyer-Peppas (Equation 3.7) and Hixson-Crowell (Equation 3.8) kinetic models to assist in the elucidation of the primary drug release mechanisms (Cheow and Hadinoto, 2012).

$$C = K_0 t \quad (3.4)$$

Where K_0 is the Zero-order release constant at time t.

$$LogC = logC_0 - Kt/2.303 \quad (3.5)$$

Where C_0 is the initial drug concentration and K is the First-order rate constant at time t.

$$Q = Kt^{1/2} \quad (3.6)$$

Where Q reflects % drug release and K is the design variable of the system at time t.

$$Q_0^{1/3} - Q_t^{1/3} = K_{HC} t \quad (3.7)$$

Where Q_0 is the initial quantity of drug in the formulations, Q_t is the residual quantity of RFP at time t and K_{HC} is the rate constant.

$$M_t/M_\infty = Kt^n \quad (3.8)$$

Where M_t/M_∞ is the fractional drug release at time t, K is the release rate constant and n is the release exponent.

3.2.2.12. Analysis of the hydrodynamic and swelling characteristics of the RFP-loaded lipopolysaccharide PEC tableted PEC particulates

Analysis of the *in vitro* hydrodynamic and swelling behaviour of the SL-CT-RFP nanoparticulate tableted formulation was performed via Magnetic Resonance Imaging (MRI) (Oxford Instruments Magnetic Resonance, Oxon, UK) equipped with a 0.5 Tesla permanent

magnet stabilized at 37°C and a dissolution flow-through cell containing PBS pH 6.8. Live-image capture of the SL-CT-RFP 1:1 and 3:1 tablets were obtained at 10-minute intervals over a period of 16 hours, respectively, utilizing MARAN-i Version 1.0 software.

3.2.2.13. *Ex vivo* Permeability of RFP from the Lipopolysaccharide PEC Particulates across Porcine Intestinal Tissue

Ex vivo permeability studies were performed, using static Franz Diffusion Cell Apparatus (Logan Instruments Corp., NJ, USA), to evaluate the permeability of RFP from the formulated PEC particulate systems (SL-CT-RFP 1:1 and SL-CT-RFP 3:1) and the free RFP across adult porcine intestinal epithelium of the large white pig. According to standard operating procedures and approval from the Animal Ethics Screening Committee of the University of the Witwatersrand (Clearance No. AESC-2014/38/C and Ref.14-11-14 O), the pig was euthanized, and the intestinal tissue was excised, cleaned and separated from the serosa then stored in PBS pH 6.8 until further use. Within 60 min of harvesting, the intestinal tissue was assessed for viability and integrity via potential difference measurements across the tissue sections using a Seven Multi GmbH S40 electrical conductivity meter (Mettler-Toledo, Zurich, Switzerland), over 8 h. Thereafter, the tissues were fixed between the donor and receptor compartments of the diffusion cells (permeation area 1.77 cm^2). The receptor chamber solution consisted of 12 mL PBS (pH 6.8), was continuously stirred with a magnetic bar and maintained at 37°C. The donor chamber consisted of 3 mL of the lipopolysaccharide PEC particulate dispersion containing 1.25 mg/mL of RFP. Samples of 3 mL were withdrawn from the receptor compartment at predetermined time intervals over 8 h and replaced with an equal volume of fresh PBS (pH 6.8) to maintain sink conditions. The samples were measured for the quantity of RFP using UV-Vis spectroscopy set at λmax = 475 nm. Equations (3.9) and (3.10) were used to determine the quantity and flux of RFP, respectively, that traversed the intestinal tissue and Equation (3.11) was used to determine permeation. Experimental data were obtained in triplicate and all values are representative of mean ± SD (n = 3).

$$\text{Cumulative amount of RFP permeated} = \frac{Q}{A}\ (\text{mg/cm}^2) \qquad (3.9)$$

where A is area of exposed membrane (cm^2) and Q is quantity of RFP crossing the membrane (mg).

$$J = \frac{Q}{AT}\ (\text{mg/cm}^2\text{/min}) \qquad (3.10)$$

where J is the flux of RFP, Q is the quantity of RFP permeated, A is the cross-sectional area of the membrane, and T is the time of exposure expressed in minutes.

$$-ln\left(1 - \frac{2C_T}{C_0}\right) = \frac{2A}{V} \times P \times T \qquad (3.11)$$

where C_T is the concentration of RFP in the receptor chamber at time T, C_0 is the original concentration of RFP in the donor chamber, V is the volume of solution in the two compartments, and A is the area of permeation.

3.3. Results and Discussion

3.3.1. Evaluation of particle size and zeta potential

The average hydrodynamic diameters of the fabricated bioactive-loaded and empty PEC particulates as obtained from the Zetasizer® Nano-ZS were found to be in the range of 151.6 to 292.1 nm with a polydispersity index (PDI) of less than 0.3, as shown in Table 3.1. The low PDI reveals a very narrow size distribution which is considered acceptable for an ideal nanoparticle (Sonvico *et al.*, 2006). Furthermore, the obtained size range may indicate enhanced permeation of the PEC particulates across the intestinal mucosa thereby allowing for higher systemic levels of the formulation (Norris and Sinko, 1997; Liu *et al.*, 2014). The average zeta potential of all the nano-suspensions ranged from +22.2 to +33.0mV revealing the stability of the nano-suspension (Jain *et al.*, 2018) in respect to coagulation, flocculation, aggregation, sedimentation and creaming phenomena through strong electrostatic repulsion between the charged particles keeping them apart.

Table 3.1. Particle size, zeta potential, conductivity and PdI of RFP-loaded and RFP-free nanoparticle formulations.

Formulation	Particle Size (nm)	Surface charge (mV)	Conductivity (mS/cm)	PdI
SL-CT 1:1	292.1	+25.6	0.194	0.292
SL-CT 3:1	232.8	+22.2	0.081	0.273
SL-CT-RFP 1:1	151.6	+33.0	0.102	0.247
SL-CT-RFP 3:1	274.2	+30.7	0.057	0.262

3.3.2. Determination of RFP loading capacity and encapsulation efficiency in response to changes in SL concentrations

Determination of the drug-loading capacity (%LC) and encapsulation efficiency (%EE) of the lipopolysaccharide system (as shown in Table II) revealed that the 3:1 SL-CT PEC particulates achieved increased RFP drug-loading (73.21%) compared to the 1:1 system (64.25%). This

could be attributed to hydrophobic interactions and association of RFP with the SL lipid bilayer architecture (Laridi *et al.*, 2003). A similar observation was noted by Were and co-workers, 2003, who reported increased drug encapsulation with increased phosphatidylcholine concentration (Jain *et al.*, 2018), thereby, inferring that drug encapsulation may be tuned to the preferred dose by adjusting SL concentration (Pattabhi, Howdary and Ao, 2004).

Table 3.2. Encapsulation efficiency (%EE) and Loading capacity (%LC) of RFP-loaded and RFP-free nanoparticle formulations.

Formulation	%EE	%LC
SL-CT 1:1	-	-
SL-CT 3:1	-	-
SL-CT-RFP 1:1	64.25	5.84
SL-CT-RFP 3:1	73.21	5.10

3.3.3. Determination of mucoadhesive properties in response to SL: CT and RFP variations

Mucoadhesion is thought to be the ability of polymeric materials to adsorb onto the surface mucous of mucosal membranes (Cevher *et al.*, 2008), thereby lengthening the resident time of these materials at the target site. Furthermore, mucoadhesion allows permeation of mucoadhesive nanocarriers into the mucosal lasyer thereby potentiating an increase in absorption and bioavailability (Pattabhi, Howdary and Ao, 2004). In this regard, the mucoadhesive property of CT could enhance the oral delivery of RFP. Surface interactions between mucoadhesive polymers and the mucosal membrane has been identified to be either ionic, covalent, hydrophobic or physical in nature (Smart, 2005).

Studies on the *in vitro* interaction of the RFP-loaded and RFP-free PEC particulates using PM indicated the mucoadhesion propensity of CT. As shown in Table III and Figure 2, all the formulations reached equilibrium adsorption at 120 minutes following immersion in mucin solution. Mucoadhesive studies revealed a %MBE of more than 10% (14-30%) for all the nanoparticle formulations except SL-CT-RFP (3:1) which demonstrated a %MBE of 8.25%. This is most likely attributed to the low amount of CT in this formulation in ratio to SL.

Furthermore, it was observed that RFP-loading and increase SL concentration caused a decrease in %MBE, hence, demonstrating that only CT contributes to the mucin-binding property of the complex system. The downregulation of CT mucin binding property imparted by RFP-loading and increased SL amount could be attributed to a reduced CT surfaces available for mucin interaction. This implies that increased availability of CT surfaces for mucin interaction and subsequent adsorption produces an expected increase in the %MBE of the nanoparticulate complex system. The mechanism of mucoadhesion is likely a result of electrostatic interaction that exist between the polysaccharide shell (positively charged) and GI mucus membrane (negatively charged) (Zhang, Wardwell and Bader, 2013; Shtenberg *et al.*, 2018). Whilst the surface positive charge contributed by chitosan coating enhanced ionic interaction with the negatively charged mucin layer, the hydrophilicity of the hybrid system could have also encouraged hydrogen bonding formation, and contributing to the enhance %MBE (Luo et al., 2015). This interaction could be of biopharmaceutical benefit to oral delivery of therapeutics, as sufficient gastrointestinal residence is necessary for nanocarrier mucosa penetration and gastrointestinal epithelium absorption, consequently promoting bioavailability of the cargo.

Table 3.3. %MBE comparison of RFP-loaded and RFP-free nanoparticle formulations as a function of time.

Time (Min)	**SL-CT 1:1**	**SL-CT 3:1**	**SL-CT-RFP 1:1**	**SL-CT-RFP 3:1**
30	6.12	3.99	1.23	0.88
60	14.40	9.47	4.12	2.00
90	21.60	16.57	9.00	5.81
120	29.77	25.02	14.10	8.25
150	29.56	25.14	14.22	8.31
300	29.63	25.09	14.14	8.29

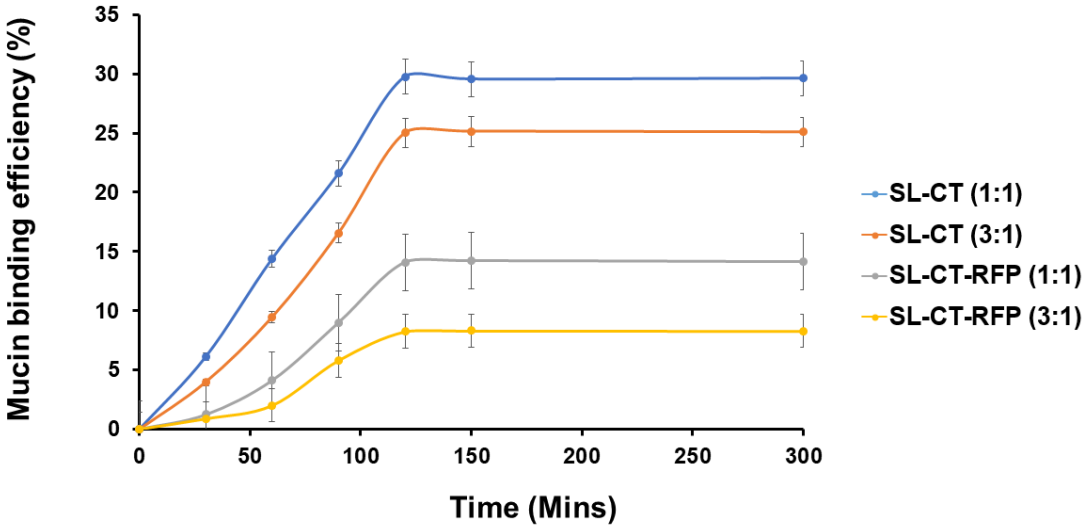


Figure 3.2. Representation of %MBE of RFP-loaded and RFP-free nanoparticle formulations in response to SL: CT and RFP variations. All values represented as mean ± SD (n=3).

3.3.4. Analysis of molecular vibrational transitions indicating PEC formation

FTIR spectra of the native polymers, SL-CT complex and SL-CT-RFP PEC particulates are illustrated in Figure 3.3. FTIR for pristine CT (Figure 3.3d) showed characteristic peaks at wave numbers 3284 cm^{-1}, 1375 cm^{-1} and 1023 cm^{-1} which corresponded to N-H, C-N and C-O stretching of the amide, respectively, while the peak at 1583 cm^{-1} indicated N-H bending. For pristine SL (Figure 3.3e), noted peaks at 3011 cm^{-1}, 1726 cm^{-1} and 1378 cm^{-1} were assigned to O-H, C=O and P=O vibrations, respectively (Dora *et al.*, 2017a) . A critical observation of the spectrum of SL-CT (Figure 3.3b) complex in comparison with the native polymers, indicated that similar bands for C=O, C-N and P=O exist at wave numbers 1736 cm^{-1}, 1375 cm^{-1} and 1241 cm^{-1}, respectively (Dora *et al.*, 2017a). It is noted that the band corresponding to the P=O vibration of SL has shifted to a lower wavenumber, thus, indicating electrostatic interaction and possible complexation with the amide groups of CT. The N-H stretching vibration of the RFP-loaded complex (Figure 3.3a) shifted to a lower wavenumber of 3253 cm^{-1} with a P-O-C vibration peak observed at 988cm^{-1}. These shifts may further suggest PEC formation occurring between the phospholipid (SL) and CT which originates from the interaction between the amino groups (NH^{3+}) of chitosan and the phosphate groups (PO^{3-}) of the phospholipid resulting in an aminophosphate-functionalized system.

The FTIR spectrum of RFP (Figure 3.3c) shows characteristic peaks at 2938 cm^{-1} (C-H stretching), 1732 cm^{-1} (-C=O acetyl stretching), 1650 cm^{-1} (-C=N asymmetric stretching), 1569 cm^{-1} (C=C stretching), 1373 cm^{-1} (C-N stretching) and 1254 cm^{-1} (-C-O-C- ether group) (Date,

Samad and Devarajan, 2010). Similar bands were demonstrated by the RFP-loaded nanoparticle spectrum: C-H stretching, –C=O acetyl stretching and C-N stretching at 2923 cm^{-1}, 1735 cm^{-1} and 1377 cm^{-1}, respectively (Bachhav *et al.*, 2017a), hence, suggesting RFP encapsulation. The encapsulation of RFP into the polymeric complex induced structural changes as noted on the spectrum of RFP-loaded PEC particulates when compared to the drug-free PEC particulates. A noticeable increase in peak intensity is evident from bands 2923 cm^{-1} – 968 cm^{-1} in the SL-CT-RFP spectrum when compared to the RFP-free nanoparticle spectrum. This further confirms the successful loading of RFP into the system, however, it may suggest that RFP could have interfered with or obscured the NH^{3+} and PO^{3-} PEC reaction sites (Singh *et al.*, 2014).

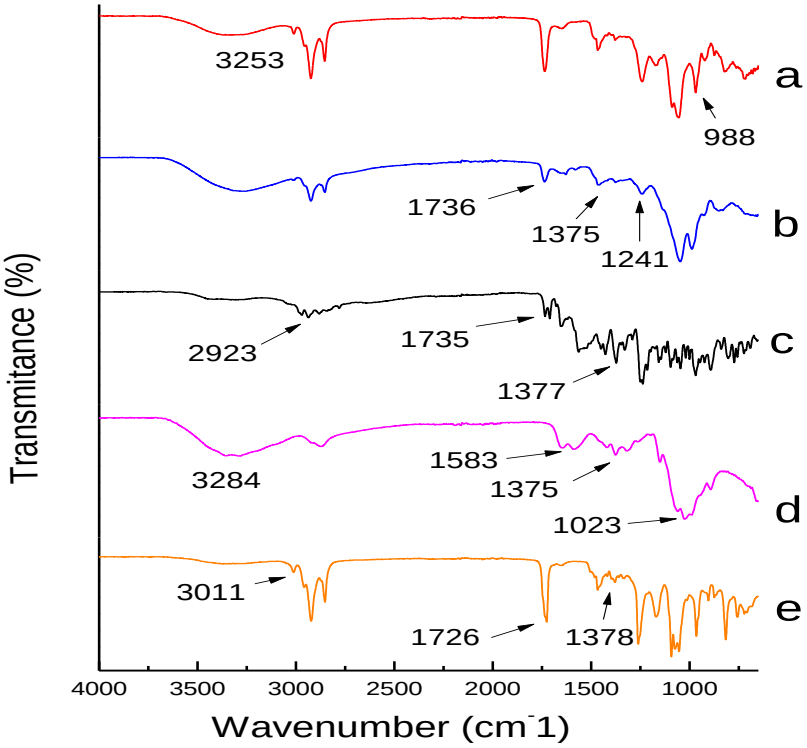


Figure 3.3. FTIR spectra of a) SL-CT-RFP, b) SL-CT, c) RFP, d) CT and e) SL.

3.3.5. Analysis of thermal stability and degradation induced by SL-CT-RFP polyelectrolyte complexation

DSC analysis, depicted in Figure 3.4, allowed the elucidation of transitions in melting points and thermal degradation in response to variations of SL ratios and RFP encapsulation. Although no significant changes were noted in the thermal properties of RFP-loaded and RFP-free formulations, the formation of a PEC induced shifts of the degradation peaks towards higher temperatures. It is noted that formulations SL-CT-RFP 3:1 and 1:1 (Figure 3.4a and b, respectively) and the corresponding RFP-free SL-CT 3:1 and 1:1 (Figure 3.4c and d,

respectively) PEC formulations exhibited the onset and endset of thermal degradation between a range of 288°C and 325°C, respectively, whereas the pristine CT (Figure 3.4e) and SL (Figure 3.4f) parent polymers exhibited lower thermal stability with the initiation of degradation occurring at 275°C. The thermogram of SL (Figure 3.4f) presented with two melting points at 146°C and 222°C. The melting point at 222°C is observed to maintain its presence in the RFP-free and RFP-loaded formulations with a gradual shift of this peak towards higher temperatures where a marked increase to 242°C in the SL-CT-RFP 3:1 formulation is noted. These changes further confirm the formation of a PEC resulting from interaction of phosphate ions present in SL with the amines of CT. The melting point of pure RFP as noted at 187°C (Figure 3.4g) is undetectable in the RFP-loaded formulations which may be attributed to the formation of a stable drug-polymer complex which necessitates higher energy to cause disruption of any newly formed chemical bonds.

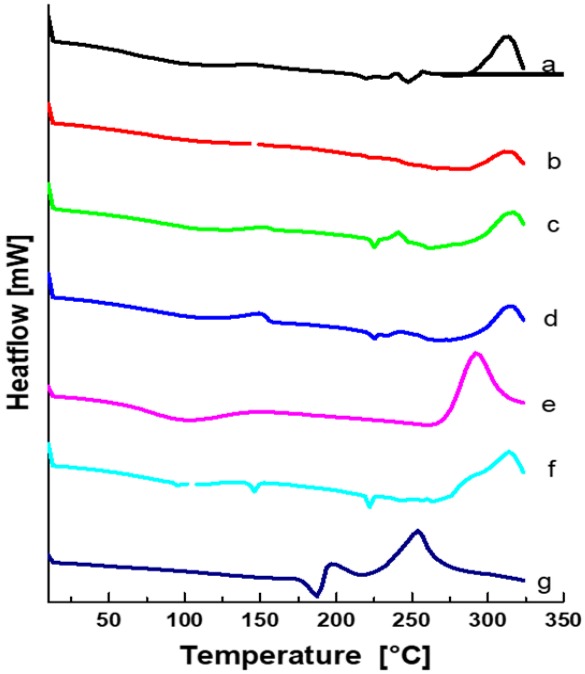


Figure 3.4. DSC thermograms of a) SL-CT-RFP 3:1, b) SL-CT-RFP 1:1, c) SL-CT 3:1, d) SL-CT 1:1, e) CT, f) SL and g) RFP

3.3.6. X-Ray Powder Diffraction (XRPD) analysis

Crystallinity transitions of polymeric materials impact the resulting physicochemical properties. Amorphous characteristics of polymeric materials and colloid and emulsion systems are preferred for biomedical applications, especially in pharmaceutical industry, since the improved solubility of amorphous states enhance bioavailability (Alkhader, Billa and Roberts, 2017). XRPD analysis performed for comparison between the characteristic crystalline

properties of the pure RFP drug, native polymers, SL-CT complex and the RFP-loaded PEC particulates, as shown in Figure 3.5. The XRPD pattern of pure chitosan, in a relatively amorphous state, has been reported to show broad peaks at 2θ = 10° and 2θ = 20° (Kumar, Dutta and Koh, 2011), which corresponds to the pattern obtained for pristine CT. The X-ray diffractogram of SL presented a semi-crystalline peak at 2θ = 20.3° indicating the amorphous regions of phosphatidylcholine (Formariz *et al.*, 2008; Cheng, 2015). A comparison of the characteristic peaks evident in the native polymers with that of the new complex (SL-CT) formed revealed that the amorphous peak of pristine CT at 2θ = 10° was absent in the formed SL-CT complex. Furthermore, the semi-crystalline peak of SL at 2θ = 20.3° transitioned to a single strong and broad peak indicative of amorphous regions in the SL-CT and SL-CT-RFP complexes. These changes in crystallinity may be attributed to the Polyelectrolyte complexation between NH^{3+} of CT and PO^{3-} of SL as described in FTIR spectra. RFP displayed well-defined narrow peaks characteristic of a highly crystalline structure. However, when encapsulated in the PEC particulates, the intense crystalline peak disappeared to form a combined singular broad peak, as depicted by the SL-CT-RFP diffractogram in Figure 5. It was observed that the XRPD pattern for the RFP-loaded system and the RFP-free system showed marked similarity which may be attributed to the relatively small amount of RFP in terms of the drug:polymer complex ratio (1:40). However, maintenance of the presented amorphous regions in the RFP-loaded SL-CT complex may suggest an improved solubility profile of the encapsulated drug in aqueous media.

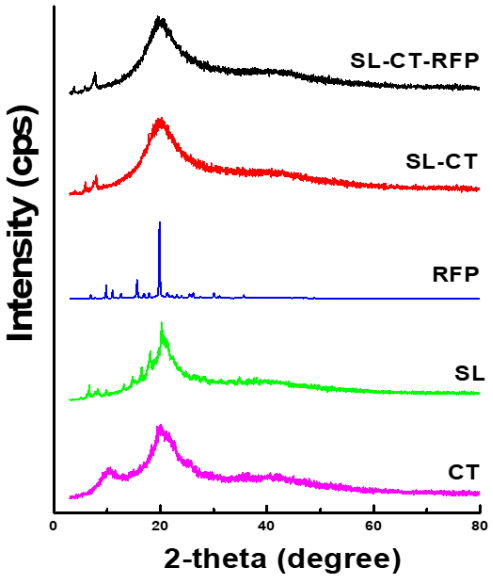


Figure 3.5. X-ray Powder Diffraction (XPRD) spectra of CT, SL, RFP, the SL-CT complex and the SL-CT-RFP PEC particulates.

3.3.7. Evaluation of rheological properties of the synthesized lipopolysaccharide complex and RFP-loaded PEC particulates

Viscoelasticity studies with regards to the gelation kinetics and real-time elasticity monitoring of SL-CT 1:1, SL-CT 3:1, SL-CT-RFP 1:1 and SL-CT-RFP 3:1 was performed as shown in Figure 3.6. The shear storage modulus (G') was given as a function of reaction time at 37 ^{0}C. It was observed that all four formulations had a relatively fast onset of gelation of less than 2 minutes. Gelation onset times of 57 seconds was observed for SL-CT 1:1, SL-CT 3:1 and SL-CT-RFP 1:1, whereas SL-CT-RFP 3:1 demonstrated a gelation onset time of 117 seconds. The delayed gelation onset observed with SL-CT-RFP 3:1 could be due to a longer time required for the reacting PEC molecules to come into contact with each other as a result of excess phosphate anions in the system causing electrostatic repulsion and interference by RFP molecules. The fast onset of gelation may be attributed to a rapid Polyelectrolyte complexation reaction between the native polymers of equal ratios with minimal interference from RFP. A progressive increase in G' for all formulations was noted over the 5-hour duration with the drug-free formulations gelling at a faster rate than the drug-loaded formulations. This may be a result of the presence of more uninterrupted reaction sites available for Polyelectrolyte complexation in the drug-free formulations, thus, supporting the FTIR-implication of possible RFP interference with NH^{3+} and PO^{3-} reaction sites. During the 5-hour gelation period, it was noted that SL-CT 1:1 and SL-CT 3:1 reached a maximum G' of 282Pa (±13) and 319Pa (±11), respectively, while SL-CT-RFP 1:1 and SL-CT-RFP 3:1 peaked at 163Pa (±10) and 242Pa (±11), respectively. This may reflect the formation of a slightly disrupted PEC matrix and gelling formation in response to RFP loading whereas the drug-free formulations are able to maintain a more compact and continuous gelling arrangement throughout the sample matrix.

3.3.8. Textural transitions in response to variations in SL in the RFP-loaded lipopolysaccharide PEC nanoparticulate tablets

Textural profiling, as presented in table 3.4, revealed that increased SL ratio in the SL-CT-RFP 3:1 formulation presented with a greater force of 12.48N and fracture energy of 0.026J to initiate a break in the tablet matrix whereas the 1:1 formulation achieved a break in the tablet structure at 10.48 N with a corresponding energy of 0.021 J. In addition to the PEC formation resulting from SL-CT electrostatic interactions, the increased mechanical strength of the 3:1 formulation could further be attributed to possible interactions arising from SL-RFP, as noted in the FTIR spectra and XRPD diffractograms. Reduced crystallinity of the

lipopolysaccharide nanoparticulate system in response to increased SL ratios, as observed in XRPD analysis, suggests the formation of a less brittle tablet matrix imparted by a slight plasticizing effect of the soy lecithin phospholipid.

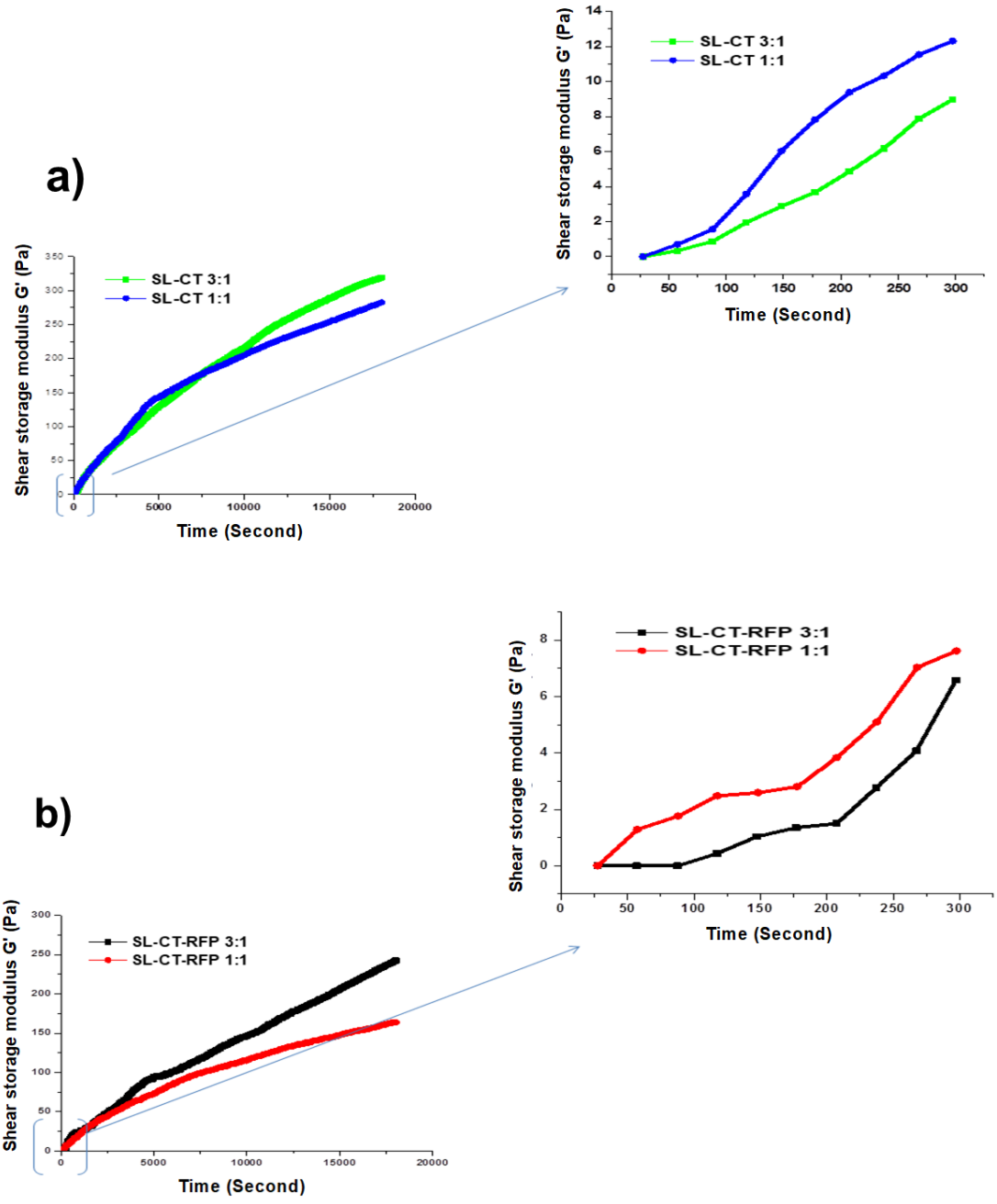


Figure 3.6. Kinetic gelation plots of a) SL-CT 1:1 and SL-CT 3:1, and b) SL-CT-RFP 1:1 and SL-CT-RFP 3:1 presenting the shear storage modulus (G') (Pa) observed over a 5-hour timeframe at 37^0C.

In this case, a portion of energy is dissipated throughout the matrix before reaching a break in the system whereas a highly brittle matrix results in immediate breakage and cracking upon application of force due to decreased deformability of the matrix system. Likewise, the enhanced mechanical attributes obtained via increased SL in the PEC particulates correspond to the enhanced elastic (G') rheological properties of the 3:1 formulation (242Pa) compared to the 1:1 formulation (163Pa).

Table 3.4. Profiling the Hardness, Compressibility and Fracture energy of SL-CT-RFP 1:1 and SL-CT-RFP 3:1 as a function of the SL: CT ratio

Formulation	Hardness (N)	Compressibility (N mm)	Fracture energy (J)
SL-CT-RFP (1:1)	10.4768	20.529	0.021
SL-CT-RFP (3:1)	12.4815	25.903	0.026

3.3.9. Optical characterization and stability of the lipopolysaccharide PEC particulates in aqueous suspension

Light scattering analysis of the synthesized drug-free (SL-CT) and drug-loaded (SL-CT-RFP) PEC particulates was performed. This analysis is based on the principle of particle migration and particle concentration variation within the sample. The phenomena of coalescence and flocculation are detected through increases in particle size of the sample. This technique measures the migration of colloidal particles toward the 1) bottom of the sample (sedimentation), 2) top of the sample (creaming) or 3) middle portion of the sample where particle aggregation leads to increased particle size (flocculation or coalescence). The result of this particle migration is expressed as the intensity of delta backscattering (ΔBS) or transmission (T) where an increase in ΔBS at the bottom of the sample with a corresponding decrease in T at the top of the sample indicates sedimentation kinetics. The reverse is true for the case of creaming kinetics; whereas in flocculation or coalescence kinetics, a decrease in ΔBS is noted throughout all three sections of the sample (Celia *et al.*, 2009).

The stability characteristics of RFP-loaded and RFP-free nanoparticle formulations was evaluated as a function of ΔBS and it was observed that all formulations showed some level of destabilization, as shown in Figure 3.7 below. However, formulations with a higher amount

of SL (depicted in Figure 3.6b and d) displayed enhanced stability as these formulations exhibited minimal changes in ΔBS of less than 5% as compared to formulations with a lower amount of SL where more than 10% ΔBS was noted (Figure 3.7a and c). This may be related to the emulsifying properties of SL (Gan *et al.*, 2014) which assists in the reduction of surface tension between the particles and the dispersion medium, thus, keeping the PEC particulates homogenously suspended in the liquid phase. Furthermore, an increase in sample particulate size at the middle and top portions of the sample indicated by increased ΔBS of 15% and 18%, respectively, was observed in Figure 3.7a of the SL-CT 1:1 complex. Similarly, The SL-CT 3:1 complex, Figure 3.7c, exhibited a ΔBS of 18% and 22% at the top and middle portion of the sample, respectively. This is indicative of possible coalescence and aggregation of the suspended particles at the top and middle portions of the samples, respectively.

The particle-migration dynamics over the 5-minute analysis period revealed that the incorporation of RFP into the lipopolysaccharide nanocomplex instigated slight changes in the stability of the formulation, indicated by changes in ΔBS and T along each time interval, compared to the RFP-free systems which maintained steady ΔBS levels over the test time-frame. This is likely due to overall increased particle size and ionic charge (Table 3.1) upon RFP-encapsulation, as particularly noted with the SL-CT 3:1 formulation demonstrating a particle size change from 232.8 nm to 274.2 nm and surface charge of +22.2 mV to +30.7 mV. However, it should be noted that the addition of increased SL plays an important function in the maintenance of stability of the nanocomplex system which may be attributed to the increased elastic response of the system as noted from the shear storage moduli of 163 Pa (1:1) to 242 Pa (3:1) in RFP-loaded formulations and from 282 Pa to 319 Pa in RFP-free formulations, respectively. As such, SL-CT-RFP 3:1 and SL-CT 3:1 displayed the highest level of stability compared to SL-CT 1:1 and SL-CT-RFP 1:1.

Dispersion stability of nanoparticulate in suspension influences the therapeutic efficacy of the formulation in terms of drug-dose obtained post-reconstitution and before oral administration. Therefore, a solid dosage form, such as tablets, may eliminate dose-administration concerns with regards to simple use and storage of the formulation.

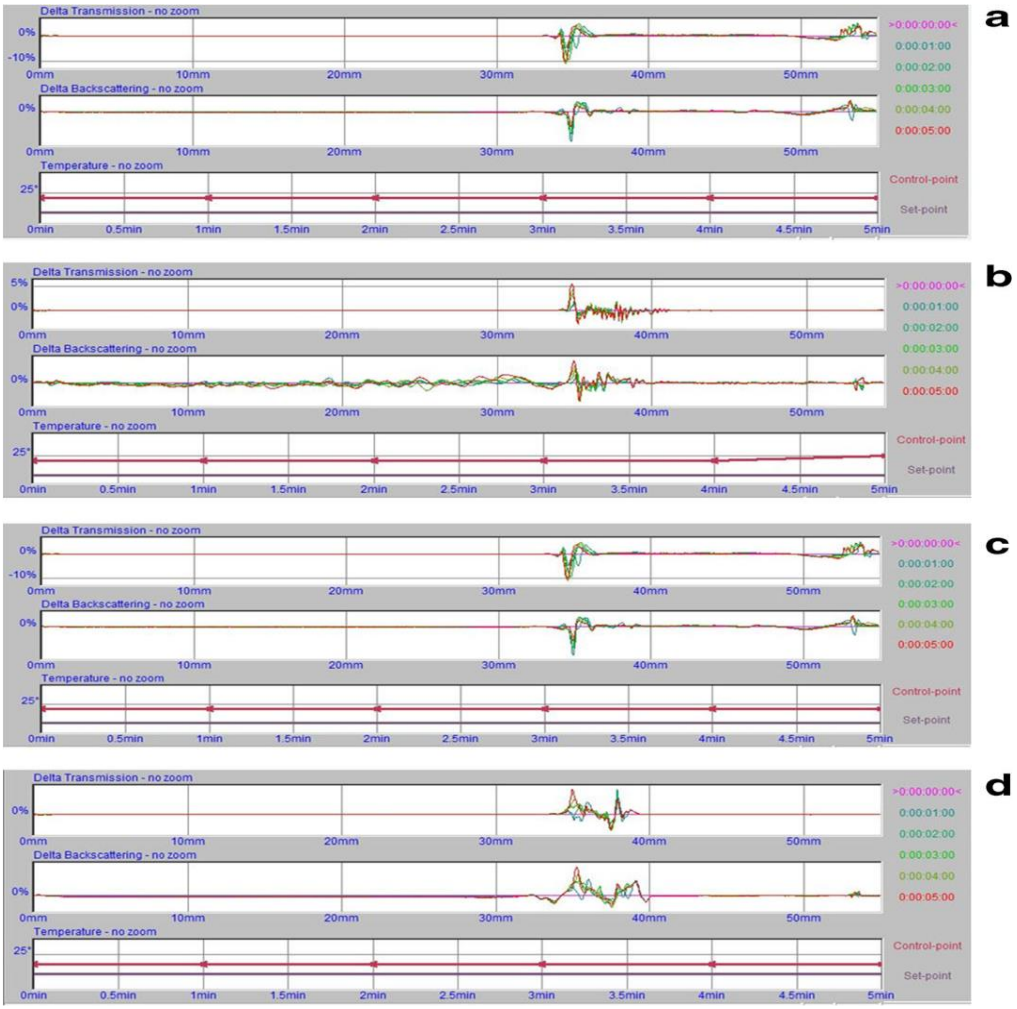


Figure 3.7. Representation of the destabilization kinetics of a) SL-CT 1:1, b) SL-CT 3:1, c) SL-CT-RFP 1:1 and d) SL-CT-RFP 3:1 suspension, indicating ΔBS and T measured at 25 ± 0.5 ^{0}C for 5-minutes duration.

3.3.10. Evaluation and mathematical modelling of RFP release from the lipopolysaccharide PEC particulates

The rate and quantity of drug release from a formulation plays a critical role in determining the dose administration frequency of a medicine. Thus, a formulation providing extended release kinetics reduces administration frequency, which is crucial in maintaining patient compliance in an infective disease-condition such as TB. The analysis of *in vitro* drug release behaviour of nanocarriers is a pertinent factor, among others (Hörter and Dressman, 1997), in determining the amount of drug available for potential absorption into the systemic circulation.

The *in vitro* release profile of RFP from the formulated lipopolysaccharide PEC particulates was investigated alongside comparator formulations (SL-CT+RFP, MSL+RFP+CT, SL+CT+RFP and Free RFP). As shown in Figure 3.8, it was observed that the *in situ* complexes of SL+CT+RFP (mixing of pristine polymers and drug powder), SL-CT+RFP 1:1

(*in situ* mixing of RFP with the formulated SL-CT 1:1 complex) and Free RFP released 90%, 64% and 28% of drug content, respectively, within the first 4 hours, hence, exhibiting the fastest release profile. Free RFP formulation released 91% of drug content within the 24-hour study period. This rapid release behaviour may be attributed to a decrease or absence of intermolecular bonds between the parent polymers of the *in situ* formulation (SL+CT+RFP) and due to RFP existing in a simple dispersed form as opposed to encapsulated within the particles of the system (SL+CT+RFP, SL-CT+RFP 1:1 and Free RFP). Such release profiles are considered unsuitable for sustained delivery of RFP as it potentiates frequent administration and reduced patient compliance. It was further observed that formulations of MSL+RFP+CT and SL-CT+RFP 3:1, which involved blending of RFP within melted SL and the SL-CT 3:1 complex, provided a cumulative drug release of 22.8% and 20.8%, respectively. In this case, the direct blending and increased ratio of SL in the formulation contributed to decreased drug release.

Formulations, involving authentic RFP encapsulation during the solvent injection method, SL-CT-RFP 1:1 and SL-CT-RFP 3:1 exhibited slower drug release rate with a cumulative drug release of 11.4% and 6.4%, respectively, obtained over the 24-hour study period. The slower release profiles could be attributed to RFP-phospholipid electrostatic interaction and barriers imparted by the phospholipid matrix as deposition of the drug most likely occurred within the lipid bilayers (Barbieri *et al.*, 2013). In addition, this concept explains the low release rates observed in formulations with a higher proportion of SL as mentioned earlier (SL-CT-RFP 3:1 and SL-CT+RFP 3:1). Furthermore, RFP entrapped within the PEC matrix of the phospholipid-polysaccharide system contributes to slower release as passage of the drug molecules out of the system is dependent on disintegration of the PEC thus, reducing release rates. PEC particulates SL-CT-RFP 1:1 and 3:1 exhibited a significantly low cumulative drug release over a 24-hour period and hence require longer time periods for complete release of loaded drug to occur. In favour of a reasonable dosing frequency and drug-interaction time, it is possible to modulate drug release rates employing enzyme-triggered drug release tactics in conjunction with adjustments in SL ratios to assist in rupture of the internal nanoparticle structure, thereby, conferring faster release (Vårum *et al.*, 1997; Barbieri *et al.*, 2013).

Mathematical modelling of the drug release data (as listed in Table 3.5) was performed to offer insight into the underlying drug release mechanisms governing the observed release profiles in response to variations in polymer ratios and tablet-preparation methods. It is noted that tablets prepared by simple mixing of the pristine polymer and drug powders (SL+CT+RFP) followed the First-order release model (R^2 = 0.7231) where drug release occurred via non-Fickian anomalous transport as indicated by the *n*-value (> 0.45) of 0.5479 derived from the Korsmeyer-Peppas equation. Rapid disintegration of the compacted powders resulting in

prompt wetting and diffusional release of RFP from this formulation contributed to the fast drug release rate of 90% within the first 4 hours with complete release occurring at the end of 24 hours. Formulations involving coating of RFP with melted SL (MSL+RFP+CT) followed the Higuchi model with *n* = 0.4699 suggesting non-Fickian diffusional release where drug release was likely dependent on the extent of hydration and dissolution of the RFP-SL complex, hence the slower release rate of 22.81%.

Drug release from tablets prepared from the pre-formulated PEC (SL-CT+RFP (1:1): 64% and (3:1): 20.8%) displayed a significant decrease in release rates upon increase in SL ratio. The faster release of the 1:1 formulation (*n* = 0.2692) profile may be attributed to the dispersion of RFP molecules within the SL-CT PEC system where RFP is dispersed within the spaces of the polymer matrix but not necessarily encapsulated and complexed to the SL-CT PEC via intermolecular interactions. This arrangement of RFP throughout the tablet matrix allows for rapid water penetration, hydration and swelling of the system resulting in Fickian-diffusion of RFP molecules whereas the decreased release rates imparted by increased SL in the 3:1 formulation is possibly conferred by SL-RFP interactions in addition to the SL-CT complex. It is further noted that increased SL ratio imparts an increase in the *n*-value suggesting a gradual shift from diffusion-based release towards non-Fickian anomalous transport (*n* = 0.6013) and erosion-controlled release (Cheow and Hadinoto, 2012). This is particularly evident in the tablets prepared from the lyophilized powder of the PEC particulates obtained from the concurrent incorporation of SL, CT and RFP during the solvent injection synthesis which yielded exceptionally low drug release rates of 11.4% and 6.4% for the SL-CT-RFP 1:1 and 3:1 formulation, respectively. The release profiles transitions from Higuchi to Zero-order kinetics upon increased SL. The increase in *n*-value from 0.736 for the 1:1 PEC particulates to 1.2605 for the 3:1 PEC particulates implies the working of a super case II transport as the primary drug release mechanism where dissolution of the PEC-entrapped drug is time-dependent on polymer relaxation and erosion of the PEC particulates as opposed to only hydration and diffusion out of the system.

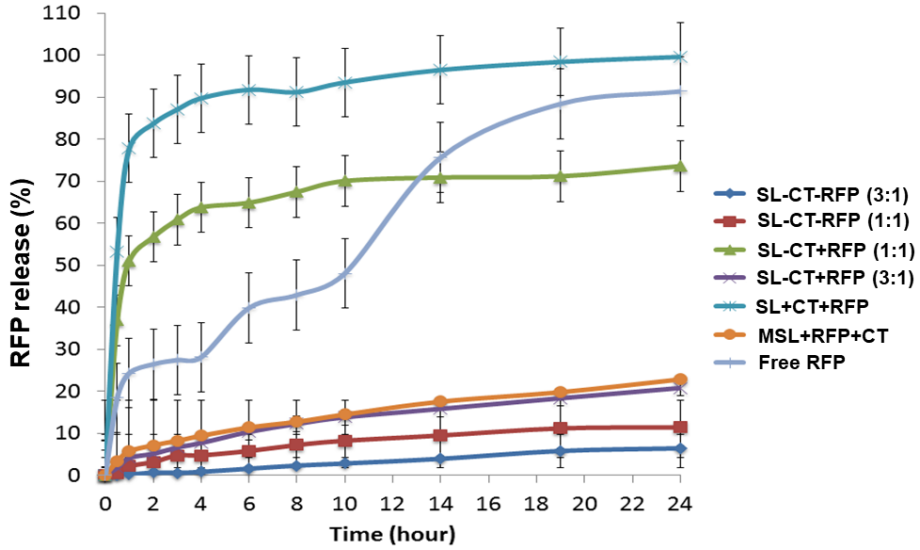


Figure 3.8. *In vitro* release profile of RFP from various indicated formulations at 37 ^{0}C and pH 6.8 (n=3, mean ± SD).

Table 3.5. Mathematical modeling for RFP release kinetics.

Formulation	Zero-order	First-order	Higuchi	Hixson-Crowell	Korsmeyer-Peppas		Best-fit model
	R^2	R^2	R^2	R^2	R^2	*n*	
SL+CT+RFP	0.5259	0.7231	0.677	0.6581	1	0.5479	First-order
MSL+RFP+CT	0.9398	0.9471	0.9879	0.9447	0.9908	0.4699	Higuchi
SL-CT+RFP 1:1	0.6942	0.7741	0.8306	0.748	0.9234	0.2692	Higuchi
SL-CT+RFP 3:1	0.9723	0.9771	0.988	0.9755	0.9794	0.6013	Higuchi
SL-CT-RFP 1:1	0.9032	0.9089	0.9678	0.907	0.89	0.736	Higuchi
SL-CT-RFP 3:1	0.9681	0.9675	0.904	0.9677	0.9811	1.2605	Zero-order

3.3.11. Evaluation of hydration dynamics controlling swelling and erosion behaviors of the RFP-loaded lipopolysaccharide PEC nanoparticulate tablets

The characteristics of fluid ingress into and hydration of the SL-CT-RFP tablets are critical in understanding the drug-release mechanisms observed in terms of swelling and erosion processes which influence the drug-release kinetics. The changes in hydration and subsequent swelling and erosion of the tablet matrix at various time points, as acquired from

MRI capture, is depicted in Figure 3.9 and 3.10. The gradual grayscale color transitions from dark to light areas indicate increased water penetration and hydration of the tablet as further swelling and subsequent erosion of the matrix ensues.

The hydration sequence of the SL-CT-RFP 1:1 formulation, depicted in Figure 3.9a, shows immediate disintegration and dissolution of the tablet matrix, into the surrounding media, occurring from the surface towards the core of the system with little or no presence of a defined swollen interface. This correlates to the drug-release kinetics obtained which indicated a slightly faster release pattern (11.4% cumulative release) controlled via a combination of diffusion and erosion processes (non-Fickian anomalous transport). In contrast, the hydration dynamics of the SL-CT-RFP 3:1 formulation, depicted in Figure 9b, shows the formation of a distinctive swollen zone (highlighted in red) surrounding an inner core of unhydrated matter. This gelled interface further retards the diffusion of RFP molecules out of the matrix (where RFP remains entrapped for a longer time in the gelled state of this layer) thereby presenting with decreased drug-release rates of 6.4% cumulative release. In this case, the predominant mechanism of super case II transport encompasses time-dependent PEC matrix hydration and subsequent swelling followed by polymer chain relaxation and erosion of the gelled region thereby following Zero-order drug-release kinetics where the matrix system does not disintegrate but maintains its bulk in a swollen or gelled state.

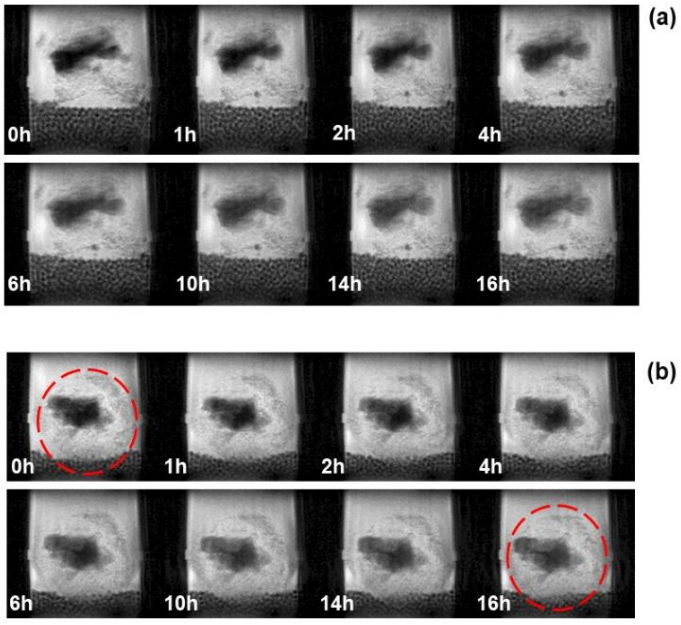


Figure 3.9. MRI acquisition illustrating the progression of fluid ingress and hydration of nanoparticulate tablets formulated from a) SL-CT-RFP 1:1 and b) SL-CT-RFP 3:1 (formation of a distinct swelling zone encircled in red) over a time-period of 16 hours.

3.3.12. Ex vivo Evaluation of RFP Permeation Across Porcine Intestinal Tissue from the Lipopolysaccharide PEC Particulates

The rate and extent of drug permeation through the intestinal barrier is governed by several factors, such as physiological, biological, and anatomical properties of the tissue and physicochemical properties of the drug and dosage form (Mariappan TT, Singh S., 2006), which ultimately influence drug solubility and bioavailability at the targeted delivery site. The Biopharmaceutics Classification System (BCS) has categorized RFP as a Class II drug (high permeability, low solubility); however, several studies have queried this classification and prior research has established RFP as a drug of low permeability and low solubility (BSC Class IV) (Buckley *et al.*, 2012; Collett, Tanianis-hughes and Warhurst, 2004; Ha, 2004).

The permeability kinetics of RFP from the lipopolysaccharide PEC particulate formulations (SL-CT-RFP 1:1 and SL-CT-RFP 3:1) were evaluated alongside capsulated free RFP, as represented in Fig. 3.11 and Table 3.6.

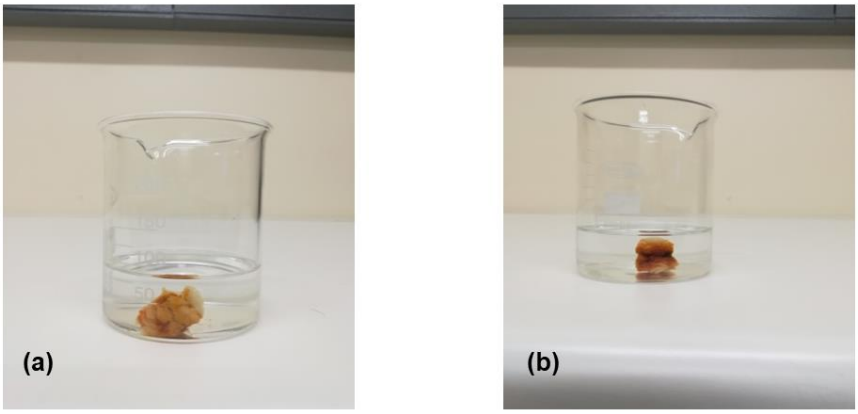


Figure 3.10. Images representing the instant hydration and swelling behaviours of (a) SL-CT-RFP 3:1 and (b) SL-CT-RFP 1:1 nanoparticle tablet after a 5-minute contact with PBS solution (pH6.8).

It was revealed that RFP release from SL-CT-RFP 1:1 and SL-CT-RFP 3:1 significantly demonstrated enhanced permeability over the 8-h study period as compared to that of free RFP, with an average flux of 1.22×10^{-3} mg cm^{-2} min^{-1}, 1.27×10^{-3} mg cm^{-2} min^{-1}, and 0.61×10^{-3} mg cm^{-2} min^{-1}, respectively. Furthermore, the effective permeability (P) of RFP was found to be 21.89×10^{-6} cm sec^{-1}, 22.85×10^{-6} cm sec^{-1} and 10.53×10^{-6} cm sec^{-1} in SL-CT-RFP 1:1,

SL-CT-RFP 3:1, and free RFP, respectively. The high permeability of RFP from the lipopolysaccharide PEC particulate formulations may be attributed to an amphiphilic property imparted by the PEComplexation which improved its interaction with the phospholipid bilayer of the intestinal membrane thereby contributing to a high migration of RFP molecules from the donor to the receptor chambers (Danaei *et al.*, 2018). The permeation of RFP from the PEC particulate formulations may occur via molecular transport across the membrane through the transcellular routes that often favours compounds of amphiphilic nature (Were *et al.*, 2003). Furthermore, as per FTIR analysis in Fig. 3.3a, the spontaneous chelation of RFP to CT and its encapsulation within the lipopolysaccharide PEC system could confer the drug molecule with increased solubility and hence, improved permeation upon dissolution. Compared to free RFP, the lipopolysaccharide PEC particulates proved as efficient nanocarriers of drug. The data obtained, showed no significant change in the permeability profile of RFP with increase in the SL-CT mass ratio as observed with SL-CT-RFP 1:1 and SL-CT-RFP 3:1 formulation, suggesting that CT (with constant mass in both formulation) played the major role in regards to the solubilization property of the lipopolysaccharide hybrid system towards dissolution and intestinal permeability of RFP.

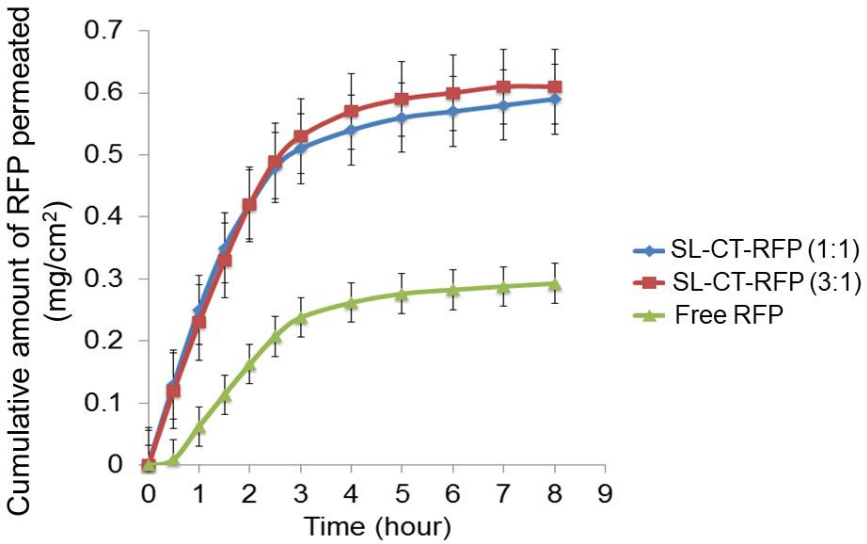


Figure 3.11. Cumulative RFP permeation across pig intestinal tissue from SL-CT-RFP 1:1, SL-CT-RFP 3:1 and Free RFP formulations (37°C).

Table 3.6. Cumulative amount of RFP permeated (M), Flux Value (J), and permeability (P) of RFP from SL-CT-RFP 1:1, SLCTLWCT-RFP 3:1, and free RFP formulations after 8-h exposure time.

Formulation	**M** (mg)	**J** (10^{-3} mg cm^{-2} min^{-1})	**P** (10^{-6} cm sec^{-1})
SL-CT 1:1	1.037	1.22	21.89
SL-CT 3:1	1.079	1.27	22.85
FREE RFP	0.518	0.61	10.53

RFP rifampicin, SL soy lecithin, CT low-molecular-weight chitosan

3.4. Conclusion

Conventional RFP delivery systems have been identified with several drawbacks, which include but are not limited to, poor bioavailability and sustained-release properties. The lipopolysaccharide PEC particulates synthesized by the solvent injection technique, reported in the present study, has shown efficacy in promoting a sustained-release profile with reduced drug release rates imparted by molecular interaction and subsequent encapsulation of RFP within a PEC system where polymer-polymer and polymer-drug interactions are likely, as confirmed by FTIR and DSC. MRI analysis further revealed and confirmed the drug release mechanism which involved entrapment of RFP within a swollen gel interface. A series of comparator formulations further demonstrated the importance of the solvent injection technique in acquiring a successfully formulated SL-CT-RFP complex wherein drug is bound within the PEC complex as opposed to dispersed around the PEC matrix. Increase in amorphous regions, indicated by XRD, suggests an improved solubility profile of the encapsulated RFP thereby, potentially improving bioavailability. The concentration-dependent incorporation of SL provides a means for adjusting particle-suspension stability and drug release rates while conferring enhanced viscoelasticity and deformability of the system. Furthermore, *ex vivo* permeation studies revealed that RFP permeability can be improved by incorporating it within PEC structure of SL-CT, thus favouring bioavailability. *In vivo* analysis is required to evaluate the therapeutic efficacy of the lipopolysaccharide PEC particulates in delivering adequate quantities of RFP via the oral delivery route.

3.5. References

Al-Remawi, M. *et al.* (2017) 'Chitosan/lecithin liposomal nanovesicles as an oral insulin delivery system', Pharmaceutical Development and Technology, 22(3), pp. 390–398. doi: 10.1080/10837450.2016.1213745.

Alkhader, E., Billa, N. and Roberts, C. J. (2017) 'Mucoadhesive Chitosan-Pectinate Nanoparticles for the Delivery of Curcumin to the Colon'. AAPS PharmSciTech, 18(4). doi: 10.1208/s12249-016-0623-y.

Amarnath, R. *et al.* (2016) 'Targeted delivery of rifampicin to tuberculosis-infected macrophages: design, in-vitro, and in-vivo performance of rifampicin-loaded poly (ester amide) s nanocarriers', International Journal of Pharmaceutics. Elsevier B.V., 513(1–2), pp. 628–635. doi: 10.1016/j.ijpharm.2016.09.080.

Bachhav, S. S. *et al.* (2017) 'Erratum to "Rifampicin Lipid-Polymer hybrid nanoparticles (LIPOMER) for enhanced Peyer's patch uptake" (International Journal of Pharmaceutics (2017) 532 (612–622) (S0378517317309067) (10.1016/j.ijpharm.2017.09.040))', International Journal of Pharmaceutics. Elsevier, 534(1–2), pp. 387–390. doi: 10.1016/j.ijpharm.2017.11.013.

Barbieri, S. *et al.* (2013) 'Lecithin/chitosan-controlled release nanopreparations of tamoxifen citrate: Loading, enzyme-trigger release and cell uptake', Journal of Controlled Release. Elsevier B.V., 167(3), pp. 276–283. doi: 10.1016/j.jconrel.2013.02.009.

Bawa, P. *et al.* (2011) 'Research Article: Composite Polyelectrolytic Matrix for Controlled Oral Drug Delivery', 12(1). doi: 10.1208/s12249-010-9576-8.

Bhise, K. S. *et al.* (2007) 'Effect of oppositely charged polymer and dissolution medium on swelling, erosion, and drug release from chitosan matrices.', AAPS PharmSciTech, 8(2), p. Article 44. doi: 10.1208/pt0802044.

Buckley, S. T. *et al.* (2012) 'European Journal of Pharmaceutical Sciences In vitro models to evaluate the permeability of poorly soluble drug entities: Challenges and perspectives', European Journal of Pharmaceutical Sciences. Elsevier B.V., 45(3), pp. 235–250. doi: 10.1016/j.ejps.2011.12.007.

Ceccaldi, C. *et al.* (2017) 'Validation and application of a nondestructive and contactless method for rheological evaluation of biomaterials', Journal of Biomedical Materials Research - Part B Applied Biomaterials, 105(8), pp. 2565–2573. doi: 10.1002/jbm.b.33797.

Celia, C. *et al.* (2009) 'Turbiscan Lab® Expert analysis of the stability of ethosomes® and ultradeformable liposomes containing a bilayer fluidizing agent', Colloids and Surfaces B: Biointerfaces, 72(1), pp. 155–160. doi: 10.1016/j.colsurfb.2009.03.007.

Cevher, E., Taha, M. A. M., Orlu, M., & Araman, A. (2008) 'Evaluation of Mechanical and Mucoadhesive Properties of Clomiphene Citrate Gel Formulations Containing Carbomers and Their Thiolated Derivatives', Drug Delivery, 15(1), pp. 57–67. doi: 10.1080/10717540701829234.

Cheng, W., Luo, Z., Li, L., & Fu, X. (2015) 'Preparation and Characterization of Debranched-Starch/Phosphatidylcholine Inclusion Complexes', Journal of Agricultural and Food Chemistry, 63(2), 634–641. doi:10.1021/jf504133c

Cheow, W. S. and Hadinoto, K. (2012) 'Self-assembled amorphous drug-polyelectrolyte nanoparticle complex with enhanced dissolution rate and saturation solubility', Journal of Colloid and Interface Science. Elsevier Inc., 367(1), pp. 518–526. doi: 10.1016/j.jcis.2011.10.011.

Collett, A., Tanianis-hughes, J. and Warhurst, G. (2004) 'Rapid induction of P-glycoprotein expression by high permeability compounds in colonic cells in vitro: a possible source of transporter mediated drug interactions ?', 68, pp. 783–790. doi: 10.1016/j.bcp.2004.05.006.

Costa, A. *et al.* (2016) 'The formulation of nanomedicines for treating tuberculosis', Advanced Drug Delivery Reviews. Elsevier B.V., 102, pp. 102–115. doi: 10.1016/j.addr.2016.04.012.

Costa, A., Sarmento, B. and Seabra, V. (2018) 'European Journal of Pharmaceutical Sciences Mannose-functionalized solid lipid nanoparticles are effective in targeting alveolar macrophages', European Journal of Pharmaceutical Sciences. Elsevier, 114(October 2017), pp. 103–113. doi: 10.1016/j.ejps.2017.12.006.

Danaei, M. *et al.* (2018) 'Impact of particle size and polydispersity index on the clinical applications of lipidic nanocarrier systems', Pharmaceutics, 10(2), pp. 1–17. doi: 10.3390/pharmaceutics10020057.

Date, P. V., Samad, A. and Devarajan, P. V. (2010) 'Freeze Thaw: A Simple Approach for Prediction of Optimal Cryoprotectant for Freeze Drying', AAPS PharmSciTech, 11(1), pp. 304–313. doi: 10.1208/s12249-010-9382-3.

Devi, N. and Maji, T. K. (2009) 'Preparation and Evaluation of Gelatin/Sodium Carboxymethyl Cellulose Polyelectrolyte Complex Microparticles for Controlled Delivery of Isoniazid', AAPS PharmSciTech, 10(4), pp. 1412–1419. doi: 10.1208/s12249-009-9344-9.

Dora, C. P. *et al.* (2017) 'Improved metabolic stability and therapeutic efficacy of a novel molecular gemcitabine phospholipid complex', International Journal of Pharmaceutics. Elsevier B.V., 530(1–2), pp. 113–127. doi: 10.1016/j.ijpharm.2017.07.060.

El-ridy, M. S. *et al.* (2007) 'Biological evaluation of pyrazinamide liposomes for treatment of Mycobacterium tuberculosis', 330, pp. 82–88. doi: 10.1016/j.ijpharm.2006.09.017.

Esmaeili, F., Hosseini-nasr, M. and Rad-malekshahi, M. (2007) 'Preparation and antibacterial activity evaluation of rifampicin-loaded poly lactide-co-glycolide nanoparticles', 3, pp. 161–167. doi: 10.1016/j.nano.2007.03.003.

Formariz, T. P. *et al.* (2008) 'Structural changes of biocompatible neutral microemulsions stabilized by mixed surfactant containing soya phosphatidylcholine and their relationship with doxorubicin release', 63, pp. 287–295. doi: 10.1016/j.colsurfb.2007.12.021.

Gan, L. J. *et al.* (2014) 'Emulsifying properties of lecithin containing different fatty acids obtained by immobilized lecitase ultra-catalyzed reaction', JAOCS, Journal of the American Oil Chemists' Society, 91(4), pp. 579–590. doi: 10.1007/s11746-013-2396-8.

Hämäläinen, M. D., & Frostell-Karlsson, A. (2004) 'Predicting the intestinal absorption potential of hits and leads', Drug Discovery Today: Technologies, 1(4), 397–405. doi:10.1016/j.ddtec.2004.09.004

Heinen, C. *et al.* (2013) 'Mechanistic basis for unexpected bioavailability enhancement of polyelectrolyte complexes incorporating BCS class III drugs and carrageenans', European Journal of Pharmaceutics and Biopharmaceutics. Elsevier B.V., 85(1), pp. 26–33. doi: 10.1016/j.ejpb.2013.03.010.

Hörter, D. and Dressman, J. B. (1997) 'Influence of physicochemical properties on dissolution of drugs in the gastrointestinal tract', Advanced Drug Delivery Reviews, 25(1), pp. 3–14. doi: 10.1016/S0169-409X(96)00487-5.

Jain, S. *et al.* (2018) 'Amphotericin B Loaded Chitosan Nanoparticles: Implication of Bile Salt Stabilization on Gastrointestinal Stability, Permeability and Oral Bioavailability', AAPS PharmSciTech. AAPS PharmSciTech, (10). doi: 10.1208/s12249-018-1153-6.

Kumar, S., Dutta, P. K. and Koh, J. (2011) 'International Journal of Biological Macromolecules A physico-chemical and biological study of novel chitosan – chloroquinoline derivative for biomedical applications', International Journal of Biological Macromolecules. Elsevier B.V., 49(3), pp. 356–361. doi: 10.1016/j.ijbiomac.2011.05.017.

Laridi, R. *et al.* (2003) 'Liposome encapsulated nisin Z: Optimization, stability and release during milk fermentation', International Dairy Journal, 13(4), pp. 325–336. doi: 10.1016/S0958-6946(02)00194-2.

Liu, M. *et al.* (2014) ‘Developments of mucus penetrating nanoparticles’, Asian Journal of Pharmaceutical Sciences. Elsevier Ltd, 10(4), pp. 275–282. doi: 10.1016/j.ajps.2014.12.007.
Luo, Y. et al. (2015) ‘Solid lipid nanoparticles for oral drug delivery: Chitosan coating improves stability, controlled delivery, mucoadhesion and cellular uptake’, Carbohydrate Polymers, 122, pp. 221–229. doi: 10.1016/j.carbpol.2014.12.084.
Mariappan TT, Singh S. (2006) 'Positioning of rifampicin in the biopharmaceutics classification system (BCS)', Clin Res Regul Af f ., 2 3 (1), pp. 1 – 1 0. h t t p s : / / d o i . o rg / 1 0 . 1 0 8 0 /10601330500533990.
Nagpal, K., Singh, S. K. and Mishra, D. N. (2010) ‘Chitosan Nanoparticles: A Promising System in Novel Drug Delivery’, Chemical & Pharmaceutical Bulletin, 58(11), pp. 1423–1430. doi: 10.1248/cpb.58.1423.

Norris, D. A. and Sinko, P. J. (1997) ‘Effect of size, surface charge, and hydrophobicity on the translocation of polystyrene microspheres through gastrointestinal mucin’, Journal of Applied Polymer Science, 63(11), pp. 1481–1492.

Ohashi, K. *et al.* (2009) ‘One-step preparation of rifampicin / poly (lactic-co-glycolic acid) nanoparticle-containing mannitol microspheres using a four- fl uid nozzle spray drier for inhalation therapy of tuberculosis’, Journal of Controlled Release. Elsevier B.V., 135(1), pp. 19–24. doi: 10.1016/j.jconrel.2008.11.027.

Patidar, A. et al. (2010) ‘A review on novel lipid based nanocarriers’, International Journal of Pharmacy and Pharmaceutical Sciences, 2(4), pp. 30–35.

Patil, J. *et al.* (2015) ‘A novel approach for lung delivery of rifampicin-loaded liposomes in dry powder form for the treatment of tuberculosis’, Lung India, 32(4), p. 331. doi: 10.4103/0970-2113.159559.

Pattabhi, K., Howdary, R. C. and Ao, Y. S. R. R. (2004) ‘Mucoadhesive Microspheres for Controlled Drug Delivery’, 27(11), pp. 1717–1724.

Pawar, H., Douroumis, D. and Boateng, J. S. (2012) ‘Colloids and Surfaces B : Biointerfaces Preparation and optimization of PMAA – chitosan – PEG nanoparticles for oral drug delivery’, Colloids and Surfaces B: Biointerfaces. Elsevier B.V., 90, pp. 102–108. doi: 10.1016/j.colsurfb.2011.10.005.

Pepic, I., Hafner, A. and Lovric, J. (2011) ‘Lecithin / chitosan nanoparticles for transdermal delivery of melatonin’, 28(8), pp. 807–815. doi: 10.3109/02652048.2011.622053.

Petkar, K. C. *et al.* (2018) ‘Development of Novel Octanoyl Chitosan Nanoparticles for Improved Rifampicin Pulmonary Delivery: Optimization by Factorial Design’, AAPS

PharmSciTech. AAPS PharmSciTech, 19(4), pp. 1758–1772. doi: 10.1208/s12249-018-0972-9.

Pinheiro, M. and Reis, S. (2011) 'Liposomes as drug delivery systems for the treatment of TB R eview', 6, pp. 1413–1428.

Rappuoli, R. and Aderem, A. (2011) 'A 2020 vision for vaccines against HIV, tuberculosis and malaria', Nature. Nature Publishing Group, 473(7348), pp. 463–469. doi: 10.1038/nature10124.

Rawal, T. *et al.* (2018) 'Chitosan Nanoparticles of Gamma-Oryzanol: Formulation, Optimization, and In vivo Evaluation of Anti-hyperlipidemic Activity', AAPS PharmSciTech. AAPS PharmSciTech, 19(4), pp. 1894–1907. doi: 10.1208/s12249-018-1001-8.

Sahoo, D. *et al.* (2009) 'Chitosan: A new versatile bio-polymer for various applications', Designed Monomers and Polymers, 12(5), pp. 377–404. doi: 10.1163/138577209X12486896623418.

Salomon, C., Goycoolea, F. M. and Moerschbacher, B. (2017) 'Recent Trends in the Development of Chitosan-Based Drug Delivery Systems', AAPS PharmSciTech. AAPS PharmSciTech, 18(4), pp. 933–935. doi: 10.1208/s12249-017-0764-7.

Shtenberg, Y. *et al.* (2018) 'Mucoadhesive alginate pastes with embedded liposomes for local oral drug delivery', International Journal of Biological Macromolecules, 111, pp. 62–69. doi: 10.1016/j.ijbiomac.2017.12.137.

Singh, C. *et al.* (2014) 'Novel rifampicin-phospholipid complex for tubercular therapy: Synthesis, physicochemical characterization and in-vivo evaluation', International Journal of Pharmaceutics. Elsevier B.V., 460(1–2), pp. 220–227. doi: 10.1016/j.ijpharm.2013.10.043.

Singh, C. *et al.* (2017) 'In Vitro-In Vivo Evaluation of Novel Co-spray Dried Rifampicin Phospholipid Lipospheres for Oral Delivery', AAPS PharmSciTech, 18(1), pp. 138–146. doi: 10.1208/s12249-016-0491-5.

Siyawamwaya, M. *et al.* (2015) 'A Review: Overview of Novel Polyelectrolyte Complexes as Prospective Drug Bioavailability Enhancers', International Journal of Polymeric Materials and Polymeric Biomaterials, 64(18), pp. 955–968. doi: 10.1080/00914037.2015.1038816.

Smart, J. D. (2005) 'The basics and underlying mechanisms of mucoadhesion B', 57, pp. 1556–1568. doi: 10.1016/j.addr.2005.07.001.

Sonvico, F. *et al.* (2006) 'Formation of self-organized nanoparticles by lecithin / chitosan ionic interaction', 324, pp. 67–73. doi: 10.1016/j.ijpharm.2006.06.036.

Sosnik, A. *et al.* (2010) ‘New old challenges in tuberculosis: Potentially effective nanotechnologies in drug delivery ☆’, Advanced Drug Delivery Reviews. Elsevier B.V., 62(4–5), pp. 547–559. doi: 10.1016/j.addr.2009.11.023.

Vårum, K. M., Myhr, M. M., Hjerde, R. J. N., & Smidsrød, O. (1997) ‘In vitro degradation rates of partially N-acetylated chitosans in human serum’, Carbohydrate Research, 299(1-2), pp. 99–101. doi:10.1016/s0008-6215(96)00332-1

Were, L. M. *et al.* (2003) ‘Size, Stability, and Entrapment Efficiency of Phospholipid Nanocapsules Containing Polypeptide Antimicrobials’, Journal of Agricultural and Food Chemistry, 51(27), pp. 8073–8079. doi: 10.1021/jf0348368.

Zhang, N., Wardwell, P. R. and Bader, R. A. (2013) ‘Polysaccharide-based micelles for drug delivery’, Pharmaceutics, 5(2), pp. 329–352. doi: 10.3390/pharmaceutics5020329.

CHAPTER 4

DESIGN OF MANNOSE-FUNCTIONALIZED HYBRID LIPOPOLYSACCHARIDE NANOPARTICLES FOR MACROPHAGE-TARGETED DELIVERY OF RIFAMPICIN AND ISONIAZID

4.1. Introduction

Tuberculosis (TB), caused by *Mycobacterium tuberculosis* (Mtb), is an infectious disease ravaging the healthcare system of the world, however it is predominantly found in Africa, Asia and South America countries, killing more people than any other infectious disease (Kaur, Garg and Narang, 2016). In 2018, World Health Organization (WHO) reported an estimated 10 million new cases and 1.5 million deaths from TB infection (WHO 2019). The disease manifestation and virulent nature of the causative organism presented serious challenge to chemotherapeutic management. Mtb-infected macrophages usually form clusters, called granulomas, which are enclosed by several immune cells, cholesterol, and fatty acids. The granulomas naturally function to eliminate infectious agents that invade the body system by localizing and containing the infection, preventing it from growing and replicating. However, these cells are unable to destroy Mtb or inhibit their energy generating ability, thus making the macrophage cells a major haven for Mtb (Donnellan and Giardiello, 2019). The formation of granuloma is a characteristic manifestation of Mtb infection, especially in latent TB infection, and plays a fundamental role in immune pathogenesis, in which ten percent of cases sees bacilli escaping from granulomas and proceeding to cause active disease (Miranda *et al.*, 2012). Cells internalize particulate materials via phagocytosis, endocytosis, and pinocytosis. By taking up nanoparticles, especially when it involves macrophages where Mtb colonize, the particulate may be co-colonized with the pathogen allowing for very specific targeting.

The exploitation of nanoparticles in drug delivery formulations is versatile due to the outstanding properties provided by their nanometric size range, which includes bioactive protection, controlled release of drug content, biocompatibility, and biodegradability to a non-toxic end-product (Saraogi *et al.*, 2011). Nanocarriers have been employed to target TB, in which the design strategies mostly involve the use of polymeric or liposomal nanosystem loaded with the first-line anti-TB drugs, rifampicin (RFP) or isoniazid (ISN) (Pandey *et al.*, 2003; Pandey and Khuller, 2005; Ohashi *et al.*, 2009a; Hirota *et al.*, 2010; Aboutaleb *et al.*, 2012; Nanoparticles *et al.*, 2012; Chuan *et al.*, 2013; Dube *et al.*, 2014; Kaur, Garg and Narang, 2016; Vieira *et al.*, 2017; Hakkimane *et al.*, 2018). Studies have shown that infected macrophages can be specifically targeted using nanocarriers with surface modification to

deliver encapsulated anti-TB drugs, thus producing therapeutic drug concentration at this site (Vieira *et al.*, 2018; Costa, Sarmento and Seabra, 2018b). This could help reduce the dose required to achieve therapeutic concentration at infection site and consequently minimizing dose-dependent side effect and drug toxicity. Macrophages have several surface receptors (e.g. mannosyl, galactosyl, lectin, and Fc) which is used to recognise and take up particulate nanocarriers. Owing to this fact, nanocarriers containing ligands to the respective receptors are better internalized by the macrophages when compared with nanocarriers without such ligands (Kaur, Jain and Tiwary, 2008). Among all nanocarrier system (e.g. liposomes, dendrimers, polymeric and solid lipid nanoparticles) that have been used for macrophage targeting, engineered nanoparticles have been recognized to possess better accumulation in organs that are rich in macrophage such as liver, lungs, and spleen because of their preferential uptake (Kumar *et al.*, 2006; Jain *et al.*, 2008; Kaur, Jain and Tiwary, 2008; Nimje *et al.*, 2009). They are better oriented to target and deliver the loaded drug selectively to the alveolar macrophages.

The nanoparticulate of lipopolysaccharide origin is renowned for their outstanding biocompatibility, biodegradability, adaptability, drug loading capacity and encapsulation efficiency, safety and cost-effectiveness (Patidar *et al.*, 2010; Salomon, Goycoolea and Moerschbacher, 2017). Furthermore, due to their inherent polyelectrolyte complex structure as well as the cationic surface provided by the nanostructure, they may provide several modification opportunities for conjugating with, for example, specific ligand for cell targeting purpose, cross-linkers, and coating substances. Considering the above, this study aimed to synthesize and characterize mannose-functionalized hybrid lipopolysaccharide nanoparticles (Mn-CT-SL) loaded with RFP and ISN, and to study the concurrent release of the loaded bioactive in simulated physiological environment. Furthermore, we also evaluated the cytocompatibility as well as the impact of nanoparticle mannosylation on cellular uptake and intracellular drug accumulation.

4.2. Materials and Methods

4.2.1. Materials

Low molecular weight chitosan (CT) (75-85% deacetylated), L-α-Lecithin soybean (a concentrate of soybean lecithin with 94% phosphatidylcholine and < 2% triglycerides), ethylenediaminetetraacetic acid (EDTA), fluorescein isothiocyanate (FITC) probe, rifampicin (RFP), isoniazid (ISN), phosphate-buffered saline (PBS) and dimethyl sulfoxide (DMSO) were purchased from Sigma-Aldrich (St. Louise, MO, USA). Ethanol (ETOH), concentrated sulphuric acid, phenol and glacial acetic acid were procured from Merck Pty Ltd., South Africa. Murine macrophage RAW 264.7 cell line was purchased from ATCC, Virginia USA. Dulbecco's

Modified Eagle's medium (DMEM), fetal bovine serum (FBS), Penicillin-streptomycin antibiotic, Trypsin-EDTA, and 3-(4,5-dimethylthiazol-2-yl)-2,5-diphenyltetrazolium bromide (MTT) were from Life Bioscience (Oakleigh, VIC, Australia). All chemicals were of analytical reagent grade and used without prior modification. Double deionized water (DDW) was used for all the preparations.

4.2.2. Methods

4.2.2.1. Preparation of the Lipopolysaccharide Formulations

4.2.2.1.1. Preparation of Hybrid Chitosan-Lecithin RFP-ISN-loaded (CT-SL-RFP-ISN) Nanoparticles

CT-SL-RFP-ISN nanoparticles were prepared using a modified solvent injection technique as previously described in our lab (Sumaila *et al.*, 2019). Briefly, a 10 mL of 30 mg/mL ethanolic solution of L-α-Lecithin soybean (SL) was prepared followed by an addition of 30 mg of RFP which was thoroughly dissolved to obtain a homogenous SL-RFP solution. Similarly, CT-ISN solution was prepared by dissolving 100 mg of the polymer in 70 mL of acetic acid (1% $^{v}/_{v}$) followed by an addition of 20 mL of 1.5 mg/mL DDW solution of ISN. The CT-SL-RFP-ISN nanoparticle suspension was obtained by injecting 10 mL of the previously prepared SL-RFP solution into 90 mL of CT-ISN solution via a syringe (inner diameter 0.75 mm, flow rate 40 mL/min) with subsequent mechanical stirring. The resulting nanoparticle suspension was centrifuged at 5000 rpm for 30 minutes, the clear supernatant discarded, and sediment lyophilized over 24 hours to obtain a dried nanoparticle powder. Placebo nanoparticles and FITC-loaded CT-SL were prepared following the same procedure but without the drug and with FITC probe, respectively.

4.2.2.1.2. Preparation of mannosylated Nanoparticles

Coating of the nanoparticles (CT-SL-RFP-ISN and CT-SL) with mannose was adapted from previously established methods (Pinheiro *et al.*, 2016; Vieira *et al.*, 2017; Costa, Sarmento and Seabra, 2018b) with slight modifications. In details, a 50 mM mannose solution was prepared in acetate buffer (pH 4.0) and added to the nanoparticle suspension. The mixture was left under constant and gentle stirring at room temperature for 48 hours to reach optimal conjugation. The reaction condition encouraged ring opening of the mannose molecule, and subsequent reaction of the aldehyde group with free amine functionality present at the surface of the nanoparticles resulted in the formation of a Schiff's base (–N=CH–) as shown in (Figure 4.1). The mannosylated formulation was dialyzed (dialysis bag; MWCO 12–14 kDa) against DDW for a period of 1 hour to remove the unreacted mannose and other impurities. It was further lyophilized without cryoprotectant so as to assess the attachment of the mannose to

the surface of nanoparticles by FT-IR.

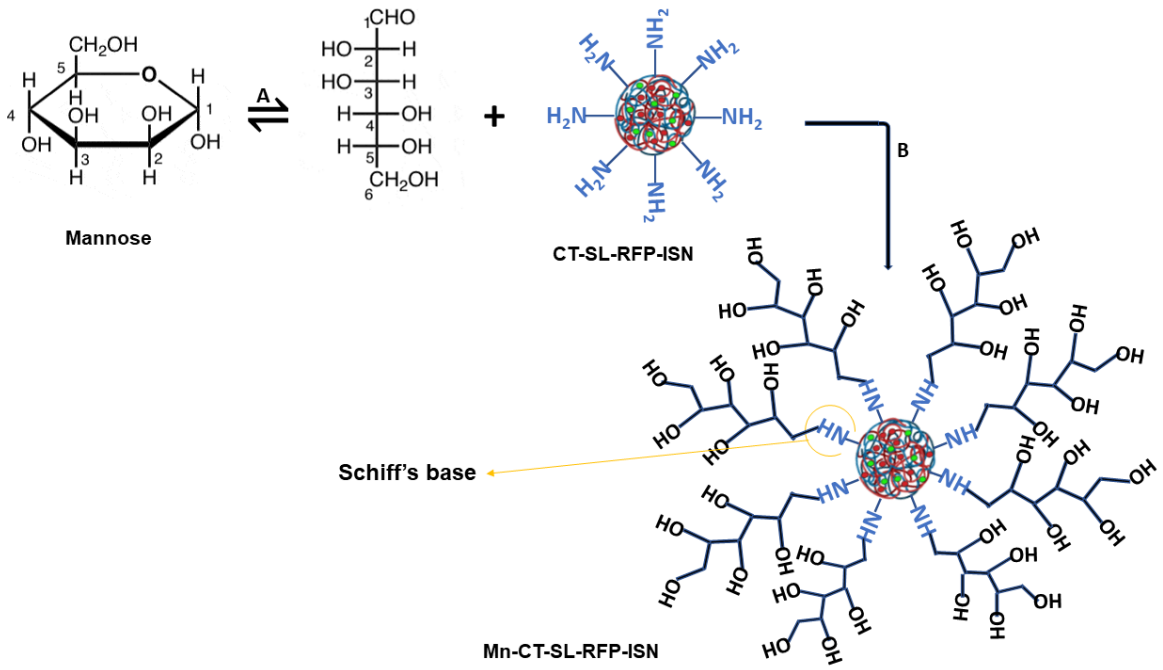


Figure 4.1: Reaction scheme for the mannosylation of CT-SL RFP-ISN-loaded nanoparticles. A = Acetate buffer at pH 4.0, B = Constant stirring for 48 hours, CT-SL-RFP-ISN = unmannosylated Rifampicin/Isoniazid-loaded nanoparticle, Mn-CT-SL-RFP-ISN = mannosylated Rifampicin/Isoniazid-loaded nanoparticle. Mannose isomerized, in the presence of acetate buffer at pH 4.0, and formed an open ring molecule, which then interacted with the positively charged suface of the CT-SL-RFP-ISN nanoparticles to produce the mannose-functionalized nanostructure, Mn-CT-SL-RFP-ISN.

4.2.2.2. Characterization of the Lipopolysaccharide Formulations

4.2.2.2.1. Evaluation of Particle Size, polydispersity index, Zeta Potential, Conductivity, and Structural Morphology

The hydrodynamic diameter, polydispersity index (PdI), surface charge, and conductivity of the nanoparticles were measured using the Malvern Zetasizer Nano ZS (Malvern Instruments, Worcestershire, UK). Briefly, 100 mg of all samples (placebo and RFP-ISN-loaded nanoparticles, and mannosylated nanoparticles) were dispersed in DDW and sonicated for 30 seconds. A 2 mL sample of the nanoparticle suspension was placed in disposable cuvettes and analyzed at 25 ^{0}C for average particle size, PdI, zeta potential, and conductivity.

The morphological characteristic of the nanoparticles was observed using Scanning Electron Microscopy (SEM). 100 µL of the synthesized nanoparticle suspension was dropped on an

aluminium specimen stub and dried overnight followed by sputter-coating with gold for four minutes at 20 kilovolts. Images of the nanoparticles were obtained from a Phenom™ scanning electron microscope (FEI Company, Hillsboro, OR, USA).

4.2.2.2.2. Quantification of mannose linkage on the surface of functionalized lipopolysaccharide nanoparticles

The density of mannose on Mn-CT-SL nanoparticles was evaluated using the previously reported phenol-sulfuric acid mannose detection assay (Carrillo-Conde *et al.*, 2011) with slight modification. Briefly, 50 µL of Mn-CT-SL nanoparticle solutions (5mg/mL) were dispensed into a 96-well plate and diluted with 50 µL DDW. Concentrated sulfuric acid (150 µL) was ejected quickly and the plate gently shaken to allow homogenous mixing of the solution. A freshly prepared 5% (w/v) solution of phenol (30 µL) was added and the reaction allowed to proceed for 30 minutes permitting adequate reduction of mannose and CT with corresponding change in colour of the solution. Unmannosylated CT-SL nanoparticles were used as controls to account for polymer interference with the assay. Absorbance of standards and unknown samples were measured at a wavelength of 490 nm using a microplate reader (Perkin Elmer VICTOR X 3 2030 MultiLabel Plate Reader). The surface coverage of mannose molecules on the functionalized nanoparticles, expressed in microgram per milligram of nanoparticle, was computed relative to standard curve. The amount of mannose attached to Mn-CT-SL nanoparticle at various mannose-CT-SL reaction time (24-, 48- and 72-hour) was calculated to evaluate the effect of mannosylation reaction time on the degree of mannose-conjugation.

4.2.2.2.3. Determination of RFP-ISN-Loading Capacity and Encapsulation Efficiency of the Nanoparticles

The loading capacity (LC) and encapsulation efficiency (EE) of RFP and ISN within the mannosylated and unmannosylated nanoparticles (Mn-CT-SL-RFP-ISN and CT-SL-RFP-ISN) were determined by the indirect method as previously reported (Pinheiro *et al.*, 2016; Vieira *et al.*, 2018). Briefly, a known amount of the drug-loaded nanoparticles (3 mg) was dispersed in 5 mL DDW, shaken vigorously, and subjected to centrifugation for one hour at 5000 rpm. An aliquot of the clear supernatant was analyzed for RFP and ISN content using an Implen Nanophotometer (IMPLEN Nanophotometer™, Implen GmbH, Munchen Germany) set at λ_{max} = 475 nm and 264 nm, respectively. Triplicate measurements were carried out to determine the LC and EE of the nanoparticles using equations (4.1) and (4.2), respectively:

$$LC = \frac{DWt - DCsVs}{Mdp} \times 100 \quad (4.1)$$

$$EE = \frac{DWt - DCsVs}{Td} \times 100 \quad (4.2)$$

Where *DWt* indicated total amount of drug, *DCs* was the concentration of drug in the supernatant, *Vs* was the volume of supernatant, *DCsVs* was the total amount of unloaded drug in the supernatant, *Mdp* was the mass of drug-loaded nanoparticles (total mass of drug and nanocarriers), and *Td* was the total initial drug amount.

4.2.2.2.4. Analysis of molecular vibrational transitions using Fourier Transform Infrared (FTIR) Spectroscopy

Powdered samples of the lyophilized placebo, CT-SL-RFP-ISN and Mn-CT-SL-RFP-ISN nanoparticles, and native polymers were evaluated for interactions resultant of polyelectrolyte complex and Schiff's base formation. Samples were analyzed at a resolution of 4 cm^{-1} over a wavelength range of 4000 cm^{-1} to 650 cm^{-1} using the FTIR Spectrophotometer (PerkinElmer; Beaconsfield, BUCKS, UK) equipped with a horizontal attenuated total reflectance (ATR) sampling accessory with a diamond crystal.

4.2.2.2.5. Analysis of the Thermodynamic Properties of the Synthesized Nanoparticles

The thermal stability and decomposition temperature of the mannosylated nanoparticles (Mn-CT-SL-RFP-ISN and Mn-SL-CT), unmannosylated nanoparticles (CT-SL-RFP-ISN and CT-SL), and the constituent pristine polymers were evaluated using a Thermo gravimetric analyzer (TGA) (PerkinElmer, TGA 4000, Llantrisant, Wales, UK). Samples of 2 – 7 mg were placed in the TGA furnace and the measurements were done under nitrogen atmosphere with a heating rate of 20 °C per minute from 30 °C to 900 °C. The changes in sample weight, as well as the thermal stability, were recorded and evaluated as a function of temperature.

4.2.2.2.6. Stability profiling and optical characterization of Mn-CT-SL-RFP-ISN and CT-SL-RFP-ISN nanoparticles in suspension

Evaluation of the nanoparticulate stability and optical interactions of Mn-SL-CT-RFP-ISN and SL-CT-RFP-ISN nanoparticle suspensions were done using the Turbiscan™ LAB (Formulaction, L'Union, France). An aliquot (20 mL) of the RFP-ISN-loaded mannosylated and unmannosylated nanoparticle suspensions were introduced into specialized sample holders and analyzed at pre-determined intervals over a 60-minute duration at 25 ^{0}C. The instrument was fixed with a pulsed near infra-red-light source moving vertically along the sample collecting data at 40 µm-intervals. In addition, this instrument was equipped with two detectors, the transmission and backscattering detectors, positioned at 180° and 45°, respectively. The transmission detector detected the light that was transmitted through the suspended nanoparticles**,** while backscattering detector detected the light that was rebounded by the suspended nanoparticles. The changes in backscatter (∆BS) measurements, as obtained from Turbiscan™ LAB, were used to delineate nanoformulation stability.

4.2.2.2.7. *In vitro* evaluation of RFP and ISN release from the Mn-CT-SL-RFP-ISN and CT-SL-RFP-ISN nanoparticles

The release profiles of RFP-ISN-loaded mannosylated and unmannosylated nanoparticles were investigated using a dissolution tester (ERWEKA, USP Apparatus II, DT 126, UK) operated at a paddle revolution of 50 rpm over a 48-hour period. 10 mL aliquots of the prepared formulations were transferred into dialysis tubes (molecular weight cut-off of 12,000-14,000 Da; Sigma-Aldrich), which were previously hydrated in DDW for three hours before use to make it glycerol- and sulphide-free. The tubes were fastened at both ends and separately suspended in 900 mL of PBS at three different pH values (4.8, 6.8, and 7.4) to simulate phagolysosome, phagosome and physiological conditions, respectively (Pinheiro *et al.*, 2016). Stainless-ring mesh assemblies were placed above the tubes within the apparatus vessel to keep the samples in place and to prevent floating due to the unstable hydrodynamics created by the paddles. At regular intervals (1, 2, 4, 6, 8, 12, 24, and 48 h), 1 mL of dissolution medium were collected and replaced with equal volume of pre-warmed fresh PBS to maintain sink conditions. The RFP and ISN contents in each sample were quantified using an Implen Nanophotometer (IMPLEN Nanophotometer™, Implen GmbH, Munchen Germany) set at λ_{max} = 475 nm and 264 nm, for RFP and ISN analysis, respectively. Experimental data were obtained in triplicate and all values are representative of mean ± SD (n=3).

4.2.2.3. Cellular studies

4.2.2.3.1. Culturing and expansion of the macrophage RAW 264.7 cell line

Murine macrophage RAW 264.7 cells were cultured in Dulbecco's Modified Eagle's medium (DMEM) supplemented with 10%($^{V}/_{V}$) fetal bovine serum (FBS) and 1.0%($^{V}/_{V}$) penicillin-streptomycin antibiotic. Cells were incubated at 37°C in a humidified incubator (RS Biotech Galaxy, Irvine, UK) with 95% oxygen and 5% carbon dioxide, and cellular growth was checked daily via microscopic observation. After attaining 70% – 80% confluence, the cells were split under sterile condition with proper use of aseptic technique throughout the culturing and analytical procedures. Briefly, cell culture medium was removed from the culture flask and cells were thoroughly rinsed with PBS (pH 7.4; 37°C; 3-5 mL) to remove the leftover of serum in the flask. About 3 mL of Trypsin-EDTA was added to the cell culture flask and cells were incubated for three minutes in the humidified incubator to enable the cells to detach. The cells were further re-suspended with fresh culture medium (approximately 3 mL) and then transferred to a sterile test tube, which was subsequently centrifuged at 800rpm for 3 minutes to obtain the pellet of cells. This pellet was immediately re-suspended in a fresh cell culture medium and then sub-cultured into three cell culture flasks, which was subsequently transferred to the humidified incubator. Cells were allowed to attach and proliferate. After

adequate expansion of the cell line, cells were suspended in a combination of cell culture medium and cryoprotectant medium (1:1) and frozen at - 70°C until further analysis.

4.2.2.3.2. Determination of cell density and viability

Cells, previously frozen, were thawed and pipetted into sterile test tubes containing cell culture medium, and this was centrifuged at 800rpm for three minutes and the supernatant discarded. The cell pellet was re-suspended in 3 - 5 mL of fresh cell culture medium and incubated for three minutes in the humidified incubator prior to use. The trypan blue exclusion assay was used to determine the concentration of viable cells based on the manufacturer's specifications. Briefly, an aliquot of cell suspension was pipetted into an Eppendorf's tube and mixed with 0.4% $^{V}/_{V}$ trypan blue solution in PBS in a 1:1 ratio. The cell-dye mixture was then loaded into both sides of a clean/dry Neubauer haemocytometer and viewed under a light microscope. The trypan blue exclusion assay is based on the principle that living cells exclude the blue dye and appears bright under the light microscope, whereas dead cells take up the dye and appears blue. The concentration of viable and dead cells was calculated using equations (4.3) and (4.4), respectively. Percentage viability (% V_C), an indication of the cells' health, was also determined by equation (4.5).

$$V_C = \frac{Number\ of\ viable\ cells\ counted \times Dilution\ factor}{Number\ of\ large\ corner\ squares\ counted} \times 10{,}000 \quad (4.3)$$

$$NV_C = \frac{Number\ of\ dead\ cells\ counted \times Dilution\ factor}{Number\ of\ large\ corner\ squares\ counted} \times 10{,}000 \quad (4.4)$$

Where, V_C = Viable count, which is the number of live cells per millilitre, and NV_C = Non-viable count, which is the number of dead cells per millilitre.

$$\%V_C = \frac{Number\ of\ viable\ cells}{Total\ number\ of\ cells} \times 100 \quad (4.5)$$

For each experiment, triplicate analysis was done, and cells of the same passage number with % $V_C \geq 95$ after freezing were used.

4.2.2.3.3. *In vitro* cytotoxicity assay of the formulated nanoparticles

The influence of Mn-CT-SL-RFP-ISN, Mn-CT-SL, CT-SL-RFP-ISN, CT-SL, and free RFP+ISN (physical mixture of equivalent amount of RFP and ISN as contained in the nanoformulations) on the metabolic activity of murine macrophage RAW 264.7 cells as well as their cytotoxicity were assessed by MTT assay. Briefly, RAW 264.7 cells were seeded in 96-well plates at a density of 2.5×10^4 cells/mL with DMEM supplemented with 10%($^{V}/_{V}$) FBS and 1.0%($^{V}/_{V}$) penicillin-streptomycin antibiotic and incubated for 24 hours prior to cell proliferation evaluation. Cells were then treated with varying concentrations (30 µg/mL, 60 µg/mL, 120 µg/mL, 250 µg/mL and 500 µg/mL) of the free RFP+ISN and nanoformulations, prepared with

a serum-free culture medium, and incubated for 24 hours. This assay also included positive and negative controls, which are cells treated with culture medium and cells treated with DMSO (4% $^{V}/_{V}$), respectively. After 24 hours of incubation, the culture medium was removed and replaced with 200 µL of 0.5 mg/mL of MTT reagent and incubated for 4 hours without light. MTT solution was discarded and 200 µL per well of DMSO was added to dissolve the formazan crystals. Adequate formazan crystals dissolution was aided by shaking the plate for 30 minutes at ambient temperature, and the absorbance was measured at 570 nm (690 nm for background deduction) using a microplate reader (Perkin Elmer VICTOR X 3 2030 MultiLabel Plate Reader).

4.2.2.3.4. Evaluation of nanoparticle internalization and drug accumulation in cultured macrophage RAW 264.7 cells

The effect of nanoparticle surface functionalization on cellular nanocarrier uptake and corresponding drug accumulation was evaluated using the macrophage RAW 264.7 cells. Cells (density, 2.5 × 10^6 cells/mL) were seeded in 12-well culture plates with DMEM supplemented with 10%($^{V}/_{V}$) FBS and 1.0%($^{V}/_{V}$) penicillin-streptomycin antibiotic and incubated for 12 hours at 37°C and 5% CO_2. Thereafter, the cells were treated with free drugs solution (RFP+ISN), SL-CT-RFP-ISN and Mn-CT-SL-RFP-ISN nanoparticle suspensions at an equal dose level (120 µg/mL) (Tiwari *et al.*, 2011) and incubated for 24 hours. In a parallel study, 0.05 M mannose was added to assess the impact of mannose receptor inhibition on cellular uptake behaviour of Mn-CT-SL-RFP-ISN nanoparticles. After 24-hour incubation period, the cells were removed from the wells and subjected to 3 rounds of washing and centrifugation (5,000 rpm, 3 minutes) with ice-cold PBS containing 0.02M EDTA to remove the surface bound nanoparticles (Wijagkanalan *et al.*, 2008). Supernatants were pooled together to quantify the extracellular drug concentration. To estimate the intracellular drug concentration, cell pellets previously stored at −80°C, were homogenized by resuspension in 100 µL of DDW and sonicated on ice (3 cycles, 1 minute) (Zhou *et al.*, 2005). Intracellular and extracellular concentrations of both RFP and ISN were estimated using Implen Nanophotometer (IMPLEN Nanophotometer™, Implen GmbH, Munchen Germany) set at λ_{max} = 475 nm and 264 nm, for RFP and ISN analysis, respectively.

The cellular uptake of FITC-labelled CT-SL and Mn-CT-SL nanoparticles (CT-SL-FITC, Mn-CT-SL-FITC) were also evaluated using a Leica MSV269 fluorescence stereomicroscope and images were obtained using a Leica DFC425C digital camera and Leica application suite software (Leica microscopy, Wetzlar, Germany). RAW 264.7 cells (1 × 10^5 cells/mL) were cultured on coverslips in a 6-well culture plate using 2 mL DMEM supplemented with 10%($^{V}/_{V}$) FBS and 1.0%($^{V}/_{V}$) penicillin-streptomycin antibiotic and incubated at 37°C and 5% CO_2 for 24 hours. Cells were washed three times with PBS solution and medium replaced with 2 mL

serum-free fresh medium containing 100 µg/mL FITC-labelled nanoparticles (CT-SL-FITC or MN-CT-SL-FITC) and cells were subsequently incubated for 24 hours at 37°C. Upon 24 hours of treatment, cells were washed twice with PBS solution followed by staining with 0.5 µM pre-warmed CellTracker™ Deep Red solution (Thermo Fisher Scientific, Waltham, MA, USA) under incubation for 30 minutes as per the product protocol. Stained cells on the coverslips were washed three times with PBS and fixed with 4% paraformaldehyde in PBS for thirty minutes at room temperature. Then, coverslips were rinsed three times with PBS solution and mounted on glass slides with 80%$^{V}/_{V}$ cooled glycerol and viewed under the fluorescence microscope. Control experiments were undertaken in parallel by omission of the FITC-labelled nanoparticles.

4.3. Results and Discussion

4.3.1. Nanoparticle synthesis and evaluation of particle size, surface charge, morphology, drug association efficiency and degree of mannose-functionalization

As illustrated in the reaction schemes in Figures 1.1, the solvent injection technique encouraged the hybridization of the polycationic CT and the polyanionic SL via polyelectrolyte interaction, which subsequently yielded a hybrid CT-SL nanostructure. Mannosylation of the CT-SL nanoparticles involved the grafting of mannose molecules to the surface of the nanoparticles through Schiff's base reaction (Figure 4.1). This surface-functionalization may enhance the performance of the nanosystem as regards the delivery of RFP and ISN to the alveolar macrophage cells.

The physical-chemical properties of the fabricated CT-SL-RFP-ISN and Mn-CT-SL-RFP-ISN nanoparticles, such as the average hydrodynamic diameters, zeta potential (ZP), conductivity and polydispersity index (PdI) are presented in Table 4.1. The nanoparticles displayed average hydrodynamic diameters within the range of 87.16 nm to 118.49 nm with a very narrow size distribution (PdI less than 0.30), and a positive average zeta potential of approximately +20 to +30 mV as shown in Figure 4.3. Mannosylated nanoparticles showed a minimal reduction in average particulate size compared with the unmannosylated nanoparticles. This could be attributed to the effect of the 48-hour dispersion stirring (Huang, Li and Zhong, 2014), necessary to drive the mannosylation reaction that gave rise to the functionalized nanoparticles. As supported by several studies (Hirota *et al.*, 2007; Champion, Walker and Mitragotri, 2008; Geiser and Ph, 2010; Yacobi *et al.*, 2010; Patel, Gupta and Ahsan, 2015), the size and surface charge of nanoparticles play an important role in macrophage uptake and internalization. To this note, the synthesized nanoparticle size range may favor cellular uptake via pinocytosis mechanisms, which could be clathrin-mediated,

caveolae-mediated, or clathrin/caveolae-independent endocytosis, or a combination mechanisms of endocytosis (Lee *et al.*, 2015). Epstein-Barash and co-workers (2010) reported an 85 ± 20 nm as the optimum size for enhanced nanoparticle uptake (Epstein-Barash *et al.*, 2010), supporting the hypothesis that Mn-CT-SL-RFP-ISN, with an average hydrodynamic diameter of 87.16 nm, has the potential to improve the delivery of RFP-ISN payload to the alveolar macrophage cells. The average nanoparticle surface charge (as seen in Figure 4.2 B and D) explained the stability profile of the nano-suspensions as regards flocculation, coagulation, aggregation, sedimentation and creaming phenomena, because the charged particles are kept apart due to the electrostatic repulsion that existed between them (Jain *et al.*, 2018). Furthermore, since macrophage cells display a negatively charged surface sialic acid (Pricer and Ashwell, 1971), the positive surface charge of the synthesized nanoparticles may encourage macrophage-particulate interaction, thus enhancing nanoparticle internalization.

Table 4.1. Physicochemical characteristics of the synthesized nanoparticles, indicating the various average hydrodynamic diameters, zeta potentials, conductivities and polydispersity indexes.

Nanoformulation	Diameter (nm)	ZP (mV)	Conductivity (mS/cm)	PdI
CT-SL	117.80	+21.10	0.30	0.25
CT-SL-RFP-ISN	118.47	+20.23	0.38	0.23
Mn-CT-SL	107.83	+21.77	2.37	0.16
Mn-CT-SL-RFP-ISN	87.16	+27.57	3.41	0.14

CT-SL: unmannosylated chitosan-lecithin nanoparticles; CT-SL-RFP-ISN: unmannosylated rifampicin-isoniazid-loaded chitosan-lecithin nanoparticles; Mn-CT-SL: mannosylated chitosan-lecithin nanoparticles; Mn-CT-SL-RFP-ISN: mannosylated rifampicin-isoniazid-loaded chitosan-lecithin nanoparticles; CT: Chitosan; SL: L-α-Lecithin soybean; RFP: rifampicin; ISN: isoniazid.

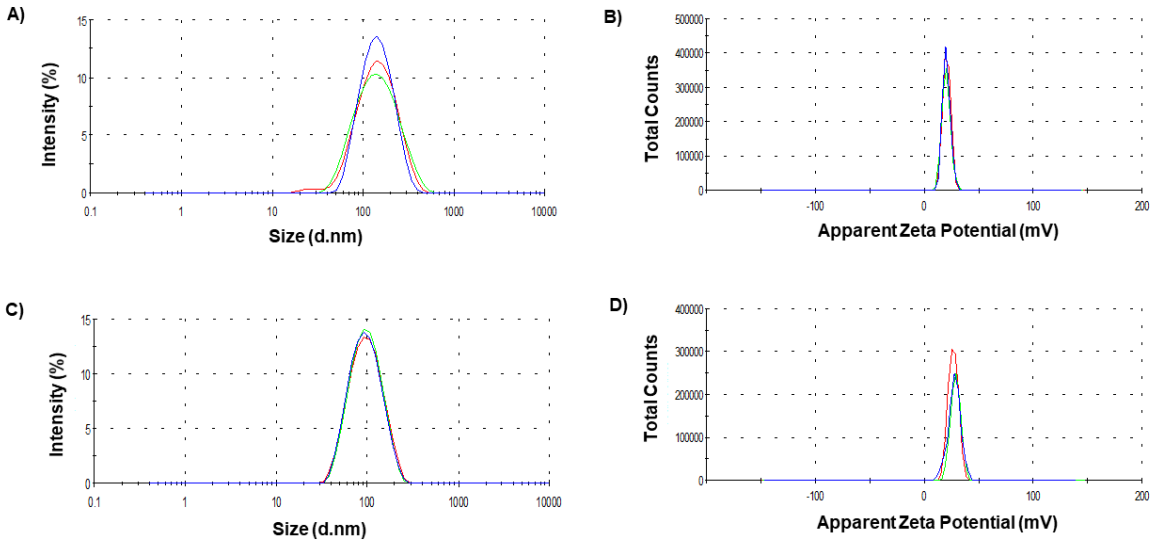


Figure 4.2. Graphical illustration of the Size distribution by intensity of CT-SL-RFP-ISN (A) and Mn-CT-SL-RFP-ISN (C) Nanoparticles, using Dynamic Light Scattering, and their Apparent zeta potentials (B and D, respectively). The nanoparticles expressed a positive surface charge, which prevents flocculation/coalescence of the nanoparticles in suspension, and this may contribute to their stability. In both formulations n=3 and SD < 0.3.

SEM imaging of the CT-SL-RFP-ISN and Mn-CT-SL-RFP-ISN nanoparticles are presented in Figure 4.3. The drug-loaded CT-SL nanoformulation was red and the lyophilized dried product was characterized with a soft and squashy appearance, as shown in Figure 4.4. Analysis of the photomicrographs, as obtained from the Phenom™ scanning electron microscope (FEI Company, Hillsboro, OR, USA), offer an in-depth understanding of the physical appearance and behavior of the nanoformulations. The nanoparticles in both formulations appeared uniformly sized and spherical with uneven surfaces. Both CT-SL-RFP-ISN and Mn-CT-SL-RFP-ISN nanoparticles presented as fairly unaggregated and well distributed throughout the nanosystem, however, while the photomicrograph of Mn-CT-SL-RFP-ISN particulate revealed a spongy matrix of polyelectrolyte complex network with the particles fairly evenly scattered all over the spongy environment (illustrated in Figure 4.3B), the micrograph of CT-SL-RFP-ISN showed distinct nanoparticles with the absence of significant matrix, as seen in Figure 4.3A. This observation could be attributed to the presence of a grafted mannose molecule on the Mn-CT-SL-RFP-ISN nanoparticle surface. The average size of the nanoparticles in both formulations, as derived from SEM images, was significantly larger than the average diameter gotten via dynamic light scattering (DLS) experiment. This could be due to a permeable gel layer formed on the surface of the dried nanoparticles arising from the drying process

undertaken during sample preparation (Tuoriniemi *et al.*, 2014). Moreover, the hydrogen bonding interactions that exist between chitosan-based nanoparticles, which is dominant during the drying process, encourages particulate aggregation (Fan *et al.*, 2012), as seen in some sections of the SEM photomicrograph. Quantification of surface mannose linkage on Mn-CT-SL nanoparticles were determined at various mannose-CT-SL reaction time via colorimetric analysis using the phenol-sulfuric acid assay method. As shown in figure 4.5, a 24-, 48-, and 72-hours stirring time produced 37.85, 50.37, and 53.15 *μg* surface sugar coverage per milligram of nanoparticle, respectively. These findings showed that extending the stirring time beyond two days yielded no significant increase in the degree of mannosylation. This could be attributed to saturation of nanoparticulate reacting surfaces.

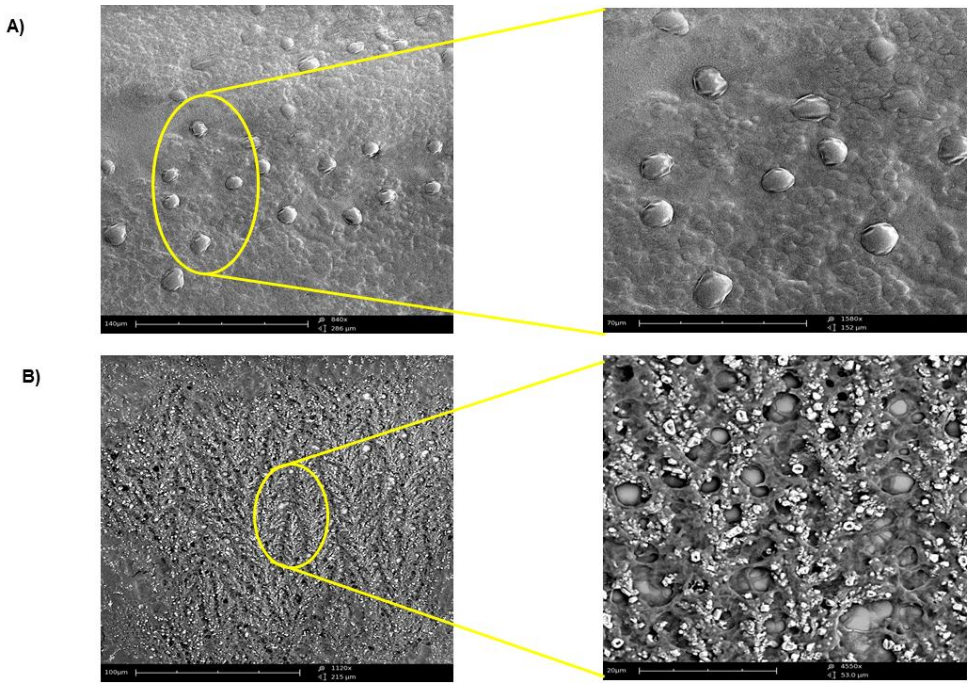


Figure 4.3. Gold sputtered scanning electron micrographs of (A) CT-SL-RFP-ISN (scale bar: 70μm; magnification: 1580x) and (B) Mn-CT-SL-RFP-ISN (scale bar: 20 μm; magnification: 4550x) nanoparticles. Particles in both formulations exhibited spherical shape morphology with uneven surfaces.

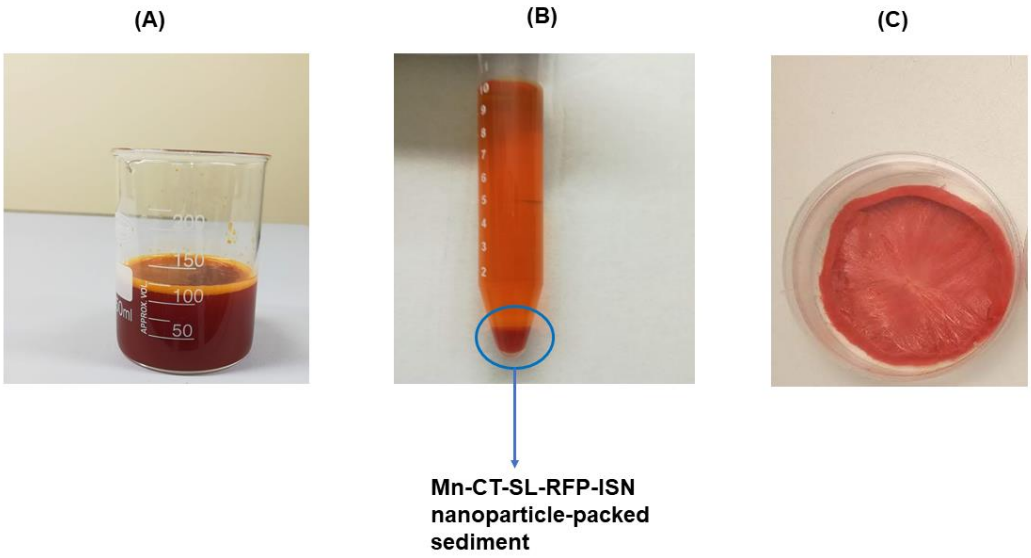


Figure 4.4. Digital images of drug-loaded mannosylated CT-SL nanoformulation (Mn-CT-SL-RFP-ISN). (A) Synthesized Mn-CT-SL-RFP-ISN nanoparticle suspension, (B) Sedimented Mn-CT-SL-RFP-ISN nanoparticles post-centrifugation, (C) Lyophilized Mn-CT-SL-RFP-ISN nanoparticles with a soft spongy appearance.

Determination of RFP-ISN loading capacity and entrapment efficiency of the synthesized nanoparticles were undertaken and result presented in Table 4.2. The findings showed no significant variation between CT-SL-RFP-ISN and Mn-CT-SL-RFP-ISN as regards the % LC and % EE. However, the slight decrease in %LC and %EE observed in the Mn-CT-SL-RFP-ISN nanoparticles could be due to drug leaching effect imparted by mannosylation reaction, which involved a 48-hour incubation period under sodium acetate buffer (pH 4) reaction medium. Similar findings had been independently reported by Jain and colleagues (2008) and Saraogi and co-workers (2011) for Didanosine-loaded Mn-GNPs and Isoniazid-entrapped Mn-G-NPs, respectively (Jain *et al.*, 2008; Saraogi *et al.*, 2011). Overall, the fabricated nanoparticles showed suitability for the encapsulation of RFP and ISN.

Table 4.2. Percentage Encapsulation Efficiency and Loading Capacity of RFP-ISN-loaded nanoformulations and corresponding placebos.

Nanoformulation	Entrapment efficiency (%)		Loading capacity (%)	
	RFP	ISN	RFP	ISN
CT-SL	-	-	-	-
CT-SL-RFP-ISN	67.37	75.01	4.39	4.89
Mn-CT-SL	-	-	-	-
Mn-CT-SL-RFP-ISN	53.52	69.80	3.03	4.55

Mn = mannose; CT = chitosan; SL = L-α-Lecithin soybean; RFP = rifampicin, ISN = isoniazid

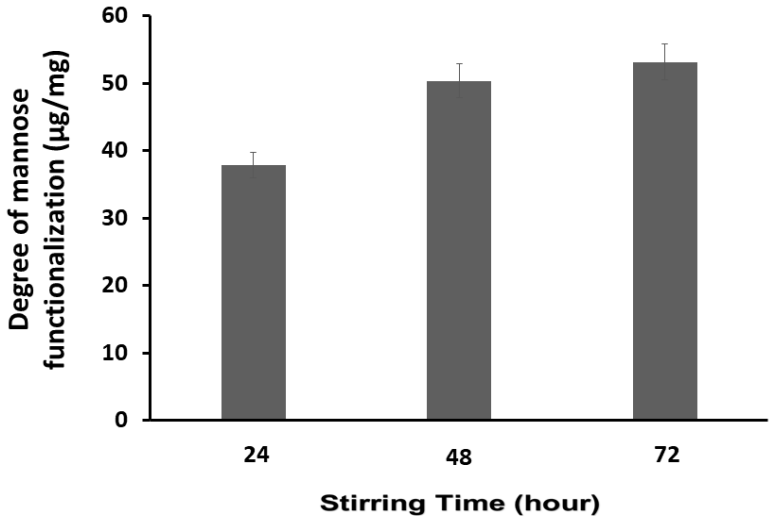


Figure 4.5. Illustration of the degree of mannose functionalization (expressed in µg/mg of nanoparticle) versus stirring time in hour. Experimental data showed an optimal surface sugar coverage of nanoparticles achieved within a 48-hour mannose-CT-SL reaction time. Further increase in stirring time produced no significant increase in surface sugar density. (n = 3, bars represent mean ± SD).

4.3.2. Evaluation of molecular vibrational transitions induced by RFP-ISN incorporation and Schiff's base formation.

FTIR spectroscopy of the pure drugs, native polymers, CT-SL-RFP-ISN, Mn-CT-SL-RFP-ISN, and placebo nanoparticles (shown in Figure 4.6) were obtained and analyzed to determine

the molecular vibrational transitions that occurred due to drug incorporation and Schiff's Base formation (confirmatory product of mannosylation reaction). Characteristic peaks of pure RFP were identified at wavenumbers 2972 cm^{-1}, 1734 cm^{-1}, and 1374 cm^{-1} for -N-CH_3, acetyl -C=O, and -C-N stretching, respectively, while the vibrational peaks at 1665 cm^{-1}, 1562 cm^{-1}, and 1218 cm^{-1}, in ISN spectrum corresponded to the carbonyl -C=O stretching, N-H bending, and N-N single bond stretching, respectively (Figure 4.6A) (Abdulla, Tan and Darwis, 2010; Sevukarajan *et al.*, 2011; Saifullah *et al.*, 2016). Analysis of CT-SL-RFP-ISN nanoparticle spectrum (Figure 4.7A) revealed similar bands: –C=O acetyl stretching, N-H bending, -C-N stretching, and N-N single bond stretching at 1733 cm^{-1}, 1552 cm^{-1}, 1377 cm^{-1}, and 1235 cm^{-1}, respectively, hence, suggesting RFP and ISN encapsulation (Saifullah *et al.*, 2016; Bachhav *et al.*, 2017b). The incorporation of RFP-ISN into the lipopolysaccharide nanostructure induced a visible increase in peak intensity from bands 1644 cm^{-1} to 1556 cm^{-1} when compared with the placebo counterpart (Figure 4.7(A)a^{I}), indicating a decrease in nanoparticle crystallinity with a corresponding increase in solubility and gastrointestinal epithelial cell permeability (Tambosi *et al.*, 2018). Moreover, broadening of the vibrational peak from bands 1052 cm^{-1} to 991 cm^{-1}, as illustrated in Figures 4.7(A)a^{II} and 4.7(B)b^{I}, further confirms the successful loading of RFP-ISN into the nanosystems; however, it may imply that the loaded drugs could have interfered with CT-SL polyelectrolyte complexation (Sumaila *et al.*, 2019).

Figure 4.6B presented the molecular vibrational transitions that accompanied nanoparticle mannosylation. The process of particulate mannose-functionalization was undertaken by mannose ring opening and followed by reaction of its −CHO group with the free amine functionalities present over the surface of CT-SL-RFP-ISN nanoparticles. The FTIR spectra of Mn-CT-SL-RFP-ISN nanoparticles showed high intensity bands between 1663 cm^{-1} and 1408 cm^{-1} wavelength when compared with the spectra of CT-SL-RFP-ISN nanoparticles. This observation could be attributed to the C=N stretching vibration produced by the formation of Schiff's base (–N=CH–) during the mannosylation reaction process (Jain *et al.*, 2010; Amato *et al.*, 2011; Xavier and Srividhya, 2014; Costa, Sarmento and Seabra, 2018c), and presumably indicating a successful surface mannose-grafting of the nanosystem.

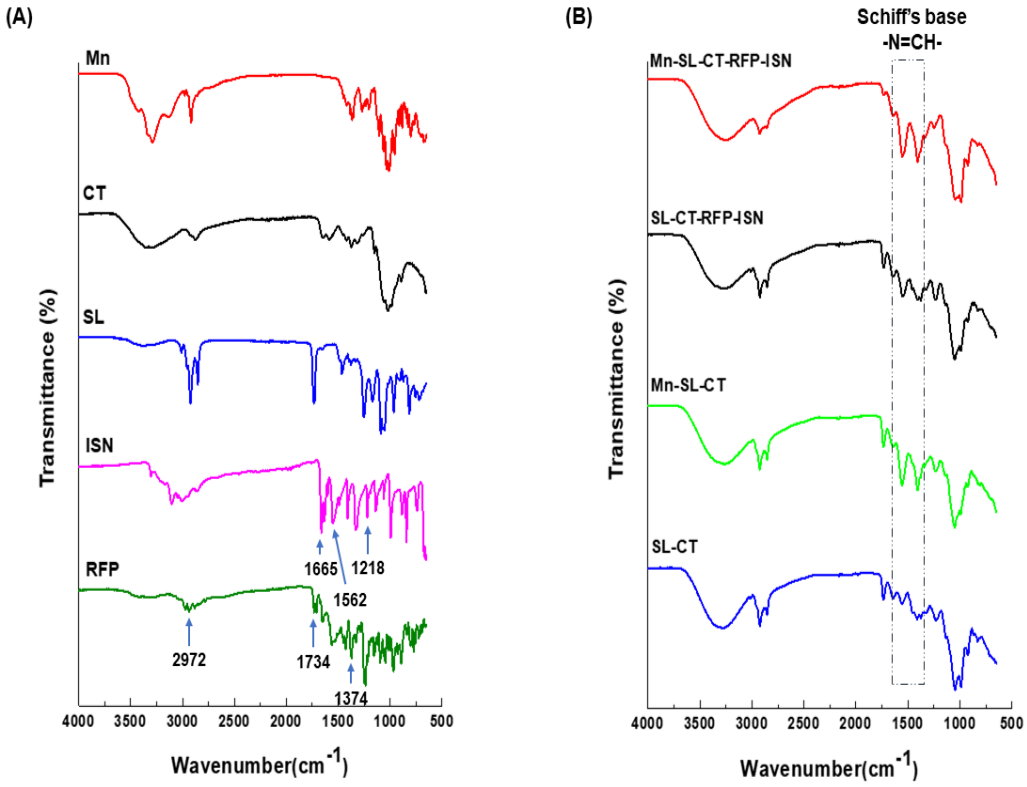


Figure 4.6. FTIR spectra of pure drugs, pristine polymers, mannosylated and unmannosylated nanoparticles showing the various molecular compositions and transitions upon polymer hybridization, drug incorporation and mannose-functionalization. (A) Mn, CT, SL, ISN, and RFP; (B) Mn-CT-SL-RFP-ISN, CT-SL-RFP-ISN, Mn-CT-SL, and CT-SL. CT-SL = unmannosylated chitosan-lecithin nanoparticles; CT-SL-RFP-ISN = unmannosylated rifampicin-isoniazid-loaded chitosan-lecithin nanoparticles; Mn-CT-SL = mannosylated chitosan-lecithin nanoparticles; Mn-CT-SL-RFP-ISN = mannosylated rifampicin-isoniazid-loaded chitosan-lecithin nanoparticles; CT = Chitosan; SL = L-α-Lecithin soybean; RFP = rifampicin; ISN = isoniazid.

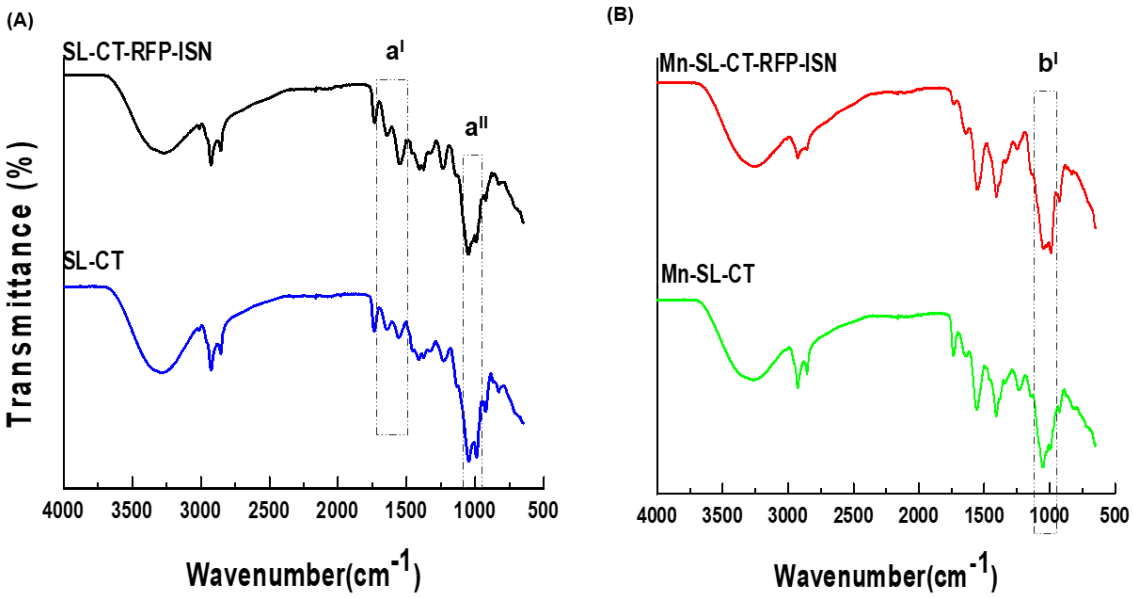


Figure 4.7. Illustrating the side-by-side comparison of the vibrational peaks of mannosylated and unmannosylated nanoparticles in order to delineate the molecular transitions of the nanosystems upon RFP-ISN incorporation. (A) CT-SL-RFP-ISN and CT-SL; (B) Mn-CT-SL-RFP-ISN and Mn-CT-SL. CT-SL = unmannosylated chitosan-lecithin nanoparticles; CT-SL-RFP-ISN = unmannosylated rifampicin-isoniazid-loaded chitosan-lecithin nanoparticles; Mn-CT-SL = mannosylated chitosan-lecithin nanoparticles; Mn-CT-SL-RFP-ISN = mannosylated rifampicin-isoniazid-loaded chitosan-lecithin nanoparticles.

4.3.3. Analysis of thermodynamic behaviour of the synthesized nanoparticles and the effect of mannosylation on nanoparticle thermal stability

Thermal stability and the decomposition temperature (D_T) of the component pristine polymers, mannosylated/unmannosylated placebo nanoparticles and the corresponding mannosylated/unmannosylated RFP-ISN-loaded nanoparticles were analyzed by TGA technique, in which the percentage mass degradation of the samples were measured as a function of temperature (shown in Figure 4.8). Mass degradation of all the analyzed samples occurred at varying stages of thermal events. The first stage in all samples, observed at temperature range 35.82 to 159.77 ^{0}C, is attributed to the loss of absorbed water (Güncüm *et al.*, 2018), and this gave rise to a minimal sample weight loss (2 – 15%). As illustrated in Figure 4.8A, the TGA thermogram of pristine CT and SL both showed a major mass degradation (CT: 45.16%, SL: 88.02%) at D_T range 250 – 480 ^{0}C in the second stage of thermal event and demonstrated a 50% weight loss at D_T 354.67 ^{0}C and 366.9 ^{0}C, respectively. This may be related to the decomposition of the polymer main chain. Conversely, the curve of CT-SL nanoparticles displayed a major degradation (66.23%) at a wider temperature range, 225.30

– 518.22 ^{0}C, presumably because of the hybridization of CT and SL polymers. Furthermore, loading of the nanoparticles with RFP-ISN decreases the D_T for 50% mass degradation from 350.25 ^{0}C to 339.68 ^{0}C, indicating a decrease in thermal stability of the drug-loaded nanoparticles. This may be due to the decrease in crystallinity of the drug-loaded nanoparticles (Ramburrun *et al.*, 2019), as observed in the FTIR analysis. Similarly, mannosylation of the nanoparticles imparted a reduced thermal stability on the nanoformulations, as it shifts the major decomposition peak from 350.25% to 290.55% and from 339.68% to 297.73% for placebo and RFP-ISN-loaded nanoparticles, respectively (Figure 4.8B), suggesting a nanosystem with less crystallinity (Ramburrun *et al.*, 2019). This analysis further confirmed the successful surface-grafting of mannose to the lipopolysaccharide nanosystem corroborating the findings from FTIR.

4.3.4. Evaluating the stability and optical characterization of Mn-CT-SL-RFP-ISN and CT-SL-RFP-ISN nanoparticles in suspension

Optical scattering analysis of Mn-CT-SL-RFP-ISN and CT-SL-RFP-ISN Nanoparticles were undertaken to access the stability profile of the synthesized nanoparticles in suspension by monitoring the sample to detect any change that may occur due to particle size variation (coalescence, flocculation) or a local variation in particle concentration (migration phenomena: sedimentation, creaming) within the sample. Figure 4.9 presented the destabilization kinetics of the experimental nanoparticulate suspensions, indicating the various transmission (T) and backscattering (BS) levels as a function of the volume fraction of the sample. Obtained results revealed that both the mannosylated and unmannosylated nanoparticle suspensions displayed a similar stability characteristic, indicating that mannosylation reaction may not have significantly impacted the destabilization kinetics of the nanosystem.

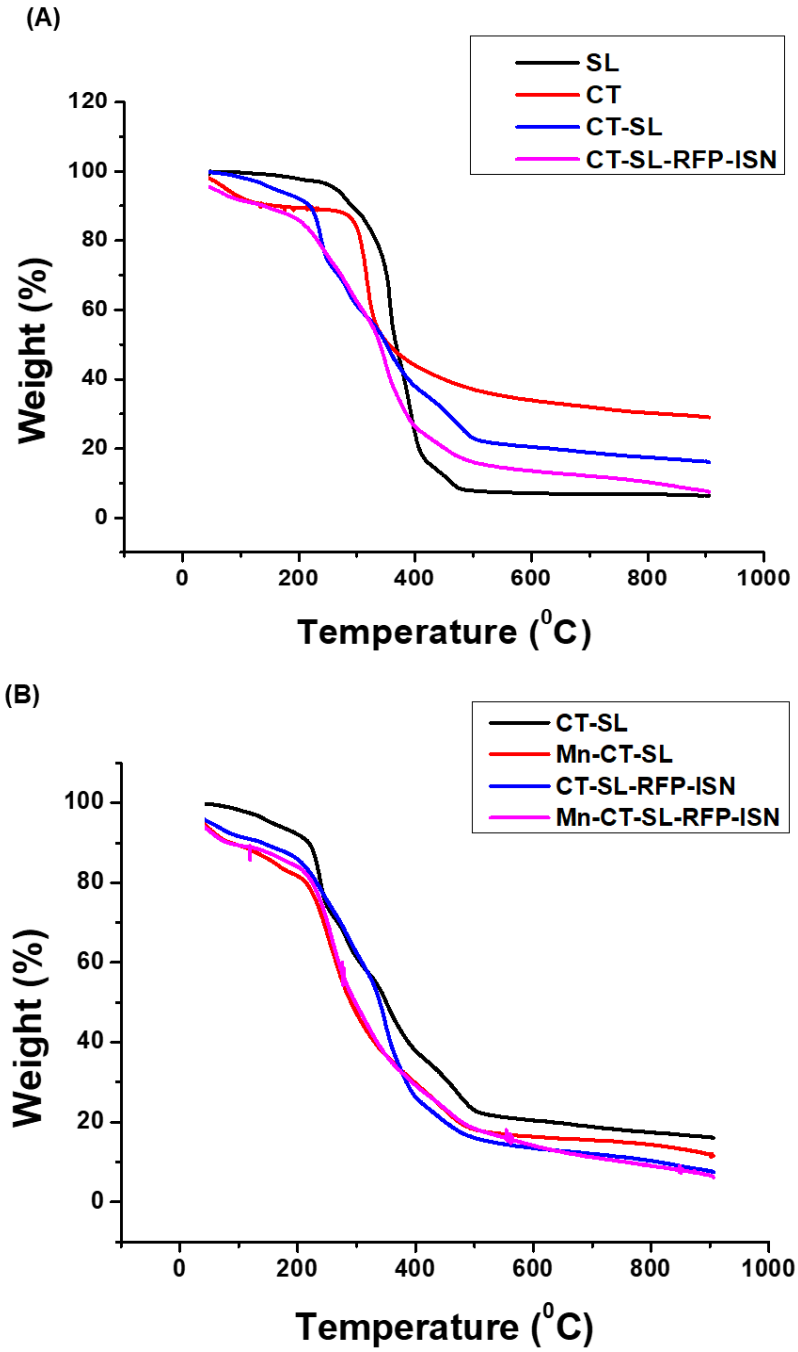


Figure 4.8. Percentage weight versus temperature thermograms depicting the transitions in thermal degradation properties of (A) CT, SL, CT-SL and CT-SL-RFP-ISN, and (B) CT-SL, Mn-CT-SL, CT-SL-RFP-ISN, and Mn-CT-SL-RFP-ISN.

The particle-migration dynamics over the 60-minutes analysis period showed no significant delta backscattering signal (ΔBS) throughout the length of the sample, suggesting good stability profile. This may be related to the electrostatic repulsion, from the ZP, that existed between the nanoparticles, thus improving stability against coagulation (Samimi *et al.*, 2019). Some amount of particle migration (< 50%) was observed around the top portion of the

samples, with CT-SL-RFP-ISN nanoparticle suspension displaying a clarified layer of relative higher thickness (~ 0.6 mm) (Figure 4.9A) when compared with the mannosylated formulation (~ 0.3 mm) (Figure 4.9B). Although, not significant, this could depict that mannosylation improved the dispersion stability of the suspended nanoparticles and minimized particle aggregation. A better steric repulsion imparted by the longer polymer chains inherent in Mn-CT-SL-RFP-ISN nanoparticles compared with the unmannosylated nanoparticles may explain this marginal variation in stability behaviour (Lee *et al.*, 2007). The BS signal observed at the top portion of the samples (Figure 4.9A and B) was overlooked because it occurred at the same portion with the transmission signal, suggesting the influence of a secondary reflections on the glass.

The stability of nanoparticle dispersion in a colloidal system impart the therapeutic efficacy of the formulation as regards dosage withdrawal post-reconstitution and prior to oral administration. To this note, a stable nanoformulation may eliminate dose-administration concerns with regard to simple use and storage of the formulation.

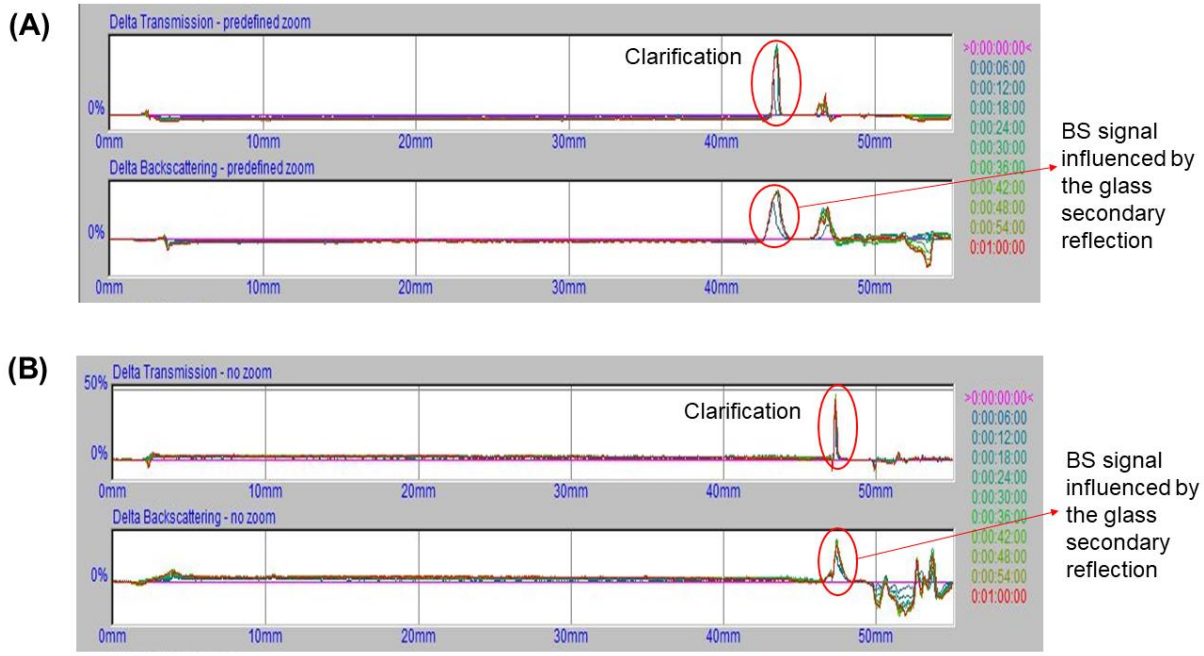


Figure 4.9. Delta transmission (top) and delta backscattering (bottom) for CT-SL-RFP-ISN nanoformulation (A) and Mn-CT-SL-RFP-ISN nanoformulation (B) measured at 25°C for 60-minutes duration. BS = Backscattering.

4.3.5. In vitro release of RFP and ISN from CT-SL-RFP-ISN and Mn-CT-SL-RFP-ISN nanoformulations

The *in vitro* release profile of RFP and ISN from the mannosylated and unmannosylated nanoformulations was investigated in phosphate buffer solution at different pH conditions (4.8, 6.8, and 7.4). Analysis of the drug release kinetics, as shown in Figure 4.10, revealed a similar pattern for both CT-SL-RFP-ISN (Figure 4.10A) and Mn-CT-SL-RFP-ISN (Figure 4.10B) nanoparticles. In both formulations, initial burst release of less than 12% was observed for RFP and ISN during the first hour in all experimental pH conditions. This may correspond to the amount of surface-bound RFP-ISN on the nanoparticles. The initial burst release was proceeded by a prolonged sustained release kinetics over the next 48-hour period, releasing less than half of the total payload (CT-SL-RFP-ISN: ~ 27% ISN, ~ 42% RFP at pH 4.8; ~ 24% ISN, ~ 34% RFP at pH 6.8; ~ 26% ISN, ~ 40% RFP at pH 7.4. Mn-CT-SL-RFP-ISN: ~ 24% ISN, ~ 45% RFP at pH 4.8; ~ 15% ISN, ~ 23% RFP at pH 6.8; ~ 18% ISN, ~ 27% RFP at pH 7.4). The slower release profile may be attributed to the barriers imparted by the phospholipid matrix as the drugs are most likely deposited within the phospholipid bilayers of the lipopolysaccharide nanostructure (Barbieri *et al.*, 2013). Moreover, RFP-ISN entrapped within the polyelectrolyte complex matrix of the CT-SL nanosystem contributes to prolong release as passage of the drug molecules out of the system is dependent on disintegration of the polyelectrolyte complex thus, reducing release rates. Further observation showed that the drug release behaviour of both CT-SL-RFP-ISN and Mn-CT-SL-RFP-ISN is pH-dependent, and this allowed the nanosystems to release more of the RFP-ISN content at acidic pH than at physiological pH. These findings suggest that majority of the loaded RFP-ISN (> 80%) may remain entrapped within the CT-SL-RFP-ISN and Mn-CT-SL-RFP-ISN architecture after administration until the nanoparticles get into the infected cells, where the acidic environment favours drug release (Vieira *et al.*, 2018; Hakkimane *et al.*, 2018) . This further support the hypothesis that CT-SL-RFP-ISN and particularly Mn-CT-SL-RFP-ISN are suitable cargo system for the delivery of RFP-ISN to the alveolar macrophages.

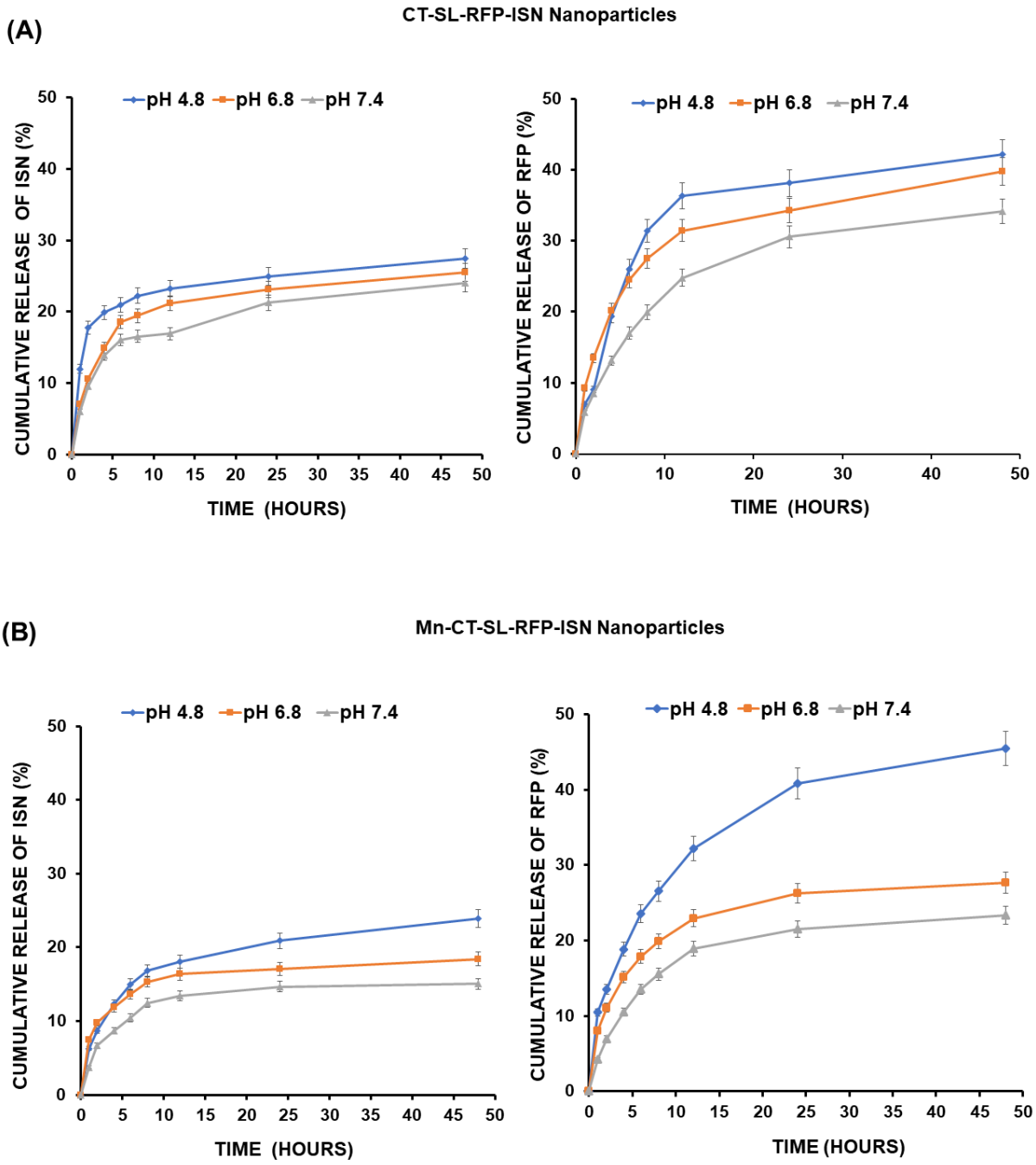


Figure 4.10. In vitro RFP and ISN release profile from CT-SL-RFP-ISN (A) and Mn-CT-SL-RFP-ISN (B) nanoparticles in pH 4.8, 6.8 and 7.4, and at 37°C (n = 3, mean ± SD).

4.3.6. Assessment of the cytotoxicity effect of the formulated nanoparticles

The effect of placebo and RFP-ISN-loaded CT-SL and Mn-CT-SL towards the proliferation of the murine macrophage RAW 264.7 cell line was evaluated for 24-hour period using the MTT (3-(4,5-dimethylthiazolyl-2)-2, 5-diphenyltetrazolium bromide) assay. This assay method was employed to measure the effect of the experimental nanoformulations on cellular metabolic activity, providing information on the cytocompatibility of the synthesized nanosystem. The

reduction of MTT to purple-coloured formazan crystals, mainly by the mitochondrial dehydrogenases (an indicator of cell viability), explains the basic principle of the MTT assay (Patravale, Dandekar and Jain, 2012).

As shown in Figure 4.11, treatment with Mn-CT-SL-RFP-ISN and CT-SL-RFP-ISN at the tested concentrations (30 to 500 µg/mL), did not significantly affect the metabolic activity of RAW 264.7 cells, displaying more than 80 percent viability for the study conditions. Therefore, RFP-ISN-loaded Mn-CT-SL and CT-SL nanoparticles could be safely employed as an effective delivery cargo for RFP and ISN up to this concentration. Placebo nanoformulations and free RFP+ISN solution showed more cytotoxic effect in comparison with RFP-ISN-loaded CT-SL nanoparticles at concentrations ≥250 µg/mL. These experimental results also revealed that encapsulation of RFP-ISN into a lipopolysaccharide architecture could help to reduce the *in vitro* cytotoxicity of the drugs. This advantage may be exploited in formulation science to design a delivery system that can safely hold a high concentration of RFP-ISN, releasing the drug content over a sustained period while maintaining optimum therapeutic concentrations and reducing dosing frequency.

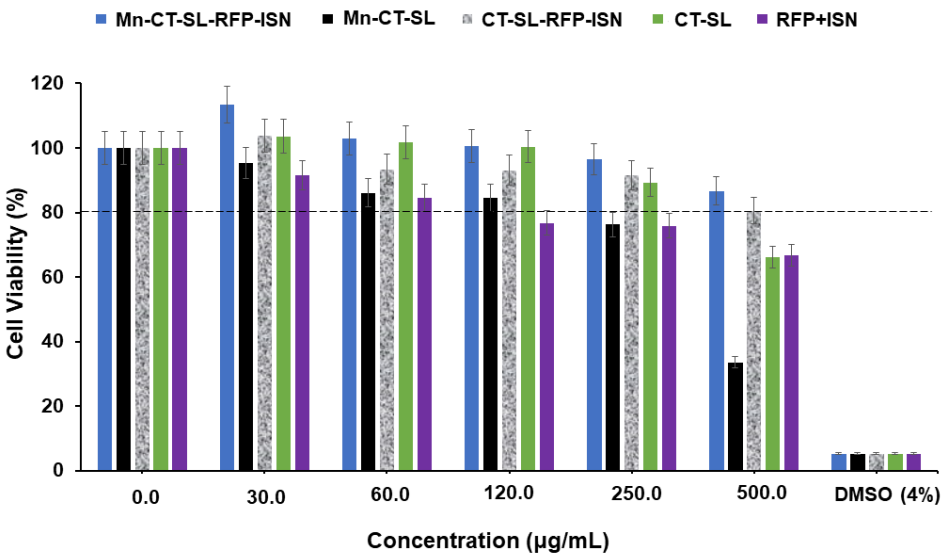


Figure 4.11. Effect of RFP-ISN-loaded nanoformulations, corresponding placebos and Free RFP+ISN solution on the viability of murine macrophage RAW 264.7 cells assessed by MTT after 24-hour period. The positive control group consisted of cells without any treatment and the negative control group consisted of cells treated with 4% DMSO. RFP+ISN was a physical mixture of RFP and ISN in equivalent concentrations as contained in the nanoformulations. (n = 3, mean ± SD).

4.3.7. Assessing the influence of CT-SL-RFP-ISN surface functionalization on nanoparticle uptake via fluorescence microscopy and drug accumulation study in cultured macrophage RAW 264.7 cells

The therapeutic efficacy of nanocarriers can be correlated with their ability to vectorize encapsulated drug(s) into the target cells. Likewise, the cellular internalization efficiency of nanocarriers strongly depend on their physicochemical characteristics; such as particle shape, size, surface charge, surface hydrophobicity/hydrophilicity and surface functionalization (Behzadi *et al.*, 2017; Foroozandeh and Aziz, 2018). In addition, these above-mentioned characteristics have been reported to also influence the route of nanoparticle endocytosis and the degree of nanocarrier cytotoxicity (Qiu *et al.*, 2010; Wu *et al.*, 2011). Though, this study was employed to evaluate the internalization efficiency of the ligand-directed CT-SL nanocarrier as compared with the unmodified nanoparticles, it is worthy to note the influence of other physicochemical factors mentioned above on particle internalization.

To assess if the CT-SL and Mn-CT-SL nanoparticles were internalized by RAW 264.7 cells, cellular uptake of the nanoformulations was investigated by fluorescence microscopy (Figure 4.12). Images obtained confirmed that both mannosylated and unmannosylated nanoparticles (shown as green fluorescence) were efficiently taken up by the macrophage RAW 264.7 cells (shown as red fluorescence) during the 24-hour treatment period (figure 4.12E and F), indicating that the lipopolysaccharide nanoformulations can effectively be applied in intracellular trafficking of anti-TB therapeutics. The cationic surfaces of the lipopolysaccharide nanoparticles could have provided a favourable interaction with the negatively charged RAW 264.7 cell surfaces (Liu *et al.*, 2013; Usman *et al.*, 2020). Additionally, RAW 264.7 cells treated with Mn-CT-SL nanoformulations exhibited a higher density of green fluorescence staining (figure 4.12E) in comparison with CT-SL nanoformulations (figure 4.12F). These findings indicate that Mn-CT-SL are more efficiently internalized than CT-SL nanoparticles as previously reported with other mannose functionalized nanosystems (Vieira *et al.*, 2017; Phanse *et al.*, 2017).

Quantitative analysis of the amount of RFP and ISN accumulated in cultured macrophage RAW 264.7 cells was undertaken and the result obtained after 24-hour incubation period is presented in Figure 4.13. Emanating results revealed that the unmannosylated CT-SL nanoformulation displayed statistically substantial nanoparticle uptake with a 7-fold and 6-fold increase in intracellular RFP (Figure 4.13A) and ISN (Figure 4.13B) contents, respectively, when compared with the free RFP+ISN solution. These findings are expected due to the improved lipophilicity and cell membrane permeability conferred by the lipopolysaccharide nanostructure (Sumaila *et al.*, 2019). Furthermore, the positively charged CT-SL nanoparticle surface could have influenced cellular uptake of the nanocarrier through electrostatic

interaction with the negatively charged surface of the cell membrane, hence, the higher RFP-ISN accumulation observed with CT-SL-RFP-ISN nanoformulation (Foroozandeh and Aziz, 2018). Moreover, spherical shaped nanoparticulates have been reported to possess a higher cellular binding effect and internalization efficacy when compared with other shapes of nanoparticle design (Verma and Stellacci, 2010; Favi *et al.*, 2015). This could also have influenced the observed CT-SL-RFP-ISN particle internalization characteristics. Surface modification of CT-SL nanoparticles, as seen with Mn-CT-SL-RFP-ISN nanoformulation, further increased the cellular uptake efficiency of the experimental system, demonstrating more than 80% each of RFP and ISN intracellular accumulation, a 13-fold and 9-fold increase in intracellular RFP and ISN concentration, respectively, in comparison with the free RFP+ISN solution. This overwhelming increase in intracellular drug content imparted by the surface-functionalized CT-SL nanoparticles could be attributed to the mannose residue, a ligand to mannose-specific membrane receptors of the macrophage cells, which actively drive the cellular uptake of the nanoparticle resulting in the higher intracellular drug accumulation (Chono *et al.*, 2008; Jain *et al.*, 2008; Tiwari *et al.*, 2011). Furthermore, a significantly low intracellular concentration of RFP and ISN was observed when cells were co-incubated with mannose prior to treatment with the Mn-CT-SL-RFP-ISN nanoformulation. This may be due to mannose receptor inhibition leading to a reduction in Mn-CT-SL-RFP-ISN particle internalization and, thus, indicating that the uptake mechanism is by mannose receptor-mediated endocytosis. Overall, these findings clearly demonstrated that Mn-CT-SL reach intracellular environment more efficiently than the unmannosylated CT-SL nanoparticles. In addition, obtained data supported the utilization of this active targeting strategy in pharmaceutical formulation design to develop a nano-delivery system for dual delivery of RFP and ISN to macrophage cells, the reservoir of *Mycobacterium tuberculosis*.

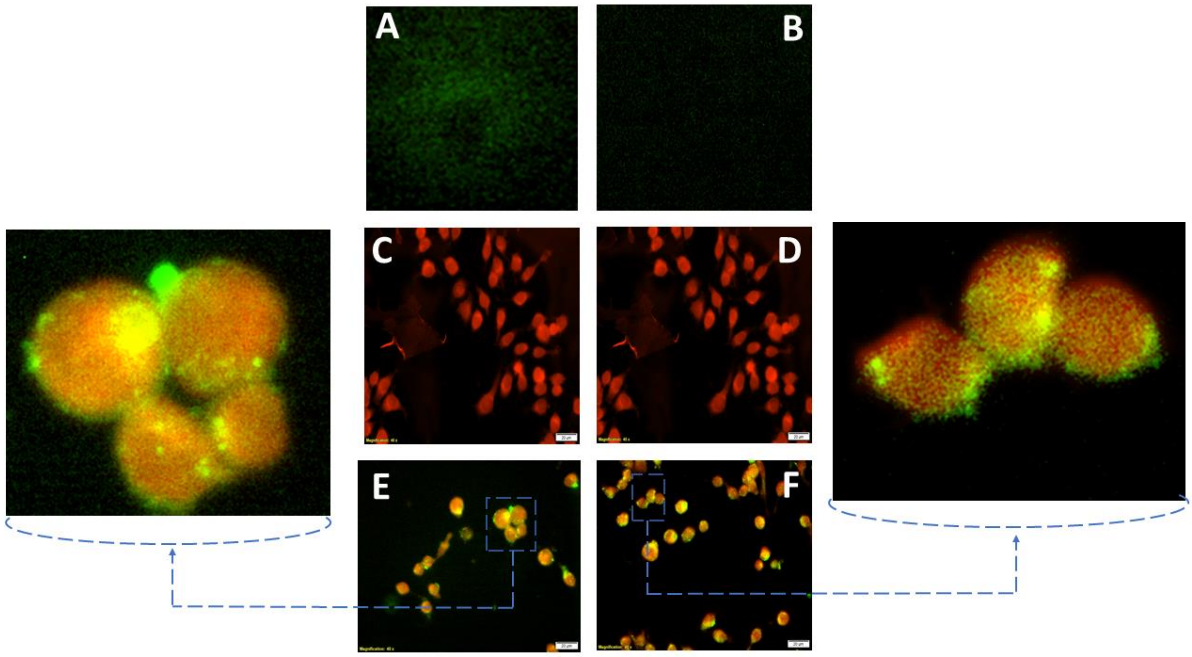


Figure 4.12. Fluorescent images illustrating the cellular uptake and internalization of FITC-labelled lipopolysaccharide nanoparticles in macrophage RAW 264.7 cells after 24-hour treatment period; (A) the fluorescence image of FITC-labelled Mn-CT-SL (green). (B) the fluorescence image of FITC-labelled CT-SL (green). (C & D) the fluorescence field of RAW 264.7 cells stained with CellTracker Deep Red dye. (E) the superimposed image of (A) and (C). (F) overlaid image of (B) and (D). (E) showed a higher density of Mn-CT-SL-FITC green fluorescence overlaid on RAW 264.7 red fluorescence indicating a greater degree of intracellular nanoparticle trafficking in comparison with CT-SL-FITC nanoparticle (overlaid red fluorescence in F). Scale bar: 20μm; magnification: 40x.

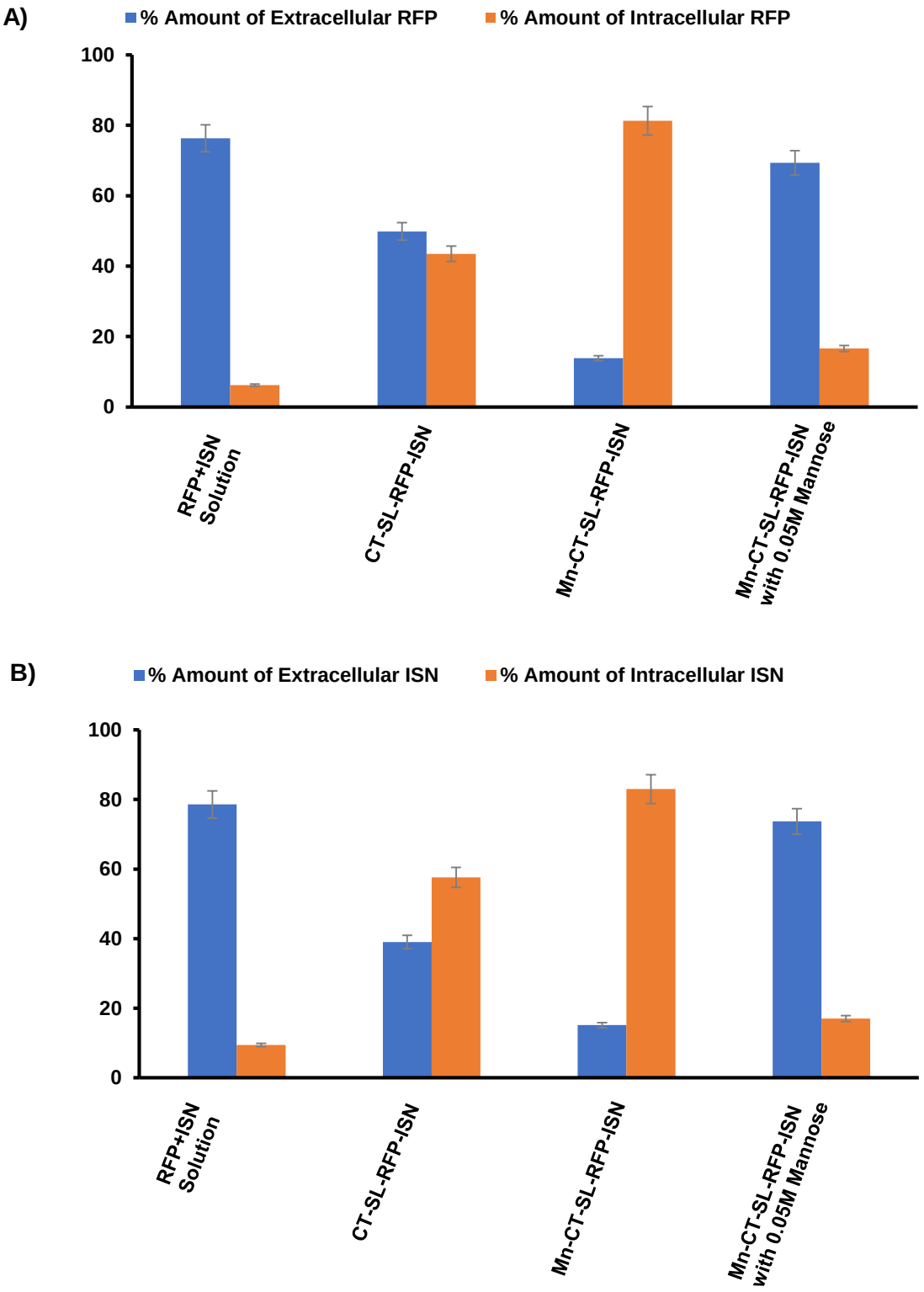


Figure 4.13. In vitro uptake characteristics of lipopolysaccharide nanoformulations by cultured RAW 264.7 cells incubated at 37 ^{0}C over a 24-hour period. (A) represent the percentage extracellular versus intracellular concentration of RFP, and (B) indicate the percentage extracellular versus intracellular concentration of ISN. (n = 3, bars represent mean ± SD).

4.4. Conclusion

In this study, we have successfully designed a novel delivery strategy that can be employed to improve anti-TB therapeutics based on mannose-functionalized lipopolysaccharide nanoparticles containing RFP and ISN, the two frontline anti-TB drugs. The lipopolysaccharide nanocarrier was developed to enhance drug uptake by the macrophages after oral administration with the aim to remedy the drawbacks, such as poor bioavailability, drug toxicity, and low patient compliance, associated with conventional TB therapeutics. The fabricated mannosylated CT-SL nanoparticle, with diameter of approximately 90 nm, possessed a positive ZP of about +27 mV, suggesting a good stability, as confirmed by Turbiscan™ analysis. Also, the positive surface charge of the nanoparticles indicated a higher propensity towards macrophage cell surface adsorption, which consequently improved particle internalization. Surface-functionalization of CT-SL nanoparticles with mannose was confirmed by the ZP variations between the unmannosylated and the mannosylated CT-SL nanoparticles as well as the TGA and FTIR spectra analysis, which allowed the detection of the Schiff's base (–N=CH–). Phenol-sulphuric acid assay revealed that optimal degree of mannose functionalization could be achieved in 48-hour mannose-nanoparticle reaction time. The %EE of more than 50% showed suitability for the encapsulation of RFP and ISN. Result from SEM revealed that all the synthesized CT-SL nanoparticles are spherical in shape. Futher physicochemical analysis showed that the incorporation of RFP-ISN and mannosylation induced a reduction in thermal stability of the nanosystem, suggesting a decrease in crystallinity of the drug-loaded nanoparticles.

In vitro release study demonstrated a sustained release profile of CT-SL nanoparticles in various simulated physiological fluids, with less than half of the nanoparticle drugs content released over 48 hours. Furthermore, cellular studies displayed a good RAW 264.7 macrophage cell cytocompartibility profile for both CT-SL-RFP-ISN and Mn-CT-SL-RFP-ISN nanoparticles, as well as their respective unloaded formulations, implying that the nanocarriers can be safely used to deliver RFP and ISN. Moreover, the higher degree of intracellular drug accumulation observed with Mn-CT-SL-RFP-ISN nanoformulation indicated a successful targeting of surface mannose receptors. Further analysis revealed that the mechanism underlying RAW 264.7 cell membrane trafficking of the mannosylated CT-SL nanoparticles was by mannose receptor-mediated endocytosis.

In summary, all the experimental results suggest that mannose-functionalized CT-SL nanoparticles represent a suitable cargo system that can be therapeutically used for disease site-specific targeting of *Mycobacterium tuberculosis* via oral administration. Thus, the fabricated MHLP nanostructure constitute a cost-effective technology that is promising for a future clinical application in TB treatment. However, further *in vivo* studies are required to

substantiate the therapeutic efficacy of the MHLP nanosystem as regards biodistribution of RFP and ISN, as well as mycobacterium clearance efficacy of the nanocarrier in an infected experimental animal model, after oral administration.

4.5. References

Abdulla, J. M. A., Tan, Y. T.-F. and Darwis, Y. (2010) 'Rehydrated Lyophilized Rifampicin-Loaded mPEG–DSPE Formulations for Nebulization', AAPS PharmSciTech, 11(2), pp. 663–671. doi: 10.1208/s12249-010-9428-6.

Aboutaleb, E. *et al.* (2012) 'Improved antimycobacterial activity of rifampin using solid lipid nanoparticles', International Nano Letters, 2(1), pp. 1–8. doi: 10.1186/2228-5326-2-33.

Adams, D. (1976) 'The Granulomatous Inflamatory Response', American Journal of Pathology, 84(1), pp. 164–192. doi: 10.1007/s12138-004-0006-8.

Adson, A. *et al.* (1994) 'Quantitative approaches to delineate paracellular diffusion in cultured epithelial cell monolayers', Journal of Pharmaceutical Sciences, 83(11), pp. 1529–1536. doi: 10.1002/jps.2600831103.

Agoram, B., Woltosz, W. S. and Bolger, M. B. (2001) 'Predicting the impact of physiological and biochemical processes on oral drug bioavailability', Advanced Drug Delivery Reviews, 50(2001), pp. S41 –S67. doi: 10.1016/S0169-409X(01)00179-X.

Aizat, M. A. and Aziz, F. (2018) 12 -Chitosan Nanocomposite Application in Wastewater Treatments, Nanotechnology in Water and Wastewater Treatment: Theory and Applications. Elsevier Inc., pp. 243-265. doi: 10.1016/B978-0-12-813902-8.00012-5.

Al-Remawi, M. *et al.* (2017) 'Chitosan/lecithin liposomal nanovesicles as an oral insulin delivery system', Pharmaceutical Development and Technology, 22(3), pp. 390–398. doi: 10.1080/10837450.2016.1213745.

Alkhader, E., Billa, N. and Roberts, C. J. (2017) 'Mucoadhesive Chitosan-Pectinate Nanoparticles for the Delivery of Curcumin to the Colon', 18(4). doi: 10.1208/s12249-016-0623-y.

Allen, A. and Carroll, N. J. H. (1985) 'Adherent and soluble mucus in the stomach and duodenum', Digestive Diseases and Sciences, 30(S11). doi: 10.1007/BF01309386.

Amarnath, R. *et al.* (2016) 'Targeted delivery of rifampicin to tuberculosis-infected macrophages : design , in-vitro , and in-vivo performance of rifampicin-loaded poly (ester amide) s nanocarriers', International Journal of Pharmaceutics, 513(1–2), pp. 628–635. doi: 10.1016/j.ijpharm.2016.09.080.

Amato, E. *et al.* (2011) ‘Synthesis, characterization and antibacterial activity against gram positive and gram negative bacteria of biomimetically coated silver nanoparticles’, Langmuir, 27(15), pp. 9165–9173. doi: 10.1021/la201200r.

de Angelis, I. and Turco, L. (2011) ‘Caco-2 cells as a model for intestinal absorption’, Current Protocols in Toxicology, (SUPPL.47), pp. 1–15. doi: 10.1002/0471140856.tx2006s47.

Azandaryani, A. H. *et al.* (2019) ‘A Comprehensive Physicochemical, In Vitro and Molecular Characterization of Letrozole Incorporated Chitosan-Lipid Nanocomplex’, Pharmaceutical Research, 36(4), pp. 1–11. doi: 10.1007/s11095-019-2597-4.

Bachhav, S. S. *et al.* (2017a) ‘Erratum to “Rifampicin Lipid-Polymer hybrid nanoparticles (LIPOMER) for enhanced Peyer’s patch uptake”, International Journal of Pharmaceutics, 534(1–2), pp. 387–390. doi: 10.1016/j.ijpharm.2017.11.013.

Bachhav, S. S. *et al.* (2017b) ‘Rifampicin Lipid-Polymer hybrid nanoparticles (LIPOMER) for enhanced Peyer’s patch uptake’, International Journal of Pharmaceutics, 532(1), pp. 612–622. doi: 10.1016/j.ijpharm.2017.09.040.

Baek, J. S. and Cho, C. W. (2017) ‘Surface modification of solid lipid nanoparticles for oral delivery of curcumin: Improvement of bioavailability through enhanced cellular uptake, and lymphatic uptake’, European Journal of Pharmaceutics and Biopharmaceutics, 117, pp. 132–140. doi: 10.1016/j.ejpb.2017.04.013.

Bai, J. P. F. and Amidon, G. L. (1992) ‘Structural Specificity of Mucosal-Cell Transport and Metabolism of Peptide Drugs: Implication for Oral Peptide Drug Delivery’, Pharmaceutical Research: An Official Journal of the American Association of Pharmaceutical Scientists, 9(8), pp. 969–978. doi: 10.1023/A:1015885823793.

Barbieri, S. *et al*. (2013) ‘Lecithin/chitosan controlled release nanopreparations of tamoxifen citrate: Loading, enzyme-trigger release and cell uptake’, Journal of Controlled Release, 167(3), pp. 276–283. doi: 10.1016/j.jconrel.2013.02.009.

Basaraba, R. J. and Hunter, R. L. (2017) ‘Pathology of Tuberculosis: How the Pathology of Human Tuberculosis Informs and Directs Animal Models’, Microbiology Spectrum, 5(3), pp. 1–13. doi: 10.1128/microbiolspec.tbtb2-0029-2016.

Basha, S. K. *et al.* (2020) ‘Materials Today : Proceedings Solid lipid nanoparticles for oral drug delivery’, Materials Today: Proceedings, (xxxx). doi: 10.1016/j.matpr.2020.04.109.

Bawa, P. *et al.* (2011) ‘Research Article A Composite Polyelectrolytic Matrix for Controlled Oral Drug Delivery’, 12(1). doi: 10.1208/s12249-010-9576-8.

Behzadi, S. *et al.* (2017) 'Cellular uptake of nanoparticles: Journey inside the cell', Chemical Society Reviews, 46(14), pp. 4218–4244. doi: 10.1039/c6cs00636a.

Benet, L. Z. *et al.* (1999) 'Intestinal MDR transport proteins and P-450 enzymes as barriers to oral drug delivery', Journal of Controlled Release, 62(1–2), pp. 25–31. doi: 10.1016/S0168-3659(99)00034-6.

Berardi, A. and Bisharat, L. (2014) 'Nanotechnology systems for oral drug delivery: challenges and opportunities', Nanotechnoloogy in Drug Delivery, (January), pp. 52–84.

Bhise, K. S. *et al.* (2007) 'Effect of oppositely charged polymer and dissolution medium on swelling, erosion, and drug release from chitosan matrices.', AAPS PharmSciTech, 8(2), p. Article 44. doi: 10.1208/pt0802044.

Brasselet, C. et al. (2019) 'Modification of chitosan for the generation of functional derivatives', Applied Sciences (Switzerland), 9(7). doi: 10.3390/app9071321.

Brown, T. D., Whitehead, K. A. and Mitragotri, S. (2020) 'Materials for oral delivery of proteins and peptides', Nature Reviews Materials, 5(2), pp. 127–148. doi: 10.1038/s41578-019-0156-6.

Buckley, A. and Turner, J. R. (2018) 'Cell Biology of Tight Junction Barrier Regulation and Mucosal Disease', pp. 1–16.

Burton, P. S., Conradi, R. A. and Hilgers, A. R. (1991) '(B) Mechanisms of peptide and protein absorption. (2) Transcellular mechanism of peptide and protein absorption: passive aspects', Advanced Drug Delivery Reviews, 7(3), pp. 365–385. doi: 10.1016/0169-409X(91)90014-4.

Campos, J., Varas-Godoy, M. and Haidar, Z. S. (2017) 'Physicochemical characterization of chitosan-hyaluronan-coated solid lipid nanoparticles for the targeted delivery of paclitaxel: A proof-of-concept study in breast cancer cells', Nanomedicine, 12(5), pp. 473–490. doi: 10.2217/nnm-2016-0371.

Carrillo-Conde, B. *et al.* (2011) 'Mannose-functionalized "pathogen-like" polyanhydride nanoparticles target C-type lectin receptors on dendritic cells', Molecular Pharmaceutics, 8(5), pp. 1877–1886. doi: 10.1021/mp200213r.

Ceccaldi, C. *et al.* (2017) 'Validation and application of a nondestructive and contactless method for rheological evaluation of biomaterials', Journal of Biomedical Materials Research - Part B Applied Biomaterials, 105(8), pp. 2565–2573. doi: 10.1002/jbm.b.33797.

Celia, C. *et al.* (2009) 'Turbiscan Lab® Expert analysis of the stability of ethosomes® and ultradeformable liposomes containing a bilayer fluidizing agent', Colloids and Surfaces B:

Biointerfaces, 72(1), pp. 155–160. doi: 10.1016/j.colsurfb.2009.03.007.

Cevher, E., Taha, M. A. M., Orlu, M., & Araman, A. (2008) 'Evaluation of Mechanical and Mucoadhesive Properties of Clomiphene Citrate Gel Formulations Containing Carbomers and Their Thiolated Derivatives', Drug Delivery, 15(1), pp. 57–67. doi: 10.1080/10717540701829234.

Champion, J. A., Walker, A. and Mitragotri, S. (2008) 'Role of particle size in phagocytosis of polymeric microspheres', Pharmaceutical Research, 25(8), pp. 1815–1821. doi: 10.1007/s11095-008-9562-y.

Chan, C. C. *et al.* (2014) 'Therapeutic Delivery Solutions', Therapeutic Delivery Solutions, 9781118111, pp. 1–410. doi: 10.1002/9781118903681.

Chen, W. L. *et al.* (2016) 'Liposomes coated with N-trimethyl chitosan to improve the absorption of harmine in vivo and in vitro', International Journal of Nanomedicine, 11, pp. 325–336. doi: 10.2147/IJN.S95540.

Chen, Y. D. *et al.* (2015) 'Development of oral dispersible tablets containing prednisolone nanoparticles for the management of pediatric asthma', Drug Design, Development and Therapy, 9, pp. 5815–5825. doi: 10.2147/DDDT.S86075.

Cheng, W., Luo, Z., Li, L., & Fu, X. (2015) 'Preparation and Characterization of Debranched-Starch/Phosphatidylcholine Inclusion Complexes', Journal of Agricultural and Food Chemistry, 63(2), 634–641. doi:10.1021/jf504133c

Cheow, W. S. and Hadinoto, K. (2012) 'Self-assembled amorphous drug-polyelectrolyte nanoparticle complex with enhanced dissolution rate and saturation solubility', Journal of Colloid and Interface Science, 367(1), pp. 518–526. doi: 10.1016/j.jcis.2011.10.011.

Cheung, J. H., Stockton, W. B. and Rubner, M. F. (1997) 'Molecular-level processing of conjugated polymers. 3. Layer-by-layer manipulation of polyaniline via electrostatic interactions', Macromolecules, 30(9), pp. 2712–2716. doi: 10.1021/ma970047d.

Choi, K. O. *et al.* (2016) 'Positively charged nanostructured lipid carriers and their effect on the dissolution of poorly soluble drugs', Molecules, 21(5). doi: 10.3390/molecules21050672.

Chono, S. *et al.* (2008) 'Efficient drug targeting to rat alveolar macrophages by pulmonary administration of ciprofloxacin incorporated into mannosylated liposomes for treatment of respiratory intracellular parasitic infections', Journal of Controlled Release, 127(1), pp. 50–58. doi: 10.1016/j.jconrel.2007.12.011.

Chuan, J. *et al.* (2013) 'Enhanced rifampicin delivery to alveolar macrophages by solid lipid

nanoparticles', Journal of Nanoparticle Research, 15(5), pp. 1–9. doi: 10.1007/s11051-013-1634-1.

Clark, M. A., Hirst, B. H. and Jepson, M. A. (2000) 'Lectin-mediated mucosal delivery of drugs and microparticles', Advanced Drug Delivery Reviews, 43(2–3), pp. 207–223. doi: 10.1016/S0169-409X(00)00070-3.

Collett, A., Tanianis-hughes, J. and Warhurst, G. (2004) 'Rapid induction of P-glycoprotein expression by high permeability compounds in colonic cells in vitro : a possible source of transporter mediated drug interactions ?', 68, pp. 783–790. doi: 10.1016/j.bcp.2004.05.006.

Costa, A. *et al.* (2016) 'The formulation of nanomedicines for treating tuberculosis', Advanced Drug Delivery Reviews, 102, pp. 102–115. doi: 10.1016/j.addr.2016.04.012.

Costa, A., Sarmento, B. and Seabra, V. (2018a) 'European Journal of Pharmaceutical Sciences Mannose-functionalized solid lipid nanoparticles are e ff ective in targeting alveolar macrophages', European Journal of Pharmaceutical Sciences, 114(October 2017), pp. 103–113. doi: 10.1016/j.ejps.2017.12.006.

Costa, A., Sarmento, B. and Seabra, V. (2018b) 'Mannose-functionalized solid lipid nanoparticles are effective in targeting alveolar macrophages', European Journal of Pharmaceutical Sciences, 114(October 2017), pp. 103–113. doi: 10.1016/j.ejps.2017.12.006.

Costa, A., Sarmento, B. and Seabra, V. (2018c) 'Mannose-functionalized solid lipid nanoparticles are effective in targeting alveolar macrophages', European Journal of Pharmaceutical Sciences, 114(December 2017), pp. 103–113. doi: 10.1016/j.ejps.2017.12.006.

Danaei, M. *et al.* (2018) 'Impact of particle size and polydispersity index on the clinical applications of lipidic nanocarrier systems', Pharmaceutics, 10(2), pp. 1–17. doi: 10.3390/pharmaceutics10020057.

Date, P. V., Samad, A. and Devarajan, P. V. (2010) 'Freeze Thaw: A Simple Approach for Prediction of Optimal Cryoprotectant for Freeze Drying', AAPS PharmSciTech, 11(1), pp. 304–313. doi: 10.1208/s12249-010-9382-3.

Decher, G. and Hong, J. D. (1991) 'Buildup of Ultrathin Multilayer Films by a Self-Assembly Process: II. Consecutive Adsorption of Anionic and Cationic Bipolar Amphiphiles and Polyelectrolytes on Charged Surfaces', Berichte der Bunsengesellschaft für physikalische Chemie, 95(11), pp. 1430–1434. doi: 10.1002/bbpc.19910951122.

Deli, M. A. (2009) 'Potential use of tight junction modulators to reversibly open membranous

barriers and improve drug delivery', Biochimica et Biophysica Acta - Biomembranes, 1788(4), pp. 892–910. doi: 10.1016/j.bbamem.2008.09.016.

Devi, N. and Maji, T. K. (2009) 'Preparation and Evaluation of Gelatin/Sodium Carboxymethyl Cellulose Polyelectrolyte Complex Microparticles for Controlled Delivery of Isoniazid', AAPS PharmSciTech, 10(4), pp. 1412–1419. doi: 10.1208/s12249-009-9344-9.

Dong, W. *et al.* (2018) 'Chitosan based polymer-lipid hybrid nanoparticles for oral delivery of enoxaparin', International Journal of Pharmaceutics, 547(1–2), pp. 499–505. doi: 10.1016/j.ijpharm.2018.05.076.

Donnellan, S. and Giardiello, M. (2019) ' Nanomedicines towards targeting intracellular Mtb for the treatment of tuberculosis ', Journal of Interdisciplinary Nanomedicine, 4(3), pp. 76–85. doi: 10.1002/jin2.61.

Dora, C. P. *et al.* (2017a) 'Improved metabolic stability and therapeutic efficacy of a novel molecular gemcitabine phospholipid complex', International Journal of Pharmaceutics, 530(1–2), pp. 113–127. doi: 10.1016/j.ijpharm.2017.07.060.

Dora, C. P. *et al.* (2017b) 'Improved oral bioavailability and therapeutic efficacy of erlotinib through molecular complexation with phospholipid', International Journal of Pharmaceutics, 534(1–2), pp. 1–13. doi: 10.1016/j.ijpharm.2017.09.071.

Du, X. J. *et al.* (2018) 'The effect of surface charge on oral absorption of polymeric nanoparticles', Biomaterials Science, 6(3), pp. 642–650. doi: 10.1039/c7bm01096f.

Dube, A. *et al.* (2014) 'Multimodal nanoparticles that provide immunomodulation and intracellular drug delivery for infectious diseases', Nanomedicine: Nanotechnology, Biology, and Medicine, 10(4), pp. 831–838. doi: 10.1016/j.nano.2013.11.012.

El-ridy, M. S. *et al.* (2007) 'Biological evaluation of pyrazinamide liposomes for treatment of Mycobacterium tuberculosis', 330, pp. 82–88. doi: 10.1016/j.ijpharm.2006.09.017.

Engman, H. A. *et al.* (2001) 'CYP3A4, CYP3A5, and MDR1 in human small and large intestinal cell lines suitable for drug transport studies', Journal of Pharmaceutical Sciences, 90(11), pp. 1736–1751. doi: 10.1002/jps.1123.

Ensign, L. M., Cone, R. and Hanes, J. (2012) 'Oral drug delivery with polymeric nanoparticles: The gastrointestinal mucus barriers', Advanced Drug Delivery Reviews, 64(6), pp. 557–570. doi: 10.1016/j.addr.2011.12.009.

Epstein-Barash, H. *et al.* (2010) 'Physicochemical parameters affecting liposomal bisphosphonates bioactivity for restenosis therapy: Internalization, cell inhibition, activation of

cytokines and complement, and mechanism of cell death', Journal of Controlled Release, 146(2), pp. 182–195. doi: 10.1016/j.jconrel.2010.03.011.

Erdine, S. and De Andrés, J. (2006) 'Drug delivery systems', Pain Practice, 6(1), pp. 51–57. doi: 10.1111/j.1533-2500.2006.00059.x.

Esmaeili, F., Hosseini-nasr, M. and Rad-malekshahi, M. (2007) 'Preparation and antibacterial activity evaluation of rifampicin-loaded poly lactide-co-glycolide nanoparticles', 3, pp. 161–167. doi: 10.1016/j.nano.2007.03.003.

Fan, W. *et al.* (2012) 'Formation mechanism of monodisperse, low molecular weight chitosan nanoparticles by ionic gelation technique', Colloids and Surfaces B: Biointerfaces, 90(1), pp. 21–27. doi: 10.1016/j.colsurfb.2011.09.042.

Farer, L., Lowell, A. and Meador, M. (1979) 'Extrapulmonary tuberculosis in the United States', Am J Epidemiol, 109(2), pp. 205–217. doi: 10.1164/ajrccm/141.2.347.

Favi, P. M. *et al.* (2015) 'Shape and surface effects on the cytotoxicity of nanoparticles: Gold nanospheres versus gold nanostars', Journal of Biomedical Materials Research - Part A, 103(11), pp. 3449–3462. doi: 10.1002/jbm.a.35491.

Formariz, T. P. *et al.* (2008) 'Structural changes of biocompatible neutral microemulsions stabilized by mixed surfactant containing soya phosphatidylcholine and their relationship with doxorubicin release', 63, pp. 287–295. doi: 10.1016/j.colsurfb.2007.12.021.

Foroozandeh, P. and Aziz, A. A. (2018) 'Insight into Cellular Uptake and Intracellular Trafficking of Nanoparticles', Nanoscale Research Letters, 13. doi: 10.1186/s11671-018-2728-6.

Fricker, G. and Drewe, J. (1996) 'Current concepts in intestinal peptide absorption.', Journal of peptide science : an official publication of the European Peptide Society, 2(4), pp. 195–211. doi: 10.1002/psc.66.

Gan, L. J. *et al.* (2014) 'Emulsifying properties of lecithin containing different fatty acids obtained by immobilized lecitase ultra-catalyzed reaction', JAOCS, Journal of the American Oil Chemists' Society, 91(4), pp. 579–590. doi: 10.1007/s11746-013-2396-8.

Ganesan, P. *et al.* (2018) 'Recent developments in solid lipid nanoparticle and surface-modified solid lipid nanoparticle delivery systems for oral delivery of phyto-bioactive compounds in various chronic diseases', International Journal of Nanomedicine, 13, pp. 1569–1583. doi: 10.2147/IJN.S155593.

Geiser, M. and Ph, D. (2010) 'Update on Macrophage Clearance of Inhaled', Journal of

Aerosol Medicine and Pulmonary Drug Delivery, 23(4), pp. 207–217. doi: DOI: 10.1089=jamp.2009.0797.

Grosset, J. (2003) 'Mycobacterium tuberculosis in the extracellular compartment: An underestimated adversary', Antimicrobial Agents and Chemotherapy, 47(3), pp. 833–836. doi: 10.1128/AAC.47.3.833-836.2003.

Güncüm, E. *et al.* (2018) 'Development and characterization of polymeric-based nanoparticles for sustained release of amoxicillin–an antimicrobial drug', Artificial Cells, Nanomedicine and Biotechnology, 46(sup2), pp. 964–973. doi: 10.1080/21691401.2018.1476371.

Hakkimane, S. S. *et al.* (2018) 'Antimycobacterial susceptibility evaluation of rifampicin and isoniazid benz-hydrazone in biodegradable polymeric nanoparticles against Mycobacterium tuberculosis H37Rv strain', International Journal of Nanomedicine, 13, pp. 4303–4318. doi: 10.2147/IJN.S163925.

Hallan, S. S. *et al.* (2016) 'Lipid polymer hybrid as emerging tool in nanocarriers for oral drug delivery', Artificial Cells, Nanomedicine and Biotechnology, 44(1), pp. 334–349. doi: 10.3109/21691401.2014.951721.

Hamman, J. H., Schultz, C. M. and Kotzé, A. F. (2003) 'N-trimethyl chitosan chloride: Optimum degree of quaternization for drug absorption enhancement across epithelial cells', Drug Development and Industrial Pharmacy, 29(2), pp. 161–172. doi: 10.1081/DDC-120016724.

Hamman, J. H., Stander, M. and Kotzé, A. F. (2002) 'Effect of the degree of quaternisation of N-trimethyl chitosan chloride on absorption enhancement: In vivo evaluation in rat nasal epithelia', International Journal of Pharmaceutics, 232(1–2), pp. 235–242. doi: 10.1016/S0378-5173(01)00914-0.

Hanifi, A., Fathi, M. H. and Mir Mohammad Sadeghi, H. (2010) 'Effect of strontium ions substitution on gene delivery related properties of calcium phosphate nanoparticles', Journal of Materials Science: Materials in Medicine, 21(9), pp. 2601–2609. doi: 10.1007/s10856-010-4123-4.

Harde, H., Das, M. and Jain, S. (2011) 'Solid lipid nanoparticles: An oral bioavailability enhancer vehicle', Expert Opinion on Drug Delivery, 8(11), pp. 1407–1424. doi: 10.1517/17425247.2011.604311.

Heinen, C. et al. (2013) 'Mechanistic basis for unexpected bioavailability enhancement of polyelectrolyte complexes incorporating BCS class III drugs and carrageenans', European Journal of Pharmaceutics and Biopharmaceutics, 85(1), pp. 26–33. doi: 10.1016/j.ejpb.2013.03.010.

Hirota, K. *et al.* (2007) 'Optimum conditions for efficient phagocytosis of rifampicin-loaded PLGA microspheres by alveolar macrophages', Journal of Controlled Release, 119(1), pp. 69–76. doi: 10.1016/j.jconrel.2007.01.013.

Hirota, K. *et al.* (2010) 'Delivery of rifampicin-PLGA microspheres into alveolar macrophages is promising for treatment of tuberculosis', Journal of Controlled Release, 142(3), pp. 339–346. doi: 10.1016/j.jconrel.2009.11.020.

Holmes, R., Hourihane, D. O. B. and Booth, C. C. (1961) 'The mucosa of the small intestine', Postgraduate Medical Journal, 37(434), pp. 717–724. doi: 10.1136/pgmj.37.434.717.

Homayun, B., Lin, X. and Choi, H. J. (2019) 'Challenges and recent progress in oral drug delivery systems for biopharmaceuticals', Pharmaceutics, 11(3). doi: 10.3390/pharmaceutics11030129.

Hörter, D. and Dressman, J. B. (1997) 'Influence of physicochemical properties on dissolution of drugs in the gastrointestinal tract', Advanced Drug Delivery Reviews, 25(1), pp. 3–14. doi: 10.1016/S0169-409X(96)00487-5.

Huang, X., Li, Y. and Zhong, X. (2014) 'Effect of experimental conditions on size control of Au nanoparticles synthesized by atmospheric microplasma electrochemistry', Nanoscale Research Letters, 9(1), pp. 1–7. doi: 10.1186/1556-276X-9-572.

Jain, A. *et al.* (2010) 'Mannosylated solid lipid nanoparticles as vectors for site-specific delivery of an anti-cancer drug', Journal of Controlled Release, 148(3), pp. 359–367. doi: 10.1016/j.jconrel.2010.09.003.

Jain, S. *et al*. (2018) 'Amphotericin B Loaded Chitosan Nanoparticles: Implication of Bile Salt Stabilization on Gastrointestinal Stability, Permeability and Oral Bioavailability', AAPS PharmSciTech, (10). doi: 10.1208/s12249-018-1153-6.

Jain, S. K. *et al.* (2008) 'Mannosylated gelatin nanoparticles bearing an anti-HIV drug didanosine for site-specific delivery', Nanomedicine: Nanotechnology, Biology, and Medicine, 4(1), pp. 41–48. doi: 10.1016/j.nano.2007.11.004.

Kaur, A., Jain, S. and Tiwary, A. K. (2008) 'Mannan-coated gelatin nanoparticles for sustained and targeted delivery of didanosine: In vitro and in vivo evaluation', Acta Pharmaceutica, 58(1), pp. 61–74. doi: 10.2478/v10007-007-0045-1.

Kaur, M., Garg, T. and Narang, R. K. (2016) 'A review of emerging trends in the treatment of tuberculosis', Artificial Cells, Nanomedicine and Biotechnology, 44(2), pp. 478–484. doi: 10.3109/21691401.2014.962745.

Khan, M. M. *et al.* (2019) 'Lipid-chitosan hybrid nanoparticles for controlled delivery of cisplatin', Drug Delivery, 26(1), pp. 765–772. doi: 10.1080/10717544.2019.1642420.

Kiptoo, P., Calcagno, A. M. and Siahaan, T. J. (2016) 'Physiological, Biochemical, and Chemical Barriers to Oral Dru g Delivery' in Wabg, B, Longqin Hu, and Siahaan, TJ. (eds.) Drug Delivery: Principles and Applications. USA: John Wiley & Sons, Inc, pp. 20-33.

Kompella, U. B. and Lee, V. H. L. (2001) 'Delivery systems for penetration enhancement of peptide and protein drugs: Design considerations', Advanced Drug Delivery Reviews, 46(1–3), pp. 211–245. doi: 10.1016/S0169-409X(00)00137-X.

Kumar, P. V. *et al.* (2006) 'Intracellular macrophage uptake of rifampicin loaded mannosylated dendrimers', Journal of Drug Targeting, 14(8), pp. 546–556. doi: 10.1080/10611860600825159.

Kumar, S., Dutta, P. K. and Koh, J. (2011) 'International Journal of Biological Macromolecules A physico-chemical and biological study of novel chitosan – chloroquinoline derivative for biomedical applications', International Journal of Biological Macromolecules, 49(3), pp. 356–361. doi: 10.1016/j.ijbiomac.2011.05.017.

Lamson, N. G. *et al.* (2020) 'Anionic nanoparticles enable the oral delivery of proteins by enhancing intestinal permeability', Nature Biomedical Engineering, 4(1), pp. 84–96. doi: 10.1038/s41551-019-0465-5.

Laridi, R. *et al.* (2003) 'Liposome encapsulated nisin Z: Optimization, stability and release during milk fermentation', International Dairy Journal, 13(4), pp. 325–336. doi: 10.1016/S0958-6946(02)00194-2.

Lee, J. *et al.* (2007) 'Measurement of the dispersion stability of pristine and surface-modified multiwalled carbon nanotubes in various nonpolar and polar solvents', Measurement Science and Technology, 18(12), pp. 3707–3712. doi: 10.1088/0957-0233/18/12/005.

Lee, W. H. *et al.* (2015) 'Nano- and micro-based inhaled drug delivery systems for targeting alveolar macrophages', Expert Opinion on Drug Delivery, 12(6), pp. 1009–1026. doi: 10.1517/17425247.2015.1039509.

Leung, A. N. (1999) 'Pulmonary tuberculosis: The essentials', Radiology, 210(2), pp. 307–322. doi: 10.1148/radiology.210.2.r99ja34307.

Li, W. *et al.* (2016) 'Synthesis, antioxidant and cathepsin D inhibition activity of quaternary ammonium chitosan derivatives', Carbohydrate Polymers, 136, pp. 884–891. doi: 10.1016/j.carbpol.2015.09.111.

Liang, J. *et al.* (2018) 'Chitosan-functionalized lipid-polymer hybrid nanoparticles for oral delivery of silymarin and enhanced lipid-lowering effect in NAFLD', Journal of Nanobiotechnology, 16(1), pp. 1–12. doi: 10.1186/s12951-018-0391-9.

Liao, C. D. *et al.* (2010) 'Nano/sub-microsized lignan glycosides from sesame meal exhibit higher transport and absorption efficiency in Caco-2 cell monolayer', Food Chemistry, 119(3), pp. 896–902. doi: 10.1016/j.foodchem.2009.07.056.

Liu, M. *et al.* (2014) 'Developments of mucus penetrating nanoparticles', Asian Journal of Pharmaceutical Sciences, 10(4), pp. 275–282. doi: 10.1016/j.ajps.2014.12.007.

Liu, X. *et al.* (2013) 'Surface and size effects on Cell interaction of gold nanoparticles with both phagocytic and nonphagocytic cells', Langmuir, 29(29), pp. 9138–9148. doi: 10.1021/la401556k.

Luan, F. *et al.* (2018) 'Preparation and characterization of quaternized chitosan derivatives and assessment of their antioxidant activity', Molecules, 23(3). doi: 10.3390/molecules23030516.

Luo, Y. *et al.* (2015) 'Solid lipid nanoparticles for oral drug delivery: Chitosan coating improves stability, controlled delivery, mucoadhesion and cellular uptake', Carbohydrate Polymers, 122, pp. 221–229. doi: 10.1016/j.carbpol.2014.12.084.

Madara, J. L. (1998) 'Regulation of the movement of solutes across tight junctions', Annual Review of Physiology, 60, pp. 143–159. doi: 10.1146/annurev.physiol.60.1.143.

Mandal, B. *et al.* (2013) 'Core-shell-type lipid-polymer hybrid nanoparticles as a drug delivery platform', Nanomedicine: Nanotechnology, Biology, and Medicine, 9(4), pp. 474–491. doi: 10.1016/j.nano.2012.11.010.

Mei, L. *et al.* (2013) 'Pharmaceutical nanotechnology for oral delivery of anticancer drugs', Advanced Drug Delivery Reviews, 65(6), pp. 880–890. doi: 10.1016/j.addr.2012.11.005.

Miranda, M. *et al.* (2012) 'The tuberculous granuloma: An unsuccessful host defence mechanism providing a safety shelter for the bacteria?', Clinical and Developmental Immunology, 2012, pp. 1-14. doi: 10.1155/2012/139127.

Mohamed, N. A. *et al.* (2013) 'Quaternized N-substituted carboxymethyl chitosan derivatives as antimicrobial agents', International Journal of Biological Macromolecules, 60, pp. 156–164. doi: 10.1016/j.ijbiomac.2013.05.022.

Mohammadzadeh, R. (2013) 'Nanosilver as a novel agent in keloid therapy', Journal of the European Academy of Dermatology and Venereology, 27(2), pp. 1–2. doi: 10.1111/j.1468-

3083.2012.04594.x.

Mohammadzadeh, R. and Javadzadeh, Y. (2018) ‘An overview on oral drug delivery via nano-based formulations’, Pharmaceutical and Biomedical Research, 4(1), pp. 1–7. doi: 10.18502/pbr.v4i1.139.

Mohammed, M. A. *et al.* (2017) ‘An Overview of Chitosan Nanoparticles and Its Application in Non-Parenteral Drug Delivery’. doi: 10.3390/pharmaceutics9040053.

Müller, R. H., Radtke, M. and Wissing, S. A. (2002) ‘Solid lipid nanoparticles (SLN) and nanostructured lipid carriers (NLC) in cosmetic and dermatological preparations’, Advanced Drug Delivery Reviews, 54(SUPPL.), pp. 131–155. doi: 10.1016/S0169-409X(02)00118-7.

Mustafa, S. *et al.* (2015) ‘Nanocarrier-based interventions for the management of MDR/XDR-TB’, Journal of Drug Targeting, 23(4), pp. 287–304. doi: 10.3109/1061186X.2015.1009076.

Nachiappan, A. C. *et al.* (2017) ‘Pulmonary tuberculosis: Role of radiology in diagnosis and management’, Radiographics, 37(1), pp. 52–72. doi: 10.1148/rg.2017160032.

Nagpal, K., Singh, S. K. and Mishra, D. N. (2010) ‘Chitosan Nanoparticles: A Promising System in Novel Drug Delivery’, Chemical & Pharmaceutical Bulletin, 58(11), pp. 1423–1430. doi: 10.1248/cpb.58.1423.

Nassar, T. *et al.* (2009) ‘Novel double coated nanocapsules for intestinal delivery and enhanced oral bioavailability of tacrolimus, a P-gp substrate drug’, Journal of Controlled Release, 133(1), pp. 77–84. doi: 10.1016/j.jconrel.2008.08.021.

Nimje, N. *et al.* (2009) ‘Mannosylated nanoparticulate carriers of rifabutin for alveolar targeting.’, Journal of drug targeting, 17(10), pp. 777–787. doi: 10.3109/10611860903115308.

Nirbhavane, P. *et al*. (2017) ‘Lipid Nanocarrier-Mediated Drug Delivery System to Enhance the Oral Bioavailability of Rifabutin’, 18(3), pp. 0–8. doi: 10.1208/s12249-016-0559-2.

Norris, D. A. and Sinko, P. J. (1997) ‘Effect of size, surface charge, and hydrophobicity on the translocation of polystyrene microspheres through gastrointestinal mucin’, Journal of Applied Polymer Science, 63(11), pp. 1481–1492. doi: 10.1002/(SICI)1097-4628(19970314)63:11<1481::AID-APP10>3.0.CO;2-5.

Ohashi, K. *et al.* (2009a) ‘One-step preparation of rifampicin/poly(lactic-co-glycolic acid) nanoparticle-containing mannitol microspheres using a four-fluid nozzle spray drier for inhalation therapy of tuberculosis’, Journal of Controlled Release, 135(1), pp. 19–24. doi: 10.1016/j.jconrel.2008.11.027.

Ohashi, K. *et al.* (2009b) ‘One-step preparation of rifampicin / poly (lactic-co-glycolic acid)

nanoparticle-containing mannitol microspheres using a four- fl uid nozzle spray drier for inhalation therapy of tuberculosis', Journal of Controlled Release, 135(1), pp. 19–24. doi: 10.1016/j.jconrel.2008.11.027.

Ortona, O. *et al.* (2008) 'The aggregative behavior of hydrophobically modified chitosans with high substitution degree in aqueous solution', Carbohydrate Polymers, 74(1), pp. 16–22. doi: 10.1016/j.carbpol.2008.01.009.

Pandey, R. *et al.* (2003) 'Nanoparticle encapsulated antitubercular drugs as a potential oral drug delivery system against murine tuberculosis', Tuberculosis, 83(6), pp. 373–378. doi: 10.1016/j.tube.2003.07.001.

Pandey, R. and Khuller, G. K. (2005) 'Solid lipid particle-based inhalable sustained drug delivery system against experimental tuberculosis', Tuberculosis, 85(4), pp. 227–234. doi: 10.1016/j.tube.2004.11.003.

Patel, B., Gupta, N. and Ahsan, F. (2015) 'Particle engineering to enhance or lessen particle uptake by alveolar macrophages and to influence the therapeutic outcome', European Journal of Pharmaceutics and Biopharmaceutics, 89(December), pp. 163–174. doi: 10.1016/j.ejpb.2014.12.001.

Patidar, A. *et al.* (2010) 'A review on novel lipid based nanocarriers', International Journal of Pharmacy and Pharmaceutical Sciences, 2(4), pp. 30–35.

Patil, J. *et al.* (2015) 'A novel approach for lung delivery of rifampicin-loaded liposomes in dry powder form for the treatment of tuberculosis', Lung India, 32(4), p. 331. doi: 10.4103/0970-2113.159559.

Patil, T. S. and Deshpande, A. S. (2018) 'Nanostructured lipid carriers-based drug delivery for treating various lung diseases : A State - of - the - Art Review', International Journal of Pharmaceutics, 547(1–2), pp. 209–225. doi: 10.1016/j.ijpharm.2018.05.070.

Patravale, V., Dandekar, P. and Jain, R. (2012) 'Nanotoxicology: evaluating toxicity potential of drug-nanoparticles', Nanoparticulate Drug Delivery, pp. 123–155. doi: 10.1533/9781908818195.123.

Pawar, H., Douroumis, D. and Boateng, J. S. (2012) 'Colloids and Surfaces B : Biointerfaces Preparation and optimization of PMAA – chitosan – PEG nanoparticles for oral drug delivery', Colloids and Surfaces B: Biointerfaces, 90, pp. 102–108. doi: 10.1016/j.colsurfb.2011.10.005.

Pepic, I., Hafner, A. and Lovric, J. (2011) 'Lecithin / chitosan nanoparticles for transdermal delivery of melatonin', 28(8), pp. 807–815. doi: 10.3109/02652048.2011.622053.

Petkar, K. C. *et al.* (2018) 'Development of Novel Octanoyl Chitosan Nanoparticles for Improved Rifampicin Pulmonary Delivery: Optimization by Factorial Design', AAPS PharmSciTech, 19(4), pp. 1758–1772. doi: 10.1208/s12249-018-0972-9.

Phanse, Y. *et al.* (2017) 'Functionalization promotes pathogen-mimicking characteristics of polyanhydride nanoparticle adjuvants', Journal of Biomedical Materials Research - Part A, 105(10), pp. 2762–2771. doi: 10.1002/jbm.a.36128.

Pinheiro, M. *et al.* (2016) 'Design of a nanostructured lipid carrier intended to improve the treatment of tuberculosis', Drug Design, Development and Therapy, 10, pp. 2467–2475. doi: 10.2147/DDDT.S104395.

Pinheiro, M. and Reis, S. (2011) 'Liposomes as drug delivery systems for the treatment of TB R eview', 6, pp. 1413–1428.

Poon, Z. *et al.* (2011) 'Controlling in vivo stability and biodistribution in electrostatically assembled nanoparticles for systemic delivery', Nano Letters, 11(5), pp. 2096–2103. doi: 10.1021/nl200636r.

Pricer, W. E. and Ashwell, G. (1971) 'The binding of desialylated glycoproteins by plasma membranes of rat liver.', Journal of Biological Chemistry, 246(15), pp. 4825–4833.

Qiu, Y. *et al.* (2010) 'Surface chemistry and aspect ratio mediated cellular uptake of Au nanorods', Biomaterials, 31(30), pp. 7606–7619. doi: 10.1016/j.biomaterials.2010.06.051.

Ramalingam, P. and Ko, Y. T. (2015) 'Enhanced oral delivery of curcumin from N-trimethyl chitosan surface-modified solid lipid nanoparticles: Pharmacokinetic and brain distribution evaluations', Pharmaceutical Research, 32(2), pp. 389–402. doi: 10.1007/s11095-014-1469-1.

Ramalingam, P. and Ko, Y. T. (2016) 'Improved oral delivery of resveratrol from N-trimethyl chitosan-g-palmitic acid surface-modified solid lipid nanoparticles', Colloids and Surfaces B: Biointerfaces, 139, pp. 52–61. doi: 10.1016/j.colsurfb.2015.11.050.

Ramburrun, P. *et al.* (2019) 'Design and characterisation of PHBV-magnesium oleate directional nanofibers for neurosupport', Biomedical Materials (Bristol), 14(6). doi: 10.1088/1748-605X/ab453c.

Rappuoli, R. and Aderem, A. (2011) 'A 2020 vision for vaccines against HIV, tuberculosis and malaria', Nature, 473(7348), pp. 463–469. doi: 10.1038/nature10124.

Rawal, T. *et al.* (2018) 'Chitosan Nanoparticles of Gamma-Oryzanol: Formulation, Optimization, and In vivo Evaluation of Anti-hyperlipidemic Activity', AAPS PharmSciTech,

19(4), pp. 1894–1907. doi: 10.1208/s12249-018-1001-8.

Reinholz, J., Landfester, K. and Mailänder, V. (2018) 'The challenges of oral drug delivery via nanocarriers', Drug Delivery, 25(1), pp. 1694–1705. doi: 10.1080/10717544.2018.1501119.

Rouge, N., Buri, P. and Doelker, E. (1996) 'Drug absorption sites in the gastrointestinal tract and dosage forms for site-specific delivery', International Journal of Pharmaceutics, 136(1–2), pp. 117–139. doi: 10.1016/0378-5173(96)85200-8.

Rubas, W. *et al.* (1996) 'Flux measurements across Caco-2 monolayers may predict transport in human large intestinal tissue', Journal of Pharmaceutical Sciences, 85(2), pp. 165–169. doi: 10.1021/js950267+.

Russell-Jones, G. J. (1996) 'The potential use of receptor-mediated endocytosis for oral drug delivery', Advanced Drug Delivery Reviews, 20(1), pp. 83–97. doi: 10.1016/0169-409X(95)00131-P.

Sahoo, D. *et al.* (2009) 'Chitosan: A new versatile bio-polymer for various applications', Designed Monomers and Polymers, 12(5), pp. 377–404. doi: 10.1163/138577209X12486896623418.

Saifullah, B. *et al.* (2016) 'Synthesis, characterization, and efficacy of antituberculosis isoniazid zinc aluminum-layered double hydroxide based nanocomposites', International Journal of Nanomedicine, 11, pp. 3225–3237. doi: 10.2147/IJN.S102406.

Sakai-Kato, K. *et al.* (2014) 'Physicochemical properties and in vitro intestinal permeability properties and intestinal cell toxicity of silica particles, performed in simulated gastrointestinal fluids', Biochimica et Biophysica Acta - General Subjects, 1840(3), pp. 1171–1180. doi: 10.1016/j.bbagen.2013.12.014.

Salomon, C., Goycoolea, F. M. and Moerschbacher, B. (2017) 'Recent Trends in the Development of Chitosan-Based Drug Delivery Systems', AAPS PharmSciTech, 18(4), pp. 933–935. doi: 10.1208/s12249-017-0764-7.

Samimi, S. *et al.* (2019) 'Lipid-Based Nanoparticles for Drug Delivery Systems, Characterization and Biology of Nanomaterials for Drug Delivery' in Mohapatra, SS., Ranjan,S., Dasgupta, N., Mishra, RK., Thomas, S., Nanoscience and Nanotechnology in Drug Delivery. Elsevier Inc., pp. 249-284. doi: 10.1016/B978-0-12-814031-4.00003-9.

Saraogi, G. K. *et al.* (2011) 'Mannosylated gelatin nanoparticles bearing isoniazid for effective management of tuberculosis', Journal of Drug Targeting, 19(3), pp. 219–227. doi: 10.3109/1061186X.2010.492522.

Savla, R. *et al.* (2017) 'Review and analysis of FDA approved drugs using lipid-based formulations', Drug Development and Industrial Pharmacy, 43(11), pp. 1743–1758. doi: 10.1080/03639045.2017.1342654.

Senna, J. P. *et al.* (2018) 'Dual alginate-lipid nanocarriers as oral delivery systems for amphotericin B', Colloids and Surfaces B: Biointerfaces, 166, pp. 187–194. doi: 10.1016/j.colsurfb.2018.03.015.

Sevukarajan, M. *et al.* (2011) 'Preparation and Pharmaceutical Characterization of Supra molecular Complex of Isoniazid with L (+) Tartaric acid', Journal of Biomedical Science, 3(2), pp. 397–402.

Seyednejad, H. *et al.* (2011) 'Functional aliphatic polyesters for biomedical and pharmaceutical applications', Journal of Controlled Release, 152(1), pp. 168–176. doi: 10.1016/j.jconrel.2010.12.016.

Shafer, R. W. and Edlin, B. R. (1996) 'Tuberculosis in patients infected with human immunodeficiency virus: Perspective on the past decade', Clinical Infectious Diseases, 22(4), pp. 683–704. doi: 10.1093/clinids/22.4.683.

Shah, D. and Shen, W. C. (1996) 'Transcellular delivery of an insulin-transferrin conjugate in enterocyte-like Caco-2 cells', Journal of Pharmaceutical Sciences, 85(12), pp. 1306–1311. doi: 10.1021/js9601400.

Shakweh, M., Ponchel, G. and Fattal, E. (2004) 'Particle uptake by Peyer's patches: A pathway for drug and vaccine delivery', Expert Opinion on Drug Delivery, 1(1), pp. 141–163.

Shepard, R. L. *et al.* (2003) 'Modulation of P-glycoprotein but not MRP1- or BCRP-mediated drug resistance by LY335979', International Journal of Cancer, 103(1), pp. 121–125. doi: 10.1002/ijc.10792.

Shi, L. L. *et al.* (2016) 'Positively Charged Surface-Modified Solid Lipid Nanoparticles Promote the Intestinal Transport of Docetaxel through Multifunctional Mechanisms in Rats', Molecular Pharmaceutics, 13(8), pp. 2667–2676. doi: 10.1021/acs.molpharmaceut.6b00226.

Shi, L. L. *et al.* (2017) 'Gastrointestinal stability, physicochemical characterization and oral bioavailability of chitosan or its derivative-modified solid lipid nanoparticles loading docetaxel', Drug Development and Industrial Pharmacy, 43(5), pp. 839–846. doi: 10.1080/03639045.2016.1220571.

Singh, C. *et al.* (2014) 'Novel rifampicin-phospholipid complex for tubercular therapy: Synthesis, physicochemical characterization and in-vivo evaluation', International Journal of

Pharmaceutics, 460(1–2), pp. 220–227. doi: 10.1016/j.ijpharm.2013.10.043.

Singh, C. *et al.* (2017) 'In Vitro-In Vivo Evaluation of Novel Co-spray Dried Rifampicin Phospholipid Lipospheres for Oral Delivery', AAPS PharmSciTech, 18(1), pp. 138–146. doi: 10.1208/s12249-016-0491-5.

Sithole, M. N. *et al.* (2017) 'Development of a Novel Polymeric Nanocomposite Complex for Drugs with Low Bioavailability', AAPS PharmSciTech, 19(1), pp. 303-314. doi: 10.1208/s12249-017-0796-z.

Siyawamwaya, M. *et al.* (2015) 'A Review: Overview of Novel Polyelectrolyte Complexes as Prospective Drug Bioavailability Enhancers', International Journal of Polymeric Materials and Polymeric Biomaterials, 64(18), pp. 955–968. doi: 10.1080/00914037.2015.1038816.

Song, S. *et al.* (2014) 'Hyaluronan-based nanocarriers with CD44-overexpressed cancer cell targeting', Pharmaceutical Research, 31(11), pp. 2988–3005. doi: 10.1007/s11095-014-1393-4.

Sonvico, F. *et al.* (2006) 'Formation of self-organized nanoparticles by lecithin / chitosan ionic interaction', 324, pp. 67–73. doi: 10.1016/j.ijpharm.2006.06.036.

Sosnik, A. *et al.* (2010) 'New old challenges in tuberculosis : Potentially effective nanotechnologies in drug delivery ☆', Advanced Drug Delivery Reviews, 62(4–5), pp. 547–559. doi: 10.1016/j.addr.2009.11.023.

Sugano, K. *et al.* (2010) 'Coexistence of passive and carrier-mediated processes in drug transport', Nature Reviews Drug Discovery, 9(8), pp. 597–614. doi: 10.1038/nrd3187.

Sumaila, M. *et al.* (2019) 'Lipopolysaccharide Polyelectrolyte Complex for Oral Delivery of an Anti-tubercular Drug', AAPS PharmSciTech, 20(3), pp. 107. doi: 10.1208/s12249-019-1310-6.

Tambosi, G. *et al.* (2018) 'Challenges to improve the biopharmaceutical properties of poorly water-soluble drugs and the application of the solid dispersion technology', Revista Materia, 23(4). doi: 10.1590/s1517-707620180004.0558.

Tiwari, S. *et al.* (2011) 'Macrophage-Specific Targeting of Isoniazid Through Mannosylated Gelatin Microspheres', 12(3), pp. 900–908. doi: 10.1208/s12249-011-9654-6.

Tuoriniemi, J. *et al.* (2014) 'Intermethod comparison of the particle size distributions of colloidal silica nanoparticles', Science and Technology of Advanced Materials, 15(3). doi: 10.1088/1468-6996/15/3/035009.

Usman, M. *et al.* (2020) 'The effect of surface charge on cellular uptake and inflammatory behavior of carbon dots', Colloids and Interface Science Communications, 35(January), p. 100243. doi: 10.1016/j.colcom.2020.100243.

Verma, A. and Stellacci, F. (2010) 'Effect of surface properties on nanoparticle-cell interactions', Small, 6(1), pp. 12–21. doi: 10.1002/smll.200901158.

Vertzoni, M. *et al.* (2019) 'Impact of regional differences along the gastrointestinal tract of healthy adults on oral drug absorption: An UNGAP review', European Journal of Pharmaceutical Sciences, 134(April), pp. 153–175. doi: 10.1016/j.ejps.2019.04.013.

Vieira, Alexandre C.C. *et al.* (2017) 'Targeted macrophages delivery of rifampicin-loaded lipid nanoparticles to improve tuberculosis treatment', Nanomedicine, 12(24), pp. 2721–2736. doi: 10.2217/nnm-2017-0248.

Vieira, Alexandre C. C. *et al.* (2018) 'Mannosylated solid lipid nanoparticles for the selective delivery of rifampicin to macrophages', Artificial Cells, Nanomedicine, and Biotechnology, 1401, pp. 1–11. doi: 10.1080/21691401.2018.1434186.

Vieira, Alexandre C.C., Chaves, L. L., Pinheiro, S., et al. (2018) 'Mucoadhesive chitosan-coated solid lipid nanoparticles for better management of tuberculosis', International Journal of Pharmaceutics, 536(1), pp. 478–485. doi: 10.1016/j.ijpharm.2017.11.071.

Were, L. M. *et al.* (2003) 'Size, Stability, and Entrapment Efficiency of Phospholipid Nanocapsules Containing Polypeptide Antimicrobials', Journal of Agricultural and Food Chemistry, 51(27), pp. 8073–8079. doi: 10.1021/jf0348368.

Wijagkanalan, W. *et al.* (2008) 'Efficient targeting to alveolar macrophages by intratracheal administration of mannosylated liposomes in rats', Journal of Controlled Release, 125(2), pp. 121–130. doi: 10.1016/j.jconrel.2007.10.011.

Wu, Y. N. *et al.* (2011) 'The selective growth inhibition of oral cancer by iron core-gold shell nanoparticles through mitochondria-mediated autophagy', Biomaterials, 32(20), pp. 4565–4573. doi: 10.1016/j.biomaterials.2011.03.006.

Xavier, D. A. and Srividhya, N. (2014) 'Synthesis and Study of Schiff base Ligands', IOSR Journal of Applied Chemistry, 7(11), pp. 06–15. doi: 10.9790/5736-071110615.

Yacobi, N. R. *et al.* (2010) 'Mechanisms of alveolar epithelial translocation of a defined population of nanoparticles', American Journal of Respiratory Cell and Molecular Biology, 42(5), pp. 604–614. doi: 10.1165/rcmb.2009-0138OC.

Zhou, H. *et al.* (2005) 'Microparticle-based lung delivery of INH decreases INH metabolism

and targets alveolar macrophages', Journal of Controlled Release, 107(2), pp. 288–299. doi: 10.1016/j.jconrel.2005.06.009.

CHAPTER 5
CONCLUSIONS, LIMITATIONS AND FUTURE RECOMMENDATIONS

5.1. Conclusions

Tuberculosis remains a chronic pathology of the pulmonary and extra pulmonary systems affecting several millions of people globally. Efforts to make the world a TB-free planet is hampered by the ineffective anti-TB therapeutics, development of resistant strains (as in Multidrug resistant TB and Extensively drug resistant TB), and the existence of human immunodeficiency virus (HIV) comorbidity. In addition, the inconsistent bioavailability, dose-related side effects, non-specific targeting and systemic toxicity associated with conventional anti-TB drugs have made TB treatment even more challenging. These multivariate challenges associated with successful TB chemotherapeutics severely compromise treatment outcome and patient quality of life. Winning the 'war' against this superbug (Mtb) should encompass an effective targeted delivery of the chemotherapeutically potent anti-TB drugs to the disease site using a smart and intelligent cargo system. The emergence of nanotechnological application in medicine has paved the way for an insight into the use of biomaterials for therapeutic purposes. Several nanomaterials, engineered for oral drug delivery of active pharmaceutical ingredient(s), take the benefit of their nanometric size to maneuver through the harsh GI environment whilst protecting the bioactive from acidic degradation, P-gp efflux, and enzymatic inactivation. In addition, the nanocarriers could protect normal healthy cells from drug toxicity, thus providing efficient and safe drug delivery to diseased site while improving drug bioavailability. Based on this concept, the aim of this study was to design a novel mannose functionalized hybrid lipopolysaccharide-based (MHLP) nanosystem that would demonstrate precised targeting to the alveolar macrophages habouring Mtb. This study explicitly demonstrated the anti-TB delivery potential of the MHLP strategy, suggesting that anti-TB therapeutics could be optimized to provide targeted drug delivery and improving therapeutic outcomes.

After reviewing the several cutting edge nanotechnological designs employing lipopolysaccharide-based polymers, a novel MHLP nanoconstruct was fabricated using the solvent injection technique. In this study, CT and SL hybrid constituted the lipopolysaccharide architecture providing a system with naturally derived and readily available polymers with affordable cost. RFP and ISN, the two most potent anti-TB drugs, were selected as the model drugs due to their inherent broad spectrum anti-mycobacterial activity as well as the formulation and therapeutic drawbacks hindering the clinical use of these compounds. More also, these drugs have poor solubility, low bioavailability and minimal cellular penetration profile obstructing the achievement of therapeutic concentration at the target site.

The synthesized MHLP nanosystem demonstrated optimal physicochemical properties suitable for formulation stability and macrophage targeting. Positive surface charge of the nanoparticles encouraged passive cell targeting due to the negatively charged macrophage surfaces. This obviously permited enhanced cellular uptake with subsequent intracellular RFP-ISN accumulation as observed from the macrophage uptake and intracellular drug accumulation studies. Additionally, an optimal degree of mannose-functionalization, achieved within a 48-hour reaction time, conferred active targeting ability on the nanosystem and further enhanced its drug delivery efficacy. A decrease in the crystallinity and hydrophilicity of RFP-ISN-loaded nanosystem, as shown with the XRPD and TGA analysis, was suggested to further enhanced cellular drug penetration. Furthermore, current research clearly demonstrated the sustained drug release property of MHLP nanosystem, and this could benefit patients as regards dose spacing and pill burden, permiting improved patients' compliance.

To validate the drug delivery efficacy MHLP nanosystem, detailed *in vitro* cellular experiments were also done using RAW 264.7 macrophages. The RFP-ISN-loaded MHLP nanoparticles showed a higher intracellular accumulation of the payload in RAW 264.7 macrophages when compared with the unmodified nanoparticles and the free drug solution. Cytotoxicity studies revealed that CT-SL-RFP-ISN and Mn-CT-SL-RFP-ISN nanoparticles, and the corresponding placebo counterpart are cytocompartible and non-toxic to healthy RAW 264.7 macrophages, implying that the synthesized nanosystem can be successfully used as a delivery system without causing any harm to healthy cells. *Ex vivo* permeability studies was done using large pig intestinal tissue to investigate the gastrointestinal permeability profile of the synthesized CT-SL drug-loaded nanoparticles in relation to the free drug solution. Experimental findings showed that the lipopolysaccharide nanosystem demonstrated an improved permeation across the gastrointestinal epithelial cells when compared with the free drug solution. This again support the hypothesis that MHLP nanosystem has the potential to improve the bioavailability of RFP and ISN.

In summary, the formulated Mn-CT-SL-RFP-ISN nanoconstruct demonstrated remarkable stability profile to validate feasibility of the formulation with regards to manufacturing, storage and clinical application. Polymeric materials used were naturally derived and generally easy to obtain and cost-effective. The nanoformulation demonstrated high target-oriented intracellular accummulation of RFP and ISN in RAW 264.7 cell line. Showed considerable safety and cytocompatibility profile towards the RAW 264.7 cell line. Thus, the MHLP nanosystem demonstrated statistically significant potential for clinical application.

5.2. Limitations of the research

Due to the unavailability of NR8383 or RAW 264.7 cell lines required for cellular studies, the research could not achieve the proposed timelines for completion as too much time was lost to application approval for cell line importation from the South Africa's department of agriculture, forestry and fishery. Additional time was lost to the importation of the cell line from LCG limited in the United Kingdom. Furthermore, the challenges related to reviving the imported cells and subsequent sub-culturing impacted the research timeline, as we lost the imported NR8383, hence using RAW 264.7 for our cell studies.

Uptake studies was significantly challenged by the inaccessibility of adequate fluorescent microscope within the WADDP labs to assess the internalization characteristics of the various nanoparticle formulations into the cells. We had to negotiate and seek approval from neighbouring departments in order to use a fluorescent microscope. This significantly impacted the research in regards to movement of samples between some distance in order to access a fluorescent microscope and the delay associated with equipment booking. Also, other cellular assay such as sub-cellular localization of nanoparticles could not be done due to inaccessible confocal laser scanning microscope.

5.3. Future recommendations

Interesting revelations about MHLP nanosystem has been made as regards the potential in affording effective anti-TB therapeutics, however, further *in vivo* pharmacokinetic and pharmacodynamic studies is recommended to substantiate this findings. In addition, *in vitro* and *in vivo* antimycobacterium assay can also be undertaken to determine the antimycobacterial impact of the RFP-ISN-loaded MHLP nanosystem.

The applicability of this nanosystem in the delivery of all the first-line, as well as the second-lines, anti-TB therapeutics can also be investigated, as precised targeting of these drugs to disease sites, particullarly in cases of MDR-TB and XDR-TB, could improve the clinical outcomes of TB treatment. Furthermore, the potential for the nanosystem to encapsulate all four first-line drugs; rifampicin, isoniazid, pyrazinamide and ethambuthol, in one system for a concurrent delivery to the disease site can also be investigated. Cellular studies for macrophage uptake should be extended to other macrophage cell lines and findings compared to that from RAW 264.7 cell line.

An outstanding characteristic of lipopolysaccharide-based nanosystem is the presence of postively charged surfaces which encourage the attachment of several negatively charged targeting moieties. Moreover, the alveolar macrophages express surface receptors, other than mannosyl, which can be explored in the design of a surface-functionalized nanosystem. To this note, it is recommended that future research delves into the feasibility of surface-modifying

CT-SL nanosystem with ligands such as galactosyl or lectin and experimental findings be compared with that of mannose-functionalized system as regards targeted delivery of anti-TB therapeutics. These alternative functionalization designs of CT-SL nanoformulation could provide even better precised delivery of anti-TB therapeutics to the diseases site.

Finally, the MHLP nanosystem can also be investigated for application in TB immunotherapeutics or chemoimmunotherapeutics. In this line of thought, MHLP could be engineered to provide a simultaneous targeted delivery of immunotherepareutic and anti-TB chemotherapeutic agents. This approach could provide a more effective therapeutic strategy for both latent and active TB infection, particularly for the MDR-TB and XDR-TB as well as for TB-HIV coinfection. Since Mtb resides mainly in macrophages, cellular immune responses become essential for inhibiting intracellular growth and limiting disease propagation. Immune response can significantly modify the proportions and absolute numbers of actively replicating Mtb within the infected macrophage cells. To this note, the incorporation of immunotheraputics, like interleukin (IL-2, IL-12), interferon (IFN-γ) or anti-tumor necrosis factor alpha (anti-TNF-α), alongside anti-TB drugs into MHLP nanosystem may be considered. Moreover, co-encapsulation of immunomodulatory agent, such as gallium, and ant-TB drugs can be explored. The co-delivery of these bioactives to macrophages could produce dual effects – regulation of cytokines release and anti-mycobacterial activity. These strategies could be a more effective approach to revolutionize TB treatment and winning the fight against the disease.

APPENDICES

APPENDIX A

Research Publication

Sumaila, M. et al. (2019) 'Lipopolysaccharide Polyelectrolyte Complex for Oral Delivery of an Anti-tubercular Drug', AAPS PharmSciTech, 20(3). doi: 10.1208/s12249-019-1310-6.

AAPS PharmSciTech (2019) 20:107
DOI: 10.1208/s12249-019-1310-6

CrossM

Research Article

Theme: Lipid-Based Drug Delivery Strategies for Oral Drug Delivery
Guest Editor: Sanyog Jain

Lipopolysaccharide Polyelectrolyte Complex for Oral Delivery of an Anti-tubercular Drug

Mumuni Sumaila,[1] Poornima Ramburrun,[1] Pradeep Kumar,[1] Yahya E. Choonara,[1] and Viness Pillay[1,2]

Received 3 October 2018; accepted 10 January 2019

Abstract. Anti-tuberculosis drug delivery has remained a challenge due to inconsistent bioavailability and inadequate sustained-release properties leading to treatment failure. To resolve these drawbacks, a lipopolysaccharide polyelectrolyte complex (PEC) encapsulated with rifampicin (RIF) (as the model drug) was fabricated, using the solvent injection technique (SIT), with soy lecithin (SLCT), and low-molecular-weight chitosan (LWCT). The average particle size and surface charge of RIF-loaded PEC particulates was 151.6 nm and + 33.0 nm, respectively, with noted decreased particle size and surface charge following increase in SLCT-LWCT mass ratio. Encapsulation efficiency (%EE) and drug-loading capacity (%LC) was 64.25% and 5.84%, respectively. Increase in SLCT-LWCT mass ratio significantly increased %EE with a marginal reduction in %LC. *In vitro* release studies showed a sustained-release profile for the PEC particulate tablet over 24 h (11.4% cumulative release) where the dominant release mechanism involved non-Fickian anomalous transport shifting towards super case II release as SLCT ratios increased (6.4% cumulative release). PEC-tablets prepared without SIT presented with rapid Fickian-diffusion-based drug release with up to 90% RIF release within 4 h. *Ex vivo* permeability studies revealed that lipopolysaccharide PEComplexation significantly increased the permeability of RIF by ~ 2-fold within the 8-h study period. These results suggest successful encapsulation of RIF within a PEC structure while imparting increased amorphic regions, as indicated by x-ray diffraction, for potential benefits in improved drug dissolution, bioavailability, and dosing.

KEY WORDS: polyelectrolyte complexation; lipopolysaccharide; PEC particulates; tuberculosis; mucoadhesion; rifampicin.

INTRODUCTION

Tuberculosis (TB) has been a major public health challenge, particularly in Africa, Asia, and South America, despite all efforts made to improve its treatment and management (WHO 2017). Moreover, TB has been associated with high mortality rates, in co-morbid human immunodeficiency virus (HIV) incidences (1). The causative organism, *Mycobacterium tuberculosis* (MTB) primarily affects the lungs as pulmonary TB; however, other parts of the body could also be affected resulting extrapulmonary TB (2). The conventional anti-TB regi involves the oral administration of rifampicin, isonia pyrazinamide or ethambutol in various combinations o dosed multiple times per day (1). Patients of this "har eradicate" bacteria (MTB) suffer severe adverse eff due to major drawbacks associated with the delivery of chemotherapy regimen (3). The current TB therape strategy is challenged with problems of low drug solubi intestinal malabsorption, pre-mature drug degradation, drug concentrations at the infection site, and poor cell-d penetration (3). All these factors impart poor bioavaila ity of TB medications. Furthermore, the long (6–9 mon and stringent treatment schedule of anti-tubercular dr (ATDs) and associated side-effect profiles (particularly second-lines ATDs) contributes to poor patient compli (4). These challenges necessitate action to develop effective delivery system capable of alleviating th concerns. A nanocarrier system capable of releas bioactives steadily in therapeutically effective quanti

Guest Editor: Sanyog Jain

Mumuni Sumaila and Poornima Ramburrun contributed equally to the research.

[1] Wits Advanced Drug Delivery Platform Research Unit, Department of Pharmacy and Pharmacology, School of Therapeutic Sciences, Faculty of Health Sciences, University of the Witwatersrand, Johannesburg, 2193, South Africa.
[2] To whom correspondence should be addressed. (e-mail: viness.pillay@wits.ac.za)

APPENDIX B

Poster Presentations

Mumuni Sumaila, Viness Pillay, Yahya E. Choonara, Lisa C. du Toit, Pradeep Kumar and PP Kondiah. Synthesis and Characterization of Lipopolysaccharide Nanoparticles for Dual Delivery of Rifampicin and Isoniazid. Poster presented at the School of Therapeutic Sciences Biennial Research day, 10 September 2019, University of the Witwatersrand, Johannesburg, South Africa. (Abstract in Appendix B).

Synthesis and Characterization of Lipopolysaccharide Nanoparticles for Dual Delivery of Rifampicin and Isoniazid

Mumuni Sumaila[1], Viness Pillay*[1], Yahya E. Choonara[1], Lisa C. du Toit[1], Pradeep Kumar[1] and PP Kondiah[1]

[1]University of the Witwatersrand, Department of Pharmacy and Pharmacology, 7 York Road, Parktown, 2193, Johannesburg, South Africa.

***Corresponding author: viness.pillay@wits.ac.za**

Purpose:
Lipopolysaccharide Nanoparticles (NPs) was evaluated as effective 'cargo' system for the dual delivery of Rifampicin (Rf) and Isoniazid (INH). Being of natural origin with a good safety profile and a sustained drug release property could be a better alternative to conventional therapeutics. Furthermore, in contrary to the conventional therapeutics, the nanoparticulate system could improve drug bioavailability, cell-drug penetration and drug protection against premature degradation while significantly reducing length of treatment.

Methods:
Preparation of Rf-INH-loaded Lipopolysaccharide Nanoparticles: Ethanolic solution of Soy Lecithin (SL) and Rf was prepared by dissolving 600mg of SL and 150mg of Rf in 20mL ethanol. 200mg of Low molecular weight chitosan (CS) and 150mg of INH were dissolved in 40mL of 1% acetic acid and 40mL double deionized water producing 80mL of CS-INH solution. Rf-INH-loaded lipopolysaccharide NPs suspension was obtained by injecting 20mL of SL-Rf solution into CS-INH solution through a syringe with subsequent mechanical stirring. NPs suspension was centrifuged (5000 rpm, 30 min) and the supernatant decanted, and sediment lyophilized to obtain a dried NP powder. SL-CS-Rf-INH NPs Characterization: The synthesized NPs were characterized for size, surface charge, chemical and functional transformation. *In Vitro* Drug Release Studies: This was performed in a dissolution tester ERWEKA, USP Apparatus II, DT 126, UK (900mL Phosphate-buffered saline solution, pH 4.8, pH 6.8 and pH 7.4 at 37°C and 50 rpm over a 48-h period, n=3).

Results:
The formulated nanoparticles were spherical as evidenced by SEM with average size of 120.4 nm and nearly uniform size distribution (PdI < 0.3). Surface charge of +37.7 mV suggested possible stability of the nanoparticulate suspension with no serious particle agglomeration. Encapsulation of the drugs favoured INH more than Rf with 75% and 67% entrapment efficiency, respectively. This could be attributed to the smaller molecular size and higher aqueous solubility of INH. FTIR spectra suggested successful encapsulation of Rf and INH within the polyelectrolyte structure of the NPs as evidenced by the structural changes observed in the drug-loaded NPs when compared with drug-free NPs. However, it may suggest that Rf and INH could have interfered with or covered the NH_3^+ and PO_3^- Polyelectrolyte Complex (PEC) reaction sites. Extended drug release was seen in all simulated physiological medium tested with less than half of both Rf and INH released within 48 h. This may be due to the nanoparticulate polyelectrolyte structure encapsulating the drugs.

Conclusion:
Conventional TB therapeutics have proved to be inefficient due to a multitude of drawbacks Lipopolysaccharide nanoparticles loaded with Rf and INH could be developed using SIT to overcome these drawbacks. Sustained drug release could be achieved, and this could be explored in product formulation to reduce dosage frequency with subsequent drug adherence benefit. Drug release was driven by diffusion and thus was a function of solubility, loading capacity and nanoparticulate PEC structure. This structure provides potential benefits in enhanced drug dissolution, bioavailability, and dosing.

APPENDIX C

Waiver letter confirming this study does not require clearance from the Animal Research Ethics Committee of the University of the Witwatersrand.

ANIMAL RESEARCH ETHICS COMMITTEE
Registration number: AREC-101210-002

January 15, 2019

To whom it may concern,

Re: Waiver from the Animal Ethics Research Committee of the University of the Witwatersrand

This letter is to confirm that Mumuni Sumaila (student number: 1821878) an MSc candidate in Forensic Science will be undertaking a study entitled "Hybrid Lipopolysaccharide-based Nanosystem for the Delivery of Anti-tuberculosis drugs"

MSc Supervisor : Professor V. Pillay

Large pig gastric and intestinal tissue is required to carry out permeability studies. Material would be collected from pigs at a commercial abattoir or other convenient source.

The study therefore does not require full Animal Ethics Research Committee clearance to undertake the work.

This letter serves as a waiver for the study.

Please contact me should you require further information.

Yours sincerely

GP Candy

Geoffrey Candy
Chair : Animal Ethics Research Committee
University of the Witwatersrand

Reference : M Sumaila: *Waiver 15012019o*

Geoffrey P Candy PhD
Associate Professor
Department of Surgery
Faculty of Health Sciences, University of the Witwatersrand, *7 York Road Parktown 2193, Johannesburg*
Tel: 27-11-717-2574; Email: geoffrey.candy@wits.ac.za

APPENDIX D

Turnitin original report indicating the similarity index.

MSc Dissertation final submission_Mumuni Sumaila

by Mumuni Sumaila

Submission date: 29-Oct-2020 09:56PM (UTC+0200)
Submission ID: 1430475166
File name: Sumaila_MSc_Dissertation_Turnitin.docx (4.57M)
Word count: 20132
Character count: 126052

MSc Dissertation final submission_Mumuni Sumaila

ORIGINALITY REPORT

8%	%	8%	%
SIMILARITY INDEX	INTERNET SOURCES	PUBLICATIONS	STUDENT PAPERS

PRIMARY SOURCES

1	Alexandre C. C. Vieira, Luíse L. Chaves, Marina Pinheiro, Sofia A. Costa Lima, Domingos Ferreira, Bruno Sarmento, Salette Reis. "Mannosylated solid lipid nanoparticles for the selective delivery of rifampicin to macrophages", Artificial Cells, Nanomedicine, and Biotechnology, 2018 Publication	1%
2	"Physiological, Biochemical, and Chemical Barriers to Oral Drug Delivery", Drug Delivery, 2016. Publication	1%
3	Marina Pinheiro, Ricardo Ribeiro, Alexandre Vieira, Fernanda Andrade, Salette Reis. "Design of a nanostructured lipid carrier intended to improve the treatment of tuberculosis", Drug Design, Development and Therapy, 2016 Publication	1%
4	"Nanoformulations in Human Health", Springer Science and Business Media LLC, 2020 Publication	1%

5	Derusha Frank, Sunaina Indermun, Mershen Govender, Pradeep Kumar, Yahya E. Choonara, Lisa C. du Toit, Viness Pillay. "Antineoplastic nano-lipobubbles for passively targeted ovarian cancer therapy", Colloids and Surfaces B: Biointerfaces, 2019 Publication	<1%
6	Yeonhee Yun, Yong Woo Cho, Kinam Park. "Nanoparticles for oral delivery: Targeted nanoparticles with peptidic ligands for oral protein delivery", Advanced Drug Delivery Reviews, 2013 Publication	<1%
7	"Patenting Nanomedicines", Springer Science and Business Media LLC, 2012 Publication	<1%
8	Samantha Donnellan, Marco Giardiello. " Nanomedicines towards targeting intracellular for the treatment of tuberculosis ", Journal of Interdisciplinary Nanomedicine, 2019 Publication	<1%
9	"Functional Chitosan", Springer Science and Business Media LLC, 2019 Publication	<1%
10	Derusha Frank, Sunaina Indermun, Mershen Govender, Pradeep Kumar, Yahya E. Choonara, Lisa C. du Toit, Viness Pillay.	<1%

	"Antineoplastic Nano-Lipobubbles for Passively Targeted Ovarian Cancer Therapy", Colloids and Surfaces B: Biointerfaces, 2019 Publication	
11	Li-Li Shi, Hongjuan Xie, Jia Lu, Yue Cao, Jiang-Yan Liu, Xiao-Xue Zhang, Hongjian Zhang, Jing-Hao Cui, Qing-Ri Cao. "Positively Charged Surface-Modified Solid Lipid Nanoparticles Promote the Intestinal Transport of Docetaxel through Multifunctional Mechanisms in Rats", Molecular Pharmaceutics, 2016 Publication	<1%
12	C.S.A. Araújo, S.A.F. Marques, M.J.T. Carrondo, L.M.D. Gonçalves. "In vitro response of the brown bullhead catfish (BB) and rainbow trout (RTG-2) cell lines to benzo[a]pyrene", Science of The Total Environment, 2000 Publication	<1%
13	Govender, Thiresen, Yahya Choonara, Pradeep Kumar, Lisa Toit, Girish Modi, Dinesh Naidoo, and Viness Pillay. "A Novel Melt-Dispersion Technique for Simplistic Preparation of Chlorpromazine-Loaded Polycaprolactone Nanocapsules", Polymers, 2015. Publication	<1%
14	Shengxiang Tao, Song Gao, Yue Zhou, Mi Cao, Weiguo Xie, Hua Zheng, Lihong Fan.	<1%

"Preparation of carboxymethyl chitosan sulfate for improved cell proliferation of skin fibroblasts", International Journal of Biological Macromolecules, 2013
Publication

---

15 Prateek Mathur, Shruti Rawal, Bhoomika Patel, Mayur M. Patel. "Oral Delivery of Anticancer Agents Using Nanoparticulate Drug Delivery System", Current Drug Metabolism, 2020 <1%
Publication

---

16 Shi, Li-Li, Hongjuan Xie, Jia Lu, Yue Cao, Jiang-Yan Liu, Xiao-Xue Zhang, Hongjian Zhang, Jing-Hao Cui, and Qing-Ri Cao. "Positively Charged Surface-Modified Solid Lipid Nanoparticles Promote the Intestinal Transport of Docetaxel through Multifunctional Mechanisms in Rats", Molecular Pharmaceutics, 2016. <1%
Publication

---

17 Valence M. K. Ndesendo, Viness Pillay, Yahya E. Choonara, Lisa C. du Toit et al. "Advanced preformulation investigations for the development of a lead intravaginal bioadhesive polymeric device", Drug Development and Industrial Pharmacy, 2011 <1%
Publication

---

18 Lucineia Alves, Leila MendonÃ§a Lima, Elisa Silva Maeda, LaÃs Carvalho et al. " infection of <1%

human Schwann cells depends on selective host kinases and pathogen-modulated endocytic pathways ", FEMS Microbiology Letters, 2004
Publication

19	Poornima Ramburrun, Pradeep Kumar, Yahya E Choonara, Lisa C du Toit, Viness Pillay. "Design and characterisation of PHBV-magnesium oleate directional nanofibers for neurosupport", Biomedical Materials, 2019 Publication	<1%
20	Daniel Hoft, Getahun Abate. "Immunotherapy for tuberculosis: future prospects", ImmunoTargets and Therapy, 2016 Publication	<1%
21	Rosa Martha Perez Gutierrez, Juan Vicente Mendez Mendez, Israel Arzate Vazquez. "A novel approach to the oral delivery of bionanostructures for systemic disease", Elsevier BV, 2017 Publication	<1%
22	"ABSTRACTS FROM THE UK-PHARMSCI CONFERENCE, 1-3 SEPTEMBER 2010", Journal of Pharmacy and Pharmacology, 09/03/2010 Publication	<1%
23	Ricardo Ribeiro. "Development and Characterization of Nanocarrier Systems for the	<1%

Delivery of Antitubercular Drugs", Repositório Aberto da Universidade do Porto, 2013.
Publication

24	Anirbandeep Bose, Tin Wui Wong. "Oral colon cancer targeting by chitosan nanocomposites", Elsevier BV, 2018 Publication	<1%
25	E. Giovannetti, L. G. Leon, S. Bertini, M. Macchia, F. Minutolo, N. Funel, C. Alecci, F. Giancola, R. Danesi, G. J. Peters. "Study of Apoptosis Induction and Deoxycytidine Kinase/Cytidine Deaminase Modulation in the Synergistic Interaction of a Novel Ceramide Analog and Gemcitabine in Pancreatic Cancer Cells", Nucleosides, Nucleotides and Nucleic Acids, 2010 Publication	<1%
26	Pietro Picconi, Rose Jeeves, Christopher William Moon, Shirin Jamshidi et al. " Noncytotoxic Pyrrolobenzodiazepine–Ciprofloxacin Conjugate with Activity against ", ACS Omega, 2019 Publication	<1%
27	Samira Nasirizadeh, Bizhan Malaekeh-Nikouei. "Solid lipid nanoparticles and nanostructured lipid carriers in oral cancer drug delivery", Journal of Drug Delivery Science and	<1%

Technology, 2020
Publication

28	Jong-Suep Baek, Cheong-Weon Cho. "Surface modification of solid lipid nanoparticles for oral delivery of curcumin: Improvement of bioavailability through enhanced cellular uptake, and lymphatic uptake", European Journal of Pharmaceutics and Biopharmaceutics, 2017 Publication	<1%
29	Haidar, Z.S.. "Protein release kinetics for core-shell hybrid nanoparticles based on the layer-by-layer assembly of alginate and chitosan on liposomes", Biomaterials, 200803 Publication	<1%
30	Amidi, M.. "Preparation and characterization of protein-loaded N-trimethyl chitosan nanoparticles as nasal delivery system", Journal of Controlled Release, 20060310 Publication	<1%
31	Akiharu Ishida, Yohei Tajima, Yasuyuki Okabe, Takeshi Matsushita et al. "Discovery and SAR Studies of Orally Active Somatostatin Receptor Subtype-2 (SSTR2) Agonists for the Treatment of Acromegaly", ACS Chemical Neuroscience, 2020 Publication	<1%
32	Olesja M. Bondarenko, Margit Heinlaan, Mariliis	

	Sihtmäe, Angela Ivask et al. "Multilaboratory evaluation of 15 bioassays for (eco)toxicity screening and hazard ranking of engineered nanomaterials: FP7 project NANOVALID", Nanotoxicology, 2016 Publication	<1%
33	"Posters", Basic & Clinical Pharmacology & Toxicology, 06/22/2010 Publication	<1%

Exclude quotes	On	Exclude matches	< 20 words
Exclude bibliography	On		